THE GEORGIA TECH REGENERATIVE ELECTRODE – A PERIPHERAL NERVE INTERFACE FOR ENABLING ROBOTIC LIMB CONTROL USING THOUGHT

A Dissertation

Presented to

The Academic Faculty

by

Akhil Srinivasan

In Partial Fulfillment

of the Requirements for the Degree

Doctor of Philosophy in the

Wallace H. Coulter Department of Biomedical Engineering

Georgia Institute of Technology

August 2015

THE GEORGIA TECH REGENERATIVE ELECTRODE – A PERIPHERAL NERVE INTERFACE FOR ENABLING ROBOTIC LIMB CONTROL USING THOUGHT

Approved by:

Dr. Ravi Bellamkonda, Advisor
Department of Biomedical Engineering
Georgia Institute of Technology

Dr. Stephanie Lacour
Institute of Microengineering
Ecole Polytechnique Fédérale de Lausanne

Dr. Mark Allen
Department of Electrical & Systems Engineering and Mechanical Engineering & Applied Mechanics
University of Pennsylvania

Dr. Garrett Stanley
Department of Biomedical Engineering
Georgia Institute of Technology

Dr. Arthur English
Department of Cell Biology
Emory University

Date Approved: April 30, 2015

To my family and Inthirai for their sacrifices and constant support

and to all those who have helped me during the last 6 years.

ACKNOWLEDGEMENTS

My graduate school career and Ph.D. have been a wonderful experience filled with personal growth and many fond memories. Everything I have accomplished and learned over the past 6 years is due to amazing individuals I have had the pleasure of getting to know, collaborate with, and learn from.

First and foremost, I would like to thank Dr. Ravi Bellamkonda who has been much more than just my Ph.D. advisor. Over the years you have guided not only my scientific growth, but personal growth as well. You have been a tremendous role model for how I approach challenges in my life and how I think about my future. I cannot thank you enough for everything you have done and the time and energy you have spent helping me mature and grow. You gave me the opportunity to write a DARPA grant which is something I still reap the benefits of. You pushed me to aim high with my research goals, to fight to actually attain them, and most importantly grow by achieving depth in pursuit of a goal instead of staying at a high level, something I am more naturally inclined to do. Finally, you encouraged me and gave me the freedom to explore numerous opportunities beyond the scientific work in our lab. All of this has led to a graduate school experience I cherish and one that drastically exceeded my expectations when I first came to Georgia Tech. You inspired me the first day I entered your lab and you continue to do so.

I would like to thank my thesis committee members, Dr. Mark Allen, Dr. Arthur English, Dr. Stephanie Lacour, and Dr. Garrett Stanley for their tremendous support during my Ph.D.. Dr. Allen, you have been instrumental in the device design and

fabrication components of my thesis. My collaboration with you and Dr. Chao Song has been one of the best collaborations I have ever had and I cannot thank you enough for it. Through this I gained tremendous experience in the cleanroom which ultimately led to my current job opportunities. You have always struck me as incredibly wise and your calm demeanor makes you a pleasure to interact with and I hope our paths cross frequently in the future.

Dr. English, you took me into your lab as one of your own for the electrophysiology aspects of my thesis. You stood by me, experimented with me, and shared some of the best and toughest experiences of my Ph.D. with me. Whenever I was in need of something, be it research related or simply a boost in spirits, you were there and always happy to help. My Ph.D. would undoubtedly not be what it is if it were not for you. Above all, you have been selfless in your support of my growth throughout my Ph.D. You have been a pleasure to work with and great company.

Dr. Lacour, despite the significant distance between us you have always been there to support me during my Ph.D. You were always willing to share you immense expertise with fabrication despite the potentially competitive nature of our research. This is something I cannot thank you enough for and something I respect you greatly for. I think you are a role model for how research and collaborations can be performed in academia despite the competitive pressure we all face. Our in-person meetings were always a highlight and I hope the future holds opportunities for us to work together.

Dr. Stanley, you gave me the opportunity to not only lead our DARPA project from a technical capacity, but also lead a team of researchers. This was a tremendous growth opportunity for me and is one of my most valued experiences from my graduate

school career. You have always treated me as an equal and encouraged me to think and act that way. Finally, you pushed me to take a deeper and more detailed look at my data and results which I truly appreciate. Your influence played a large role in ensuring I gained the depth of understanding I current have in my Ph.D.

During the last 6 years I have had the opportunity to work with amazing individuals across Georgia Tech as we collaborated on various aspects of my Ph.D.. There are a few that I would like to specifically thank for their help and mentorship. Dr. Liang Guo initially got me started in the cleanroom, teaching me the basics of photolithography and patterning. Your help and mentorship were instrumental to where I am today. Dr. Chao Song was my collaborator for much of the challenging device design and fabrication components of my thesis. Over the years I not only learned tremendously from you as a collaborator but have come to value you as a dear friend. Dr. Russell Gore and Dr. Daniel Millard both collaborated with me during my very first *in vivo* electrophysiology experiments. Without both of your support I likely would not have progressed beyond the first phase of my thesis. Your willingness to share you immense knowledge and lend a helping hand to a first-time electrophysiologist is truly appreciated. It has been a pleasure working with both of you. Yogi Patel also collaborated with me over many months when we attempted to integrate advanced amplification/multiplexing microchips into the device I developed for my thesis. While we met with many technical challenges along the way, I respect you greatly and cannot wait to see what you accomplish in the future. Poornima Venkataraman was a technician under our DARPA grant and put countless hours into cleanroom fabrication. Your patience, consistency, and dependability are truly remarkable. You had one of the most demanding jobs along with

extremely challenging deadlines yet always showed up with a smile on your face, a pleasant attitude, and willingness to jump back into the job despite numerous technical difficulties.

I would also like to thank all of the past and present members of the Bellamkonda Lab who have helped me countless times and in almost every way imaginable over the past 6 years. In particular, Dr. Vivek Mukhatyar and Dr. Isaac Clements took me under their wings when I first joined the lab. They allowed me to participate in their experiments and taught me the intricate peripheral nerve transection and device implantation surgeries, electrophysiology, and immunohistochemistry. You both have not only been amazing mentors, but are also life- long friends. Dr. Lohitash Karumbaiah played a significant role in the earlier stages of my Ph.D. pushing me to be better and do better work. You allowed me to constantly bounce my thoughts off of you and always tried to steer me clear of pitfalls and taking shortcuts that would have resulted in failure and poor quality research. I greatly appreciate your advice and mentorship over the years. Dr. Nassir Mokarram has been with me every step of the way through my Ph.D. We found numerous opportunities to collaborate and even when we weren't, we were constantly exploring ideas with each other. You helped me tremendously over the years with my experiments, my thought process, and always reminding me to look on the positive side of things and take advantage of the numerous opportunities presented to us. I have been incredibly lucky to have you as a lab mate and a dear friend. Kristin Loomis is another dear friend and lab mate who has been with me every step of the way. We shared almost every lab experience together from the beginning to the end. You helped keep me sane and moving forward and always had an ear when I needed to relieve some

frustration. Graduate school and my Ph.D. simply would not have been the same without you. Kelly Rockwell managed all of the financials and scheduling of our DARPA grant which was a constant struggle. Working with you over the years has been a pleasure and your positive, happy attitude made all of the struggles always seem surmountable. I will always fondly remember our times together. Dr. Balakrishna Pai and Ketki Patil keep our lab running. Thank you for always putting up with my constant off-cycle ordering of abnormal items that often times required personal ordering from both of you. You take a chaotic environment and maintain a level of order that allows everyone else in the lab to be successful and I am forever grateful to both of you for that.

I would also like to thank the amazing undergraduate students and technicians who have worked with me over the years. These include Jim Schwoebel, Anish Joseph, Adel Haque, Mayank Tahilramani, Adel Kharbouch, John Tipton, John Bentley, and Eric Gaupp. All of you have been wonderful to work with and made my time here a blast. We accomplished a lot together and none of this would have been possible without all of you. You made coming to lab something I looked forward to and I cannot ever thank you all enough for everything you did to help me throughout Ph.D. I am extremely proud of everything you all have already accomplished on your own and cannot wait to see what more you do in the future and the career paths you choose.

The BME staff, in particular Shannon Sullivan, Sally Gerrish, and Courtney Ferencik deserve special recognition for all the work they do behind the scenes to keep our department running and help students find jobs and internship. I have enjoyed getting to know all of you over the past years and hope to keep in touch in the future. The Georgia Tech cleanroom staff also deserves special recognition for the incredibly

difficult job of keeping the cleanrooms running and always striving to meet the incredibly diverse demands of the various users. Without them, I would never have been able to fabricate the devices in my thesis.

Finally I would like to thank all my friends here in Atlanta who given me numerous memories and experience I will cherish forever. I would also like to thank my family for all of their support and help during my thesis. My father at many times served as an additional thesis committee member with his vast experience in MEMS and was always willing to provide advice and solutions for the numerous issues I encountered. Last, but not least, I would like to thank Dr. Inthirai Somsuntharam. You have been with me and supported me for the last 6 years both with my research and personally. You put up with countless hours of my brooding and obsessing over my work and always listened as I constantly reviewed and re-thought every aspect of my thesis. You have given me a level of joy and excitement I never knew before. It is largely because of you that I have no regrets and I can look back on this time period in my life as one of the best.

TABLE OF CONTENTS

LIST OF FIGURES

LIST OF SYMBOLS AND ABBREVIATIONS

µm	Micrometer
µV	Microvolt
ANOVA	Analysis of variance
AP	Action potential
Au	Gold
CAP	Compound action potential
CNS	Central nervous system
DAPI	4‟,6-diamidino-2-phenylindole
DI water	Deionized water
DRG	Dorsal root ganglion
ECM	Extracellular matrix
FINE	Flat interface nerve electrode
GT-RE	Georgia Tech Regenerative Electrode
hr	Hour
LIFE	Longitudinal intrafascicular electrode
MEA	Microelectrode array
mJ	Millijoule
NF-160	Neurofilament 160kDa.
NR4-8000P	Photoresist
PAA	Polyacrylic acid
PBS	Physiologically buffered saline
PCB	Printed Circuit Board
PDMS	Polydimethylsiloxane
PNI	Peripheral nerve interface
PNS	Peripheral nervous system
SMD	Surface mount device
SMT	Surface mount technology
SNR	Signal to noise ratio
SPR 220-7.0	Photoresist
SU-8	Photosensitive epoxy
Ti	Titanium
TIME	Transverse intrafascicular multichannel electrode
USEA	Utah slanted electrode array
V	Volt

SUMMARY

Amputation is a life-changing event that results in a severe reduction in quality of life. In addition to the loss of a limb, there is drastic loss of function and severe mental, emotional and physical pain. In order to mitigate these negative outcomes, there is great interest in the design of 'advanced' prosthetics that cosmetically and functionally mimic the lost limb. While, the robotics side of advanced prosthetics has seen substantial progress recently, they still provide only a fraction of the natural limbs' functionality. At the heart of the issue is the *interface* between the robotic limb and the individual that needs significant development. Amputees retain significant function in their nerves post-amputation, which offers a unique opportunity to interface with the peripheral nerve.

Here we evaluate a relatively new approach to peripheral nerve interfacing by using microchannels which hold the intrinsic ability to record larger neural signals from nerves than previously developed peripheral nerve interfaces. We first demonstrate that microchannel scaffolds are well suited for chronic integration with amputated nerves and promote highly organized nerve regeneration. We then demonstrate the ability to record neural signals, specifically single unit action potentials, using microchannels permanently integrated with electrodes after chronic implantation in a terminal study. Together these studies suggest that microchannels are well suited for chronic implantation and stable peripheral nerve interfacing.

As a next step toward clinical translation, we developed fully-integrated high electrode count microchannel interfacing technology capable of functioning while implanted in awake and freely moving animal models as needed for pre-clinical evaluation. Importantly, fabrication techniques were developed that apply to a broad range of flexible devices/sensors benefiting from flexible interconnects, surface mount device (SMD) integration, and/or operation in aqueous environments. Examples include glucose sensors for diabetes, flexible skin based health monitors, and the burgeoning

flexible wearable technology industry. Finally we successfully utilized the fully-integrated microchannel interfaces to record action potentials in the challenging awake and freely moving animal model validating the microchannel approach for peripheral nerve interfacing. In the end, the findings of these studies help direct and give significant credence to future technology development enabling eventual clinical application of microchannels for peripheral nerve interfacing.

CHAPTER 1 INTRODUCTION

Currently, neural prosthetics provide only a small fraction of the functionality of a natural limb. However, compelling evidence in the last decade that amputees retain significant motor and sensory function in the peripheral nerve stump has paved the way for bidirectional sensorimotor prosthetics to restore function following amputation [1]. A bidirectional sensorimotor prosthetic aims to record volitional motor commands from peripheral nerves to control a robotic limb, while sensors on the device produce direct stimulation of peripheral nerves to deliver feedback. Advances in robotics have led to high dimensionality robotic limbs, but the peripheral nerve interface remains the "weak-link" due to issues with reliability and engaging sufficient numbers of independent and specific channels of communication with the peripheral nerve. To realize the dream of a fully functional interface for amputees, it is imperative that engineered systems interface with the periphery in a highly specific and reliable manner to deliver and receive information that is relevant for natural sensation and movement.

State of the art prosthetics often use electromyograms from various sets of muscles. However, this method provides limited prosthetic control and does not allow for proprioception, tactile feedback, and other sensation. Next generation peripheral nerve prosthetics aim to interface with the original limb's remaining nervous system by taking advantage of the retained motor and sensory function. Even here, peripheral nerve interfacing attempts have faced significant challenges stemming from a tradeoff between interfacing specifically with individual axons within a nerve and long-term reliability with the nerve. The widely used cuff electrodes, which wrap around the nerve, provide long-term stability at the physical tissue-device interface at the expense of stimulation and recording specificity because of poor proximity to central portions of the nerve [2,3]. A device that penetrates into the nerve, like the Utah Slanted Electrode Array (USEA), provides enhanced specificity over its large number of needle-like electrodes. However,

the penetration causes multiple injuries and as a result the device remains susceptible to a buildup of scar tissue and an immune response limiting chronic efficacy [4]. On the other hand, regenerative devices have the capability to circumvent the tradeoff between specificity and reliability by allowing axons to regenerate through specific geometries in close contact with electrodes. Unfortunately the Sieve electrode, the hallmark regenerative device, by design only supports axon regeneration over a small distance on the order of hundreds of microns [5]. As a result, many electrodes are rendered useless when they are far from a node of Ranvier, the point at which the signal of an axon is largest. This is in fact a fate suffered by all existing electrode technologies.

Our ***long-term goal*** is to create a novel regenerative neural interface to establish high-channel, bi-directional communication between an amputated nerve and a prosthetic limb. This interface would allow for intimate contact between electrodes and small groups of axons. The ***objective*** of this thesis was to evaluate the use of microchannels for chronic peripheral nerve interfacing and develop a fully integrated high electrode count microchannel interface, the Georgie Tech. Regenerative Electrode (GT-RE), able to perform in this application. The rationale behind the microchannel design was based upon the fact that confining an axon to a microchannel limits the volume of low impedance extracellular fluid surrounding the axon. Limiting the extracellular volume effectively increases the extracellular resistance and following from Ohm's Law, increases the extracellular potential [6]. Other interfacing approaches are forced to endure the low impedance of the surrounding volume. Furthermore, other interfaces are spatially dependent on the nodes of Ranvier, which are breaks in axon insulation where the extracellular potential is largest. Using a 3mm microchannel ensures that a node falls within the channel as they occur at least every 2mm [7]. This allows the incorporated electrodes to be spatially independent of the nodes of Ranvier. Finally, encouraging the axons to regenerate in small numbers through numerous microchannels allows for highly selective recording and stimulation based upon electrical and spatial isolation.

The long term goal and objective were achieved through the following 3 aims.

Specific Aim 1: Evaluating the Chronic Capability of Regenerative Microchannel Interfacing. [1,2]

The underlying success of a regenerative microchannel device for neural interfacing is fundamentally contingent on long term tolerance by the peripheral nervous system in amputees. Thus, the neural implant is inherently dependant on the chronic condition of the matured nerve post regeneration when original reinnervation targets are no longer present due to amputation. Accordingly, we first developed microchannel scaffolding composed of polydimethylsiloxane (PDMS) and the polymer SU-8 to enable this investigation. We evaluated cytocompatibility using an *in vitro* culture system and then focused *in vivo* on the amputated nerve lacking distal reinnvervation targets and its capability to regenerate through an artificially imposed microchannel obstacle. The nerve was characterized morphologically as a whole and on a cellular level. Growth was characterized both within the microchannels and distal to the microchannels to evaluate regenerative capability, chronic stability, and the risk of neuropathic complications. Finally, we evaluated whether neural signals from regenerated axons can be recorded using microchannels permanently integrated with electrodes after chronic implantation in a separate terminal study. The *outcomes* of this aim are discussed in Chapter 3.

---

[1] Srinivasan, A., et al., *Microchannel-based regenerative scaffold for chronic peripheral nerve interfacing in amputees.* Biomaterials, 2015. **41**: p. 151-65

[2] Srinivasan A., et al., *Regenerative microchannel electrode array for peripheral nerve interfacing.* 5th Int. IEEE/EMBS Conf. Neural Eng, 2011. p. 253–6

Specific Aim 2: Fabrication Processes for Flexible Electrode Arrays, SMT Integration, and Implantation.

In order for microchannel interfacing to be clinically translated, full integrated microchannel interfacing technology must first be developed. This includes the incorporation of large count microelectrode arrays (MEA), the ability to easily integrate surface mount technology (SMT) for multiplexing and amplification, and be capable of functioning while implanted in awake and freely moving animal models for pre-clinical evaluation. Along these lines, we designed fabrication techniques for flexible (Parylene C) and elastomeric (PDMS) based MEAs with large numbers of high-density microelectrodes generating two different GT-RE's differing only in substrate material. Second, we devised and validated a simple and broadly applicable SMT integration strategy for flexible and elastomeric devices. Third we utilized flexible and elastomeric polymer based hermetic insulation and encapsulation strategies for the GT-RE's enabling implantation and electrophysiology in awake and freely moving rats. These design and fabrication techniques, while enabling peripheral nerve interfacing with microchannels, are applicable to a broad range of flexible devices and sensors benefiting from stretchable and/or flexible interconnects, SMD integration, and/or operation in hostile aqueous environments. The *outcomes* of these fabrication techniques are discussed in Chapter 4.

Specific Aim 3: Evaluating the fully integrated high electrode count microchannel interface for clinically translatable peripheral nerve interfacing.

We then evaluated the capability of the fully integrated GT-RE microchannel interfaces to be used for challenging single unit action potential recordings. First, *in vitro* functionality of the GT-RE's was explored using artificial neural signals. Secondly, *in vitro* dorsal root ganglia (DRG) studies were utilized to assess cytocompatibility after microfabrication of the GT-RE's which involved a number of toxic processes. Finally, *in*

vivo the GT-RE's were implanted in the rat sciatic nerve transection model. *In vivo* recordings were performed while the rats were awake and ambulating to evaluate the capability to record single unit action potentials through microchannel interfaces in a clinical relevant experimental model. The *outcomes* of these evaluations studies are discussed in Chapter 5.

CHAPTER 2 LITERATURE REVIEW

2.1 Introduction

2.1.1 Amputation Occurrence and Prevalence

In general it is difficult to find up to date information regarding amputations with just a couple studies reviewing the occurrence and prevalence in the US over the last 20+ years and the most recent being in 2005. In the 2005, 1.6 million persons were living with a limb amputation (one in 190 Americans) and it has been projected that by 2050 this number will more than double to 3.6 million in the United States alone [8]. Amputations are performed for a number of reasons, but the majority stem from diabetic and dysvascular diseases, trauma, and cancer related operations. In 2005 amputations stemming from individuals suffering from dysvascular disease accounted for 54% of the total with two thirds of these individuals also suffering from diabetes. Amputation due to trauma accounted for 45% and cancer for less than 2%. The majority of amputations, approximately 65%, were of the lower extremity with over half of these being major amputations and excludes toes. Only 8% of upper limb amputations were categorized as major, excluding fingers, in comparison. [8] The larger number of lower limb amputations follows naturally from the fact that a study found in 2008 diabetes was the leading cause of non-traumatic lower limb amputations with rates approximately eight times higher than with the non-diabetic population [9]. Another study reported that the diabetic population accounted for more than 60% of lower limb amputations in 2011 [10].

Regarding the age demographics of amputees, in 2005 it was shown that the rate of amputations dramatically increased with age where 42% of all amputees and 57% of the incident cases were in adults 65 years or older. A contributing factor to this age demographic was the large tendency, 64%, of amputations occurring in individuals

suffering from dysvascular disease to also be 65 years or older. That being said, in 2005 there were approximately 1 million amputees below the age of 65 and 302,000 below the age of 45. Furthermore, over two thirds of trauma related amputations occurred in individuals below the age of 45. [8] In many cases, it is these individuals that stand to benefit the most from new advances in prosthetic technology as it will enable them to maintain a higher quality of life for their longer life expectancy.

2.1.2 Amputation and the Clinical Need

Amputation is a life-changing event that results in a severe reduction in quality of life. In addition to the loss of a limb, there is a drastic loss of function and mobility and also severe mental, emotional and physical pain. The lifestyle change and emotional challenges extend to the individual's loved ones as well. The extra care needed can also drastically increase costs of living. Finally, family income and society suffer if the amputee is unable to return to work and maintain a job.

In order to mitigate these negative outcomes after amputation, there is great interest in the design of 'advanced' or 'robotic' prosthetics that cosmetically and functionally mimic the lost appendages. Amputees want a prosthetic that returns them to their previous level of function and looks like their lost limb. In essence, these are robotic prosthetic limbs that need to be controlled and operated according to a person's will or thought as a normal arm or leg would be. Furthermore, the robotic prosthetic needs to provide sensation such as hot or cold, rough or smooth, hard or soft back to the individual so that he or she is able to feel through the prosthetic.

The robotics side of advanced prosthetics has seen many advances in the recent decade with lifelike limbs that can be programmed to perform intricate motions. They also have various integrated sensors providing data of the environment to onboard chips or computers. Examples include the 'Otto Bock C-leg' and the 'i-limb Robotic Hand'. However, these advanced prosthetics *still* only provide a small fraction of the

functionality of a natural limb. It is the ability to understand an individual's *intended* action and translate that to prosthetic movement that lags behind. Furthermore, these advanced prosthetics while having numerous integrated sensors for the environment do not send this information back to the individual in a seamless fashion and instead stop at the onboard chip for processing. Essentially it is the *interface* between the robotic limb and the individual that needs significant development to enable large scale clinical translation and market adoption of advanced robotic prosthetics.

The body's nervous system offers a unique opportunity to establish this interface between the robotic limb and the individual. The nervous system is not only responsible for generating signals resulting in limb movements, but also conveys sensation from the environment to the individual. Tapping into the nervous system could allow a seamless integration with robotic limbs enabling movement of the limbs based on thought and sensation through the limb. Based on these ideas there have been ongoing efforts to develop 'neural interfacing' technology.

Broadly speaking, neural interfacing technologies can be divided into two major segments based on location of interaction with the body's nervous system. There are central neural interfaces consisting of the brain and spine and peripheral neural interfaces consisting of nerves predominantly in the limbs. There have been a number of approaches within both of these areas, but all have met with significant difficulties and limitations. Central neural interfaces are plagued by the invasiveness of needing to implant electrodes directly in the brain and the fact that this will cause another injury in addition to the amputation of the limb. Furthermore, even after the implantation and recording of neural signals a huge obstacle of decoding these 'abstract' signals remains. Peripheral neural interfaces are significantly less invasive as they are implanted in peripheral nerves and can be implanted at the time of amputation. Another large advantage peripheral neural interfaces have is that the signals obtained from peripheral nerves, closely represents the signal intended for muscle activation. The decoding has been taken care of by the

descending pathways of the brain and spinal cord, obviating the need for artificial decoding.

2.2 Peripheral Nerve

2.2.1 Physiology

The peripheral nerve, in its physiological structure, is similar in some sense to a multi-wire electrical cable. A nerve can be thought of simplistically as a ‘cable’ comprised of many thousands of wires, termed axons. These axons are processes (extensions) of cells whose cell bodies reside in or just outside the spinal cord or at the base of the brain. The axons are the entities within a nerve that conduct motor (muscle) and sensory information to and from the brain and the body’s periphery. The ‘information’ that is conducted by the axon is termed an action potential (AP) and is an electrochemical event that propagates down the length of the axon to its end target. The electrochemical event is a local change in ion concentrations inside and outside the axon which creates a local voltage change across the axons’ cellular membrane. As a result of the voltage change of an AP, it is possible to measure or record the occurrence and magnitude of the AP signal. The magnitude of these APs however is on the order of microvolts making this an exceedingly challenging endeavor. This is especially true when considering an *in vivo* environment where much of the noise, motion artifact and electrical signals from local muscles are orders of magnitude larger.

Another similarity axons have with wires in an electrical cable is the presence of insulation. This insulation is biological in nature stemming from cells of a glial origin termed Schwann cells. These Schwann cells wrap themselves around the axons in numerous layers and produce a protein (myelin) ensheathment which makes up the insulation surrounding the axons. In addition to providing insulation, Schwann cells play an important role in providing nutrients and maintaining the health and stability of the axon [11]. However, one important difference between the insulation of a wire and that of

an axon is that the Schwann cell and myelin sheath is not continuous down the length of an axon. Instead the Schwann cell and myelin sheath extend at most 2mm before a small gap in insulation appears and another Schwann cell insulates the following portion of the axon. [7] The gaps between the Scwhann cells and myelin insulation are on the order of 1 micron and are known as the 'nodes of Ranvier'. Owing to the lack of insulation in these nodes, they are also the regions of an axon where the AP magnitude is largest. The insulation, while making the measurable AP magnitude small except at the nodes of Ranvier, help the APs propagate faster from its source to its destination through a process known as 'saltatory conduction'. In salutatory conduction, the AP is able to essentially hop from node to node down the length of the axon increasing the AP conduction speed and reducing the time for information to travel from the brain to the periphery and vice versa.

Another important cell known as a fibroblast resides within the connective tissue throughout the nerve. The fibroblast is predominantly responsible for producing and maintaining the extracellular matrix and support tissue of the nerve which is largely composed of laminin and collagen. The fibroblasts within a nerve are typically found in concentric rings or layers denoting different tissues of the nerve.

There are three major tissues known as the epineurium, perineurium, and endoneurium. The epineurium is the outer most tissue layer of the nerve and tends to be more fibrous in nature and functions as a protective layer to the nerve. The perineurium is a tissue layer that wraps around groups or bundles of axons and Schwann cells. These groupings are known as fascicles and larger nerves typically have multiple fascicles while smaller diameter nerves may not have any. The endoneurium is the extracellular matrix which resides immediately next to and surrounding the axons and Schwann cells providing a structure for support and cell adhesion. As a result the endoneurium is often observed as a tube like structure and called an endoneurial tube.

2.2.2 Peripheral Nerve Injury and Regeneration

In the case of peripheral nerve injury the nerve and cells within undergo a series of well-defined processes culminating in an attempt to regenerate and heal from the injury. In the case of nerve cut or transection a process known as Wallerian degeneration starts almost immediately after the injury. The axons distal to the transection have been separated from their cell body residing more proximally and as a result start to degenerate. The debris from the injury and axon degradation is cleared away by an influx of immune cells, predominantly macrophages [12,13], and local Schwann cells. Concurrently a fibrin protein cable forms between the proximal and distal ends of the cut nerve, bridging the gap and providing a matrix for cell migration and axon extension. [14]

Following Wallerian degeneration Schwann cells in the distal nerve proliferate and differentiate, taking on a pro-regenerative phenotype and aligning themselves within the remaining endoneurial tubes forming aligned tracts called “bands of Büngner”. These tracts help guide regenerating axons from the proximal nerve stump once they reach the distal nerve stump. Fibroblasts also proliferate and along with Schwann cells migrate from both ends of the transected nerve along the fibrin matrix enriching and restructuring the matrix to support subsequent axon regeneration [15,16]. During this time the fibroblasts and Schwann cells also secrete a milieu of growth factors and cytokines to further support regeneration and pathfinding of the newly regenerating axons from the proximal nerve stump [17,18].

At this point in the regeneration cascade, the severed axons in the proximal nerve stump form a growth cone at the severed tip. This growth cone follows the migrating Schwann cells from the proximal nerve stump and leads the regenerating axon along the enriched fibrin/cellular cable, eventually meeting the distal nerve stump and the bands of Büngner. The regenerating axons then use the endoneurial tubes and structure of the distal nerve stump to continue regenerating back to and eventually reinnervating the end

organs and distal targets in successful nerve regeneration. [19,20] It is important to note however, that often the growth cone from a regenerating axon will enter a different endoneurial tube from where it was prior to the injury. As a result that axon will follow a different path through the distal nerve and reinnervate a different target/end organ than which it was previously connected to. This manifests clinically in a common mixing of sensations post nerve regeneration where instead of feeling touch, one feels hot or cold or simply a tingling sensation, for example. The individual must 'relearn' over the course of months and years which axons are responsive to which sensations and similarly which muscles in the case of motor control. [21]

2.2.3 Peripheral Nerve Regeneration and Viability in an Amputee Scenario

When the distal stump of a nerve is missing, as in the case of amputation, reinnervation of the original distal targets cannot occur. However, the nerve itself is still capable of regenerating. Previous studies have shown that in the complete absence of the distal nerve stump, transected nerves sutured into semi-permeable conduits/tubes are capable of regenerating through the conduits [22,23]. Inserting a small nerve segment at the distal end of the conduit further helps this case as it provides a distal source of Schwann cells and fibroblasts to help support the phases of nerve regeneration. Doing so enables nerve regeneration that in some cases can even match regeneration through open conduits when the distal nerve stump is present. [24–26]

Not only is an amputated nerve capable of regeneration, but the axons and corresponding neurons remain viable and do not under cell death post amputation. Multiple studies have documented the survival of both motor neurons extending axons from within the spinal cord and sensory neurons extending axons from dorsal root ganglia next to the spinal cord after peripheral nerve transection. Motor neurons seem particularly capable of survival after axotomy whereas sensory neurons have shown at least 50% survival. [27–32] It is important to note however, that the neurons and axons

do undergo physiological changes post amputation. Notably, atrophied states are observed where the axons exhibit reduced axonal diameters. These diameters are stable over time however and as stated before, do not die away. The action potentials associated with amputated axons also undergo changes, such as slower conduction velocities, but the ability to generate and propagate action potentials is retained as well. [29,30,33]

The viability of axons/neurons and ability to generate and propagate action potentials post amputation have also been validated clinically. Wire electrodes called Longitudinal intrafascicular electrodes (LIFE) were inserted into the remaining nerves in the limbs of amputees. The amputations had occurred out to 15 years before the experiment took place. The LIFEs were successfully used to record action potentials associated with intended movements of the missing limbs. The LIFEs were also successfully used to evoke sensory action potentials and induce various sensations associated with the missing limbs. The ability to accomplish both the recording and stimulation in amputees whose amputations occurred many years in the past clearly demonstrates the chronic viability of axons/nerves and their ability to generate and propagate action potentials post amputation. [1]

2.3 Peripheral Interfacing

2.3.1 State of the Art Prosthetic Control

2.3.1.1 EMG

Myoelectric systems are the current state of the art and record electrical signals using sensors on various muscles (electromyograms) as efferent (motor) control inputs. These systems are minimally invasive but provide only limited prosthetic control and are not readily capable of providing afferent (sensory) feedback signals [1]. These systems are limited by the remaining number of muscles on a limb post amputation for input, which in the case of upper limb amputations can be quite few. The production of sweat

and shifts in the position of the prosthetic and its EMG sensors over time in relation to the remaining muscles on the amputees' limb also drastically affects it performance and interferes with its EMG recording capabilities. Furthermore, individuals must learn to use their remaining muscles for prosthetic limb movements which are completely different from the original movements of their amputated limb. This is a time intensive and challenging processes.

Surgical techniques have been developed to help increase the number of muscles available for control input to the EMG prosthetics. This technique involves surgically rerouting nerves from the amputated limb to non-critical muscles for the amputated nerve to reinnervate. This technique is known as 'targeted muscle reinnervation'. In the case of upper-limb amputees the nerves are often rerouted to the pectoral muscles. Using this technique the number of muscles available for prosthetic limb control increases and in many cases the movement is now directly synced to the individuals intended movement of their amputated limb. The amputee does not need to relearn different movements for new muscles. Of significance, it has also been shown that sensory reinnervation has occurred as well where portions of the skin in the chest region become tied to the amputated limb and the individual feels sensation on their missing limb instead of the chest region. [34,35] While these are exciting outcomes from the targeted muscle innervation technique, the surgery is extremely invasive. Furthermore, there remains a real-estate issue between EMG sensor placement and sensory feedback devices on the chest limiting the actually capability of this technique to drive a closed-loop prosthetic system. Finally, this technique still suffers from the practical issues of EMG sensor movement and sweat generation during prosthetic limb operation.

2.3.2 Peripheral Nerve Interfaces

2.3.2.1 Cuff Electrodes

Cuff electrodes, which wrap around the nerve (Figure 1A), cause little damage to the nerve and provide long-term stability at the tissue-electrode interface. They have even shown efficacy in clinical translation regarding some applications in nerve stimulation [36–38]. However, cuff electrodes achieve their stability at the expense of recording fidelity and stimulation specificity because they are not in direct contact with individual axons. [2,3,6,39] Instead, due to the fact that they reside outside of the nerve's epineurium and the distance this creates between the electrodes and individual axons, they tend to record and stimulate nerves on a fascicular level. While interfacing with fascicles is useful in some applications, it does not provide the specificity needed to control a neural prosthetic with large degrees of freedom. Attempts to improve selectivity with multiple electrode configurations and nerve compression, such as in the Flat Interface Nerve Electrode (FINE), have been somewhat successful but again not beyond the fascicular level [39,40]. Additionally many electrodes are rendered useless due to poor contact between the nerve and the electrode.

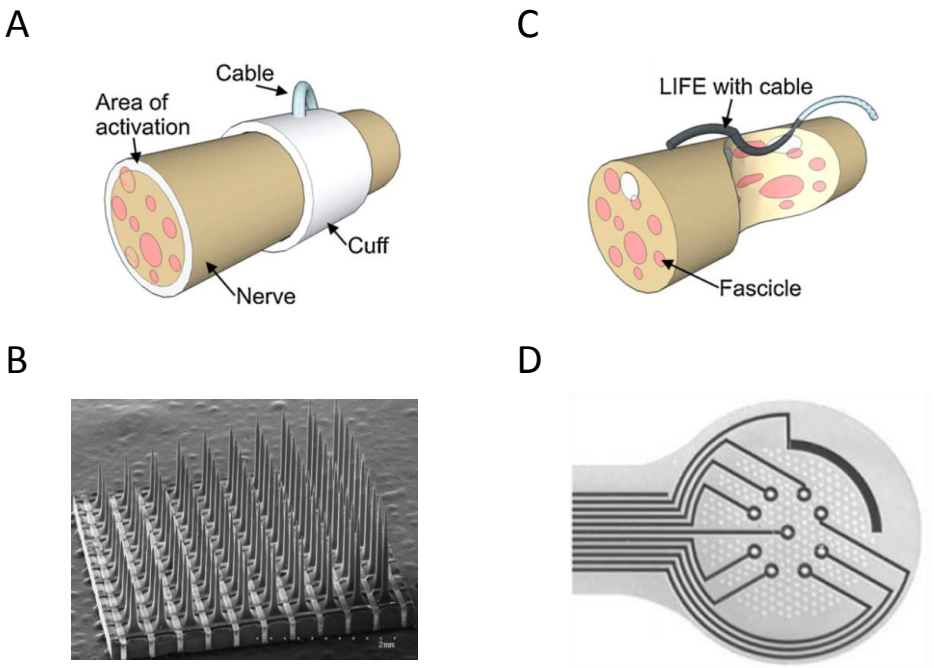

Figure 1. Traditional peripheral nerve interfaces.
(A) Cuff electrode. (B) Penetrating Utah Slanted Electrode Array. (C) Penetrating Longitudinal Intrafascicular Electrode. (D) Regenerative Sieve electrode. Adapted from Boretius, Biosensors and Bioelectronics, 2010; Branner, IEEE Transactions on Biomedical Engineering, 2004; Negredo, Neuroscience, 2004.

2.3.2.2 Penetrating Electrodes

In contrast, the Utah Slanted Electrode Array (USEA) with 100+ needle-like electrodes (Figure 1B) penetrates into the nerve and resides within individual fascicles, axon bundles. This design provides direct contact between electrodes and axons and leads has demonstrated enhanced specificity over a large number of channels in acute experiments [39,41,42]. However the insertion causes irreparable physical damage to the nerve, which would have already undergone significant trauma in the case of limb amputation. Additionally, the USEA electrodes suffer from chronic inflammation and the eventual formation of scar tissue and fibrotic encapsulation. Due to these drawbacks, the overall efficacy has been limited to 80% of the electrodes for approximately 5 months in chronic experiments [4].

The Longitudinal Intrafascicular Electrode (LIFE) is another penetrating interface with a wire like electrode that is inserted longitudinally into the nerve along the direction of the axons (Figure 1C). It also has improved stimulating and recording fidelity and specificity due to proximity of electrodes to axons but currently with only a limited number [43,44]. However, while showing a balance between specificity and reliability [45], the insertion still causes damage to the remaining viable portion of the nerve. Perhaps most importantly, by design the LIFE is limited to a small number of electrodes when compared to the FINE or USEA and simply does not scale to the level necessary for functional and viable interfaces for amputees.

2.3.2.3 Regenerative Electrodes

2.3.2.3.1 Sieve Electrode

As shown by these hallmark peripheral nerve interfaces, there exists a large tradeoff between the ability to selectively interface with individual axons versus the amount of disruption to the nerve and long-term stability as a result of trying to get in close proximity to axons.[39] In order to combat the negative outcomes of trying to get in close proximity to axons, a regenerative approach has been explored where amputated nerves are encouraged to regenerate into specific geometries within close proximity to electrodes. While this approach is dependent on a previously cut nerve and therefore limited in application, it is advantageous because it allows close proximity between axons and electrodes without the need to penetrate the nerve. [46–50] However, these approaches have met again with limited success. The Sieve Electrode, the hallmark regenerative interface, is effectively a thin perforated disk that is attached to the nerve perpendicularly so the nerve is forced to regenerate through the device. [51] Some of the perforations in the disk have ring electrodes that contact the axons regenerating through the holes (Figure 1D). [52] Theoretically, each hole could have a ring electrode allowing this device to interface with an extraordinarily large number of axons. Designs such as

the Sieve Electrode demonstrate highly selective stimulation after regeneration but limited recording fidelity. This is in large part due to the challenges of recording the very low amplitude action potentials (APs) from axons and a spatial dependence of the electrodes to the Nodes of Ranvier where the AP is largest [5,6,39,53,54].

2.3.2.3.2 Microchannel Approach

The measurable extracellular potential of action potentials is small due in large part to the extracellular volume surrounding axons and nerves. This volume, mainly water and ions, disperses the extracellular potential of the action potential due to its low impedance nature and the resulting high ionic diffusion/dispersion [6]. This in turn reduces the magnitude of the action potential outside the axonal membrane. The end result is the extremely difficult design requirement that any electrode with the hope of capturing the action potential be placed as physically close to the axon membrane as possible. It is important to note that not only are Sieve electrodes forced to endure this low signal, but all peripheral nerve interfaces to date are forced to endure it. Furthermore, all peripheral nerve interfaces that contact the nerve in a perpendicular manner (Sieve electrodes, Utah electrode arrays, etc.) have the additional design requirement of being spatially dependent on the nodes of Ranvier, breaks in axon insulation where the extracellular potential is largest. These breaks in insulation do occur fairly frequently, on average at least every 2mm [7,55]. However, it is highly impractical to attempt to target them when implanting large numbers of electrodes in a patient because they are on the order of 1 micron in length [55] and not easily located. This is yet another severe limitation and difficult design criteria state-of-the-art peripheral nerve interfacing technologies must cope with.

The present work builds upon these nerve interfacing designs by using microchannel technology, a promising new regenerative approach to peripheral nerve interfacing. In this approach, axons from an amputated nerve regenerate through a large

number of microchannels made of electrically insulating materials. Interfacing with axons within a microchannel offers three distinct advantages. First, by using electrically insulating materials for the microchannels, the axons are effectively isolated from the low impedance extracellular fluid. It has been theorized and simulated through mathematical modeling that limiting the extracellular fluid/volume offers a huge advantage by increasing the extracellular resistance and following from Ohm's Law, the extracellular potential of an axon's AP [6]. Essentially the microchannels provide a method to circumvent the reduction in AP magnitude stemming from the low impedance extracellular volume and provide an interfacing scenario as if the electrodes were placed right next to the axonal membrane.

Second, if microchannels with lengths greater than 2 mm are used, a node of Ranvier will always be contained within the microchannels. This coupled with the fact that microchannels help contain the AP signal and mitigate the reduction in magnitude, allows electrodes within microchannels to be spatially *independent* of the nodes of Ranvier. One need not attempt targeting the placement of electrodes to minimize proximity to the nodes. This unique phenomenon to microchannels has been validated *in vitro* where axons were recorded from inside a microchannel, their spatial position changed by pulling the axons further through the microchannel, and recordings were attempted again. The authors found there was no significant difference in recordings between the different axon and node of Ranvier positions. [56]

Third, if a nerve regenerates through a large number of microchannels, then the axons will be forced into small groups each held within its own microchannel made of electrically insulating materials. This allows specific interfacing capabilities unlike any of the previously developed peripheral nerve interfacing technologies because the small groups of axons are electrically and spatially isolated from each other and can be treated independently. This would allow the recording of signals from one group of axons in one microchannel, while simultaneously stimulating another group of axons in another

microchannel without worrying about cross-talk or interference. The end result is the potential for highly specific and simultaneous regimes of stimulation, conduction blocking, and recording for sensory feedback, pain blocking, and motor signal acquisition. [56]

Within the past half-decade or so, significant work has gone into evaluating the use of microchannel technology for peripheral nerve interfacing in the context of *in vivo* application. Initial work investigated the functionality and capability of nerves to regenerative through microchannels in a transection/non-amputee animal model. It was shown that axon regeneration (myelinated and unmyelinated) is highly susceptible to microchannel dimensions with cross-sections ranging from 3025 – 12100 μm^2 and lengths ranging 1 – 5mm. When regeneration is present within the microchannels, single unit action potentials can be recorded from the axons using electrodes inserted into the microchannels post-regeneration at the time of experimentation/recording [49,57]. While the animal model does not translate to an amputee population and the electrodes used to record the single unit action potentials were not actually implanted, the studies demonstrate the *potential* for chronic nerve-microchannel integration and interfacing.

Other work has focused on non-regenerative implementations of microchannel technology for peripheral nerve interfacing. These include flexible and elastomeric polydimethylsiloxane (PDMS) based microchannel interfaces with microfabricated electrodes. In these cases dorsal roots were dissected into small strands (rootlets), as opposed to being transected, and then *placed* within 'open' microchannels. Dorsal roots are the roots of a nerve passing dorsally to the spinal cord. A capping PDMS layer was finally placed on top of the microchannels to close them during the recording experiment. These microchannel interfaces have been used to record both sensory evoked and bladder responsive single unit action potentials in acute recording experiments with axons from the dissected dorsal rootlets [50,58,59]. While these microchannel interfaces do not have large electrode counts (5 electrodes per device) due to the challenging fabrication

demands of PDMS, it does not appear necessary for application in bladder control with spinal cord injury patients [58]. Furthermore this is an insightful approach to utilizing dorsal rootlets that can be dissected for bladder control. Unfortunately this approach is not easily achieved with nerves innervating limbs due to the increasing degree of dissection that would be required based on significantly larger numbers of axons and nerve roots. Regardless of the clinical application, these studies are yet another example for the viability of microchannel interfacing.

2.4 Conclusion

Building upon the promising work showing the potential of microchannels for peripheral nerve interfacing, it was warranted and the overarching aim of this thesis to investigate chronic regenerative interfacing for amputees and to develop advanced microchannel interfacing technology capable of performing in such chronic interfacing applications. The capability of microchannels and amputated nerves to integrate in a chronically stable manner was first investigated to establish the fundamental requirement that nerves be tolerant towards the foreign implant even after sustaining the massive injury of amputation. Secondly, a large electrode count microchannel based interface was designed, fabrication processes developed applicable to implantable microelectronics such as these, and predominant failure modes investigated for chronic interfacing, specifically recording APs, in the *in vivo* environment.

CHAPTER 3

Evaluating the Chronic Capability of Regenerative Microchannel Interfacing

3.1 Introduction

Prosthetics aim to restore the functional capacity once held by an amputee. A number of neural prostheses have been developed with the goal to artificially substitute or mimic sensorimotor functions in patients. For instance, this goal can be accomplished via an interface with the peripheral nervous system by means of implanted electrodes capable of neuromuscular stimulation and neural signal recording. Stable bi-directional communication could allow for a natural control over advanced prosthetic limbs and other similar assistive devices for amputees.

State of the art peripheral nerve interfacing has centered around three main types of device designs: cuff, penetrating, and regenerative sieve electrodes. Cuff and penetrating interfaces face a large tradeoff between the ability to selectively interface with individual axons versus the amount of disruption to the nerve and long-term stability as a result of trying to get in close proximity to axons [39]. Cuff electrodes, which wrap around the nerve, cause minimal damage and provide long-term stability at the expense of stimulation/recording specificity due to a lack of direct contact with individual axons [2,3,6,39]. In contrast the Utah Slanted Electrode Array (USEA) penetrates the nerve and provides enhanced specificity through direct contact between the electrodes and axons. However, the insertion causes injury and the electrodes elicit chronic inflammation and scar tissue [4]. An alternative to combat these negative outcomes is a regenerative approach, where transected axons grow into specific geometries within close proximity of electrodes [5]. The hallmark Sieve Electrode is implanted so axons are forced to regenerate through its many perforations/holes making contact with ring electrodes [52].

However, this design has few viable electrodes because the extracellular potential of an axon's action potential (AP) is small. Furthermore, there is a spatial dependence of the electrodes to the nodes of Ranvier, which occur at least every 2 mm and are where the extracellular potential is largest [7,39,53,56].

Microchannels offer a unique opportunity to take advantage of the regenerative approach while circumventing issues with small APs and the node of Ranvier dependence, as detailed elsewhere [6,49,50,56,59]. Briefly, if a nerve regenerates through electrically insulating microchannels, small groups of axons can be isolated from each other and the surrounding low impedance extracellular fluid. Limiting the extracellular volume increases the extracellular resistance and from Ohm's law, increases the extracellular potential of an axon's AP [6]. Using microchannels with a length of 3 mm ensures a node of Ranvier will always be contained within the microchannels making them spatially independent of the nodes. Such conditions have been validated *in vitro*. APs from axons were recorded from inside a microchannel, the spatial position of the axons changed, and recordings taken again without any significant difference in AP signal amplitude [56].

However, the underlying success of a regenerative microchannel interface as a dependable solution for neural interfacing is not only its ability to detect high quality APs, but also a function of long term tolerance by the peripheral nervous system. Thus, the neural implant is inherently dependent on the chronic condition of the matured nerve post-regeneration. To prevent neuropathic complications post-implantation, the device must facilitate sufficient room for nerve maturation over time while in close contact with as many axons as possible to obtain clear neural signals. The device must also facilitate healthy nerve characteristics such as a maintained tissue architecture, established myelinated fibers, and prominent axon profiles through the regeneration and maturation phases [11,52,60]. Lacking such nerve characteristics has proven to yield poor nerve functionality, compressive axonopathy, and neuromas which result in poor translation of

neural signal and loss of nerve utility [11,52,61–64]. The tendency of regenerating injured nerves to form neuromas is also a major clinical concern for amputees due to associated chronic pain as well as a major concern for specificity during neural interfacing due to characteristic random AP firing [65–69]. Neuromas not only negatively impact performance but also the tolerance of an implant by the host's PNS by creating a hostile environment not conducive to typical axon regeneration and maturation. They are abnormal in their physiological characteristics as manifested by a marked degeneration and absence of myelination and axons, myelin debris, a decrease in Schwann cell population, loss of nerve organization/structure and oriented axon growth, loose basal lamina structure surrounding axons, edema and swelling, and the overall decline of axonal health in a regenerating nerve [62,63,66–68,70]. If a regenerative microchannel interface is unable to support the maturation and chronic retention of healthy axons, then even if it can record action potentials, it still fails from a biological perspective due to these neuropathic complications.

Our long term goal is to establish a large-electrode count microchannel interface for bi-directional communication within an amputated nerve. The basic design of the microchannel architecture is inspired by work from Dr. Fawcett and Dr. Lacour while at the University of Cambridge, and is shown in Figure 2. The interface utilizes top and bottom polydimethylsiloxane (PDMS) layers with SU-8 walls forming series of adjacent microchannels. Prior to implantation, the array of microchannels is rolled onto itself forming the device filled with microchannel conduits, mimicking the general cross-sectional architecture of a nerve. The device is implanted so that the transected axons can regenerate through the microchannels and over the electrodes housed in the bottom PDMS layer for interfacing.

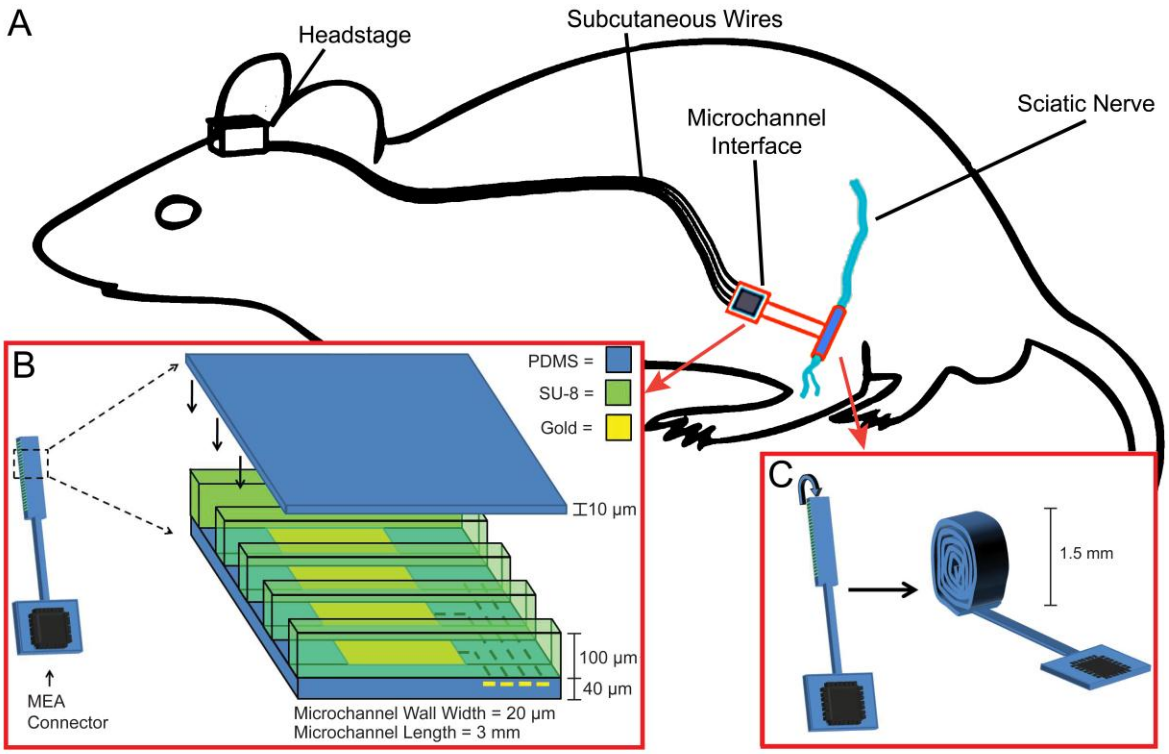

Figure 2. Microchannel interface schematic.
(A) Overview of the rat amputee model depicting the site of implantation, tracing of subcutaneous wires, and percutaneous headstage for neural interfacing. (B) Schematic of microchannel architecture detailing materials, dimensions, and possible layout of incorporated gold electrodes. (C) Depiction of final microchannel scaffold after rolling for implantation.

Here, we focus on the response of the regenerating nerve to an artificially imposed microchannel obstacle and separately the ability to obtain neural signals from these microchannels that are meaningful for the eventual goal of neural interfacing. We first validate cytocompatibility of the scaffolding materials through *in vitro* experimentation. We then explore the capability of axons in an amputated nerve that lacks distal reinnervation targets to regenerate through the device and mature in a PDMS and SU-8 based microchannel scaffolding. Furthermore, we characterize the regenerated nerve from a morphological perspective once the axons have grown out of the microchannel scaffolding and attempt to assess whether neuroma formation is a major concern by evaluating the characteristics described previously common to neuromas.

Specifically we consider the presence or lack of organization within the nerve and oriented axon regeneration, Schwann cells and myelin deposition on axons, tight basal lamina structures around axons/Schwann cell units, and edema/swelling. Finally, we evaluate the ability to record single and multi-unit action potentials through microchannels permanently integrated with microwire electrodes in a terminal study after chronic implantation in the rat sciatic nerve. The chronic terminal electrophysiology experiment allows the testing of interfacing capabilities without needing to invest in the development of advanced wiring and packaging technologies for chronic continuous behavioral studies.

3.2 Materials and Methods

3.2.1 Regenerative microchannel scaffold fabrication

To fabricate the regenerative microchannel scaffolds, a 40 μm PDMS (1:10 weight ratio Sylgard 184, Dow Corning) base layer was first spun on glass coated in titanium (10Å) and gold (50 Å) for anti-adhesion. The PDMS base layer was then briefly treated with oxygen plasma to increase the adhesion between PDMS and SU-8. A 100 μm layer of SU-8 (SU-8 2100, MicroChem Corp) was then spun on top of the PDMS. The SU-8 was cured, exposed using an experimentally determined exposure dose of 520 mJ/cm^2, and developed forming the patterned microchannel walls on the PDMS base layer. The width and length of the microchannel walls were 20 μm and 10 mm, respectively. The width of the microchannels ranged from 50, 100, or 150 μm. The dimensions and spacing between the microchannel walls were controlled by the photolithography mask used for each microchannel type. The basic fabrication process of these steps is depicted in Figure 3. Detailed methods for the fabrication of these steps can be found in literature [71].

Adding the top PDMS layer involved first spinning polyacrylic acid, a water resorbable layer, on another glass slide and drying it on a hotplate at 60°C for five min.

This was done twice. A 10 µm layer of PDMS was immediately spun on the polyacrylic acid (PAA) layers and partially cured on a hotplate at 65°C for 4 min. During this time, the bottom PDMS layer with the SU-8 microchannel walls was treated with oxygen plasma to increase the adhesion between the two layers. The two glass slides were placed together with weight on top and baked on a hotplate at 60°C for 30 min and then 90°C for 1 hr to ensure that the top PDMS layer was fully cured. Finally, the glass slide sandwich was soaked in water until the PAA dissolved and allowed for easy removal of the top glass slide. The basic process is depicted in Figure 3. Once the layer of microchannels was removed from the glass slide, they were rolled perpendicularly to the direction of the microchannels and cut to 3 mm forming microchannel scaffolds with a cylindrical shape resembling that of the rat sciatic nerve. Each microchannel scaffold type was designed to contain a different number of microchannels based on the microchannel cross-sectional area. This was necessary in order to maintain a uniform rolled scaffold cross-section of approximately 1.5 mm across all three types of microchannel scaffolds. The 150 µm x 100 µm microchannel scaffolds contained 59 microchannels, the 100 µm x 100 µm microchannel scaffolds contained 84 microchannels, and the 50 µm x 100 µm microchannel scaffolds contained 143 microchannels.

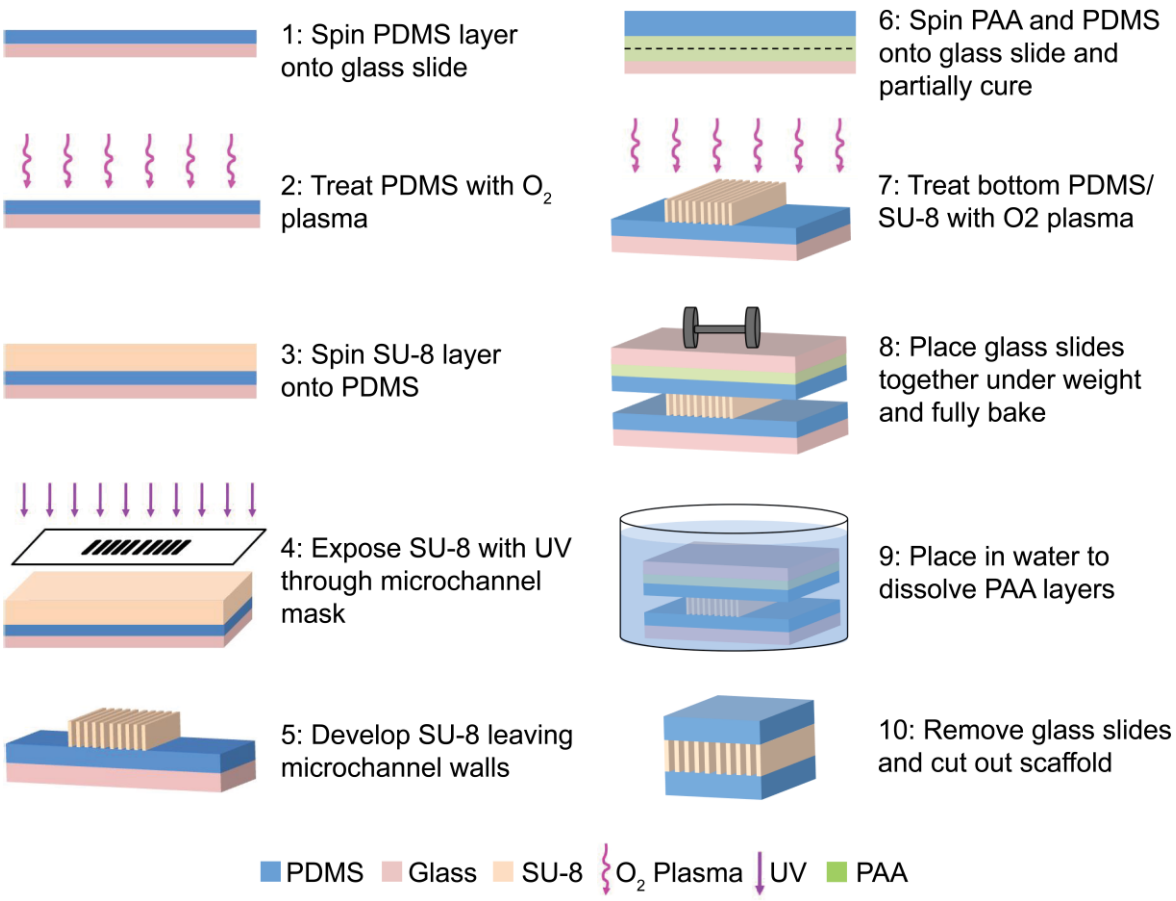

Figure 3. Microchannel scaffold fabrication.
Overview of all major fabrication processes for the regenerative microchannel scaffolds along with schematics depicting the device in each step. 'Open' microchannels from step 5 were used in *in vitro* studies. *In vivo* studies used microchannels from step 10. Drawings are not to scale.

3.2.2 Regenerative microchannel interface fabrication

The ends of eight insulated microwires (Stainless Steel 304, California Fine Wire Company) 60 µm in diameter and 10 cm in length were fed midway into eight random microchannels within the regenerative microchannel scaffold. 0.5 mm of each microwire at the end in the microchannel was de-insulated, forming the microchannel recording electrodes. The microchannel electrodes were inserted at the distal end of the regenerative microchannel scaffolds to minimally obstruct regeneration from the proximal side. Two coupled microwires were placed outside the scaffold running parallel

to the microchannels with de-insulated electrodes at both ends positioned to record from each end of the 3mm device forming a tripolar reference. This reference was held in place using standard silicone tubing placed around the reference and microchannel interface. This silicone tubing also served as a cuff to suture the proximal and distal transected nerves stumps into place during implantation. A second microwire reference was deinsulated by 0.5 mm and adhered to the outer wall of the silicone tubing using silicone adhesive (3140, Dow Corning®) forming a bipolar reference. This allowed the option of choosing either reference during electrophysiology experimentation.

3.2.3 *In vitro* cytocompatibility

Unrolled regenerative microchannel scaffolds lacking the PDMS cover layer were used for the *in vitro* experiments. Once fabricated, the 'open' regenerative microchannel scaffolds were placed at the bottom of tissue culture wells. Importantly, no protein coatings of any kind, such as laminin, were used. Lumbar dorsal root ganglia (DRGs) were explanted from P1 rat pups. The nerve roots were removed and the DRGs were placed on the open scaffolds at the entrance to the microchannels. For the first several hours, the DRGs were incubated with only a thin layer of DMEM/F12 media with 10% fetal bovine serum and 50 ng/mL nerve growth factor (NGF) (Roche). Subsequently, the wells were fully covered with the same media. The media, including NGF, were replaced every two days for a total of seven days. After seven days, the cultures of DRGs were fixed with 4% paraformaldehyde in PBS for 20 min and washed three times with 1X PBS. To visualize neurite outgrowth and non-neuronal cell migration, axons and Schwann cells of the DRGs were reacted overnight at 4°C with antibodies to the 160kDa neurofilament protein (NF160, 1:500, mouse IgG1, Sigma) and S-100 (1:250, rabbit IgG S100, Dako), respectively, followed by secondary antibodies: goat anti-mouse IgG1 Alexa 594 (1:220, Invitrogen) and goat anti-rabbit IgG Alexa 488 (1:220, Invitrogen). Cell nuclei in the DRG cultures were marked by incubation in DAPI (Invitrogen) in PBS

at a concentration of 10 µM for 15 min at room temperature. The fluorescently labeled cells and nuclei were visualized using a Zeiss upright microscope and the images were captured with an Olympus digital camera.

3.2.4 Microchannel scaffold implantation, explantation, and immunohistochemical preparation

A total of 18 regenerative microchannel scaffolds were implanted in the rat sciatic nerve amputee animal model, with an n=6 for each of the three microchannel widths studied. In isoflurane anesthetized rats, the sciatic nerve was transected at the mid-thigh and the regenerative microchannel scaffold was sutured to the proximal and distal segments of the cut nerve. The nerve was then transected again, this time two mm distal to the distal end of the device and a large portion (approximately 1cm) of the nerve distal to this second transection site was excised. The goal of this procedure is to leave a two mm 'distal nerve stump' attached to the distal end of the device so that regenerating axons may grow through the device in response to cues from the distal segment. By excising a segment of the nerve distal to this stump, we sought to prevent any regenerating axons from reinnervating their original targets. The net result is a sciatic nerve amputee model which forms a more stringent test for regenerative peripheral nerve interfaces than a conventional sciatic nerve transection and repair model.

After eight weeks, the regenerative microchannel scaffolds were explanted for histological analysis for axonal regeneration and nerve characterization. Explants were post fixed in 4% paraformaldehyde in PBS (Sigma-Aldrich) for 48 hours at 4°C and cryoprotected in 30% w/v sucrose in PBS for 72 hours at 4°C. Samples were then embedded in O.C.T compound (Tissue Tek) and stored at -80°C. A 1.5 mm segment of nerve tissue distal to the microchannel scaffolds was sectioned in a transverse plane at 16 µm thickness with a cryostat (CM30505, Leica). Cross sections of the microchannel scaffolds with regenerated nervous tissue were made at 100 µm. These thicker sections

were used to reduce mechanical stress and uncoiling which results from thinner sectioning. Sections mounted on slides were stored at -20°C until staining.

3.2.5 Immunohistochemical analysis of microchannel scaffolds

Prior to staining, slides were brought to room temperature and excess O.C.T. surrounding the samples was removed with a razor blade. Next, an encompassing square section of precision mesh netting (McMaster-Carr) was applied over the whole cross section to prevent uncoiling of the microchannels during subsequent washes. The mesh netting was secured by applying a finite drop of cyanoacrylate glue at each corner onto the glass slide. Additional care was taken during subsequent reagent pipetting under a stereomicroscope to eliminate any air bubbles trapped in the mesh netting and to prevent uncoiling due to mechanical stress from excessive fluid flow. Microchannel slides were washed in PBS and then incubated in blocking solution for one and a half hours at room temperature. Blocking solution was prepared using a 1:25 dilution of goat serum (Gibco) with 0.5% Triton X-100 prepared in PBS. After incubation in blocking solution, the samples were washed with a wash solution made of 0.5% Triton X-100 in PBS. The samples were incubated in primary antibody solutions (see above) for 24 hr at 4° C. Primary markers selected to stain for axons (NF160), Schwann cells (S100), and fibroblasts (1:500, mouse vimentin, Sigma–Aldrich) were prepared in blocking solution. The following day, the samples were again washed with wash solution and then incubated for 2 hr in secondary antibodies at room temperature. Secondary antibodies used were goat anti-rabbit IgG Alexa 488 and goat anti-mouse IgG1 Alexa 594 and prepared with wash solution. Lastly, the samples were incubated with DAPI (see above), washed with PBS, and cover slipped using fluoromount-G (SouthernBiotech). It should be noted that the goal of the immunohistochemistry method used was to stain the superficial portion of the 100 µm thick tissue samples and not the entire tissue thickness as doing so was unnecessary for the analyses performed. Tile scan images of the samples

were taken approximately 20 µm into the sample at 20x, 40x, and 100x magnification with a confocal microscope (LSM 510, Carl Zeiss) and stitched using Zen 2009 software (Carl Zeiss).

3.2.6 Immunohistochemical analysis of nerve tissue distal to the microchannel scaffolds

Glass slides with the 16 µm thick sections of nerve tissue distal to the microchannel scaffolds were brought to room temperature and rinsed three times with PBS to remove excess O.C.T. gel. Next, the samples were incubated in goat serum blocking solution for 1 hr at room temperature, as described earlier. After blocking solution incubation, the samples were washed three times with wash solution and incubated overnight at 4°C with primary antibodies. Primary markers were selected to stain for axons (NF160), Schwann cells (S100), fibroblasts (vimentin), and myelin (1:100, chicken IgY P0, Chemicon Intl.) each prepared in blocking solution. The following day, the samples were washed three times with wash solution and incubated for 1 hr in secondary antibodies at room temperature. Secondary antibodies used were goat anti-rabbit IgG Alexa 488, goat anti-mouse IgG1 Alexa 594, and goat anti-chicken IgG1 Alexa 488 (1:220, Invitrogen); all were prepared with wash solution. After secondary antibody incubations, the samples were again rinsed with wash solution three times and then incubated with DAPI, washed, and cover slipped as described above. Samples were imaged at 20x and 40x magnification with an inverted microscope (Axiovert 200, Carl Zeiss). Tile scan images were taken at 20x, 40x, and 100x with a confocal microscope (LSM 510, Carl Zeiss).

3.2.7 Microchannel interface implantation and electrophysiology

A total of five regenerative microchannel interfaces were implanted in the rat sciatic nerve. In isoflurane anesthetized rats, the sciatic nerve was transected at the mid-thigh and the regenerative microchannel interface was sutured to the proximal and distal

segments of the cut nerve. The microwires ends were led out through the musculature to lie subcutaneously in the local region. After 20 weeks (approximately five months) the rats were re-anesthetized lightly using isoflurane for induction followed by a ketamine/xylazine injection (i.p., 0.75 ml/kg). Booster shots of ketamine/xylazine (i.p., 0.25 ml/kg) were given as needed. The subcutaneous ends of the microwires were exposed and connected to a Cerebus Neural Signal Processing System (Blackrock Microsystems, USA) for signal acquisition. An 18 gauge needle was placed subcutaneously along the back of the rat serving as a distant low impedance reference.

Once the microwires were connected to the Cerebus System, spontaneous action potentials were recorded through the microchannel interface. Next, attempts were made to evoke sensory single unit action potentials using a variety of natural stimuli. These included brushing of the leg distal to the implant, foot pad and toe region, pinching of the foot pad and toe region, ankle flexion/extension, and brushing of hair follicles distal to the implant. To control for movement related artifacts, identical sensory stimuli were delivered to the contra-lateral limb.

Lastly, the sciatic nerve was exposed near the sciatic notch using the same approach as the implantation surgery. A DS8000 stimulator (World Precision Instruments Inc, USA) was used to stimulate the sciatic nerve with 100 µsec, symmetric, charged balanced, bipolar, square wave voltage pulses at 0.33 Hz through a pair of stainless steel hook electrodes with 1.5 mm electrode spacing. A stimulus ramp of pulse amplitudes ranging from zero volts to 1 V at 0.01 V increments was used to evoke a range of neural responses, from a few action potentials to a general compound action potential. These were recorded through the microchannel interface.

All recorded signals were sampled at 30 KHz (33 µsec/sample) and first filtered in hardware using a 1st order high-pass Butterworth at 0.3 Hz and a 3rd order low-pass Butterworth at 7.5 KHz. Additional filtering was performed in software using a 4th order high-pass Butterworth at 250 Hz. Single unit action potentials were isolated online using

conventional window discrimination spike sorting techniques based on spike amplitude and duration, and offline using an automated expectation-maximization algorithm though the Plexon Offline Sorter™ software package (Plexon, USA). Signal-to-noise ratios of isolated units were calculated by taking the average peak-to-peak amplitude of the unit and dividing it by 3 times the standard deviation of noise in that specific electrode.

3.2.8 Data analysis

Images from 100 µm thick histological sections through the scaffolding samples were used to analyze the number of microchannels containing axons, and number of axons and area of tissue occupied in each microchannel. The number of microchannels containing regenerated axons and the numbers of axons per microchannel across the three types of scaffolds were counted manually using ImageJ software. To evaluate the average amount of microchannels containing axons, for example in the 100 µm x 100 µm microchannel scaffolds, the percent of microchannels containing axons for each of the six 100 µm x 100 µm microchannel scaffolds scaffold were averaged together.

To evaluate the numbers of regenerating axons in each of the 100 µm x 100 µm microchannel scaffolds, up to 100 axon profiles per microchannel were counted. Using this data, the microchannels in each scaffold were categorized using arbitrary bins set at 0-10 axons, 11-100 axons, and 100+ axons. The percent of microchannels falling in these bins for the six 100 µm x 100 µm microchannel scaffolds are reported.

To evaluate the average free space in each microchannel within the 100 µm x 100 µm microchannel scaffolds, the tissue cross-sectional area in each microchannel was identified using the fibroblast stain as a proxy for the regenerated tissue cable. The area of positive staining for fibroblasts was measured and compared to the total microchannel cross-sectional area using ImageJ. These values were used to determine the percent area of a given microchannel filled with regenerated tissue. Similar to the axon counting analysis, data from the area analysis was used to categorize the microchannels of each

scaffold into arbitrary bins of 0-25%, 25-50%, 50-75%, 75-100% microchannel area filled with tissue. The percent of microchannels falling in these bins for the six 100 µm x 100 µm microchannel scaffolds are reported.

Microchannels not structurally intact due to damage from sectioning and the associated tissue located within were not included in any analysis. Data from axon counts and tissue cross-sectional areas were analyzed using one-way ANOVA followed by a Tukey's least significant difference post-hoc test, where appropriate, to determine significant differences with at least 95% confidence.

3.3 Results

3.3.1 Regenerative microchannel scaffold

An image of the fabricated regenerative microchannel scaffold prior to the bonding of the PDMS cover layer (step 5 in Figure 3) is shown in Figure 4A. In this image a reflection of the SU-8 channel walls can be seen on the PDMS base layer. The SU-8 channel walls were successfully patterned using photolithography on the PDMS base layer and the SU-8 was capable of forming 20 µm by 100 µm channel walls. These 'open' microchannel scaffolds lacking the PDMS cover layer were used for all *in vitro* studies.

Application of the PDMS cover layer resulted in adherence to the top of the SU-8 microchannel walls forming arrays of closed microchannels (Figure 4B). The PDMS cover layer is the thin line at the top of the microchannel walls. The arrays of microchannels were rolled perpendicular to the SU-8 walls forming the final regenerative microchannel scaffold for *in vivo* studies (Figure 4C and Figure 4D). The overall diameter of the scaffold was slightly larger than 1.5 mm. In these images, the SU-8 appears slightly gold and the PDMS appears grey or light blue. The microchannels are clearly visible. The dotted red line in Figure 4D shows the separation between two layers of microchannels where the PDMS cover layer of the inner microchannel roll is in

contact with the PDMS base layer of the outer microchannel roll. As a consequence of the rolling procedure, an unavoidable small open core was present in the center of the scaffolds (Figure 4C).

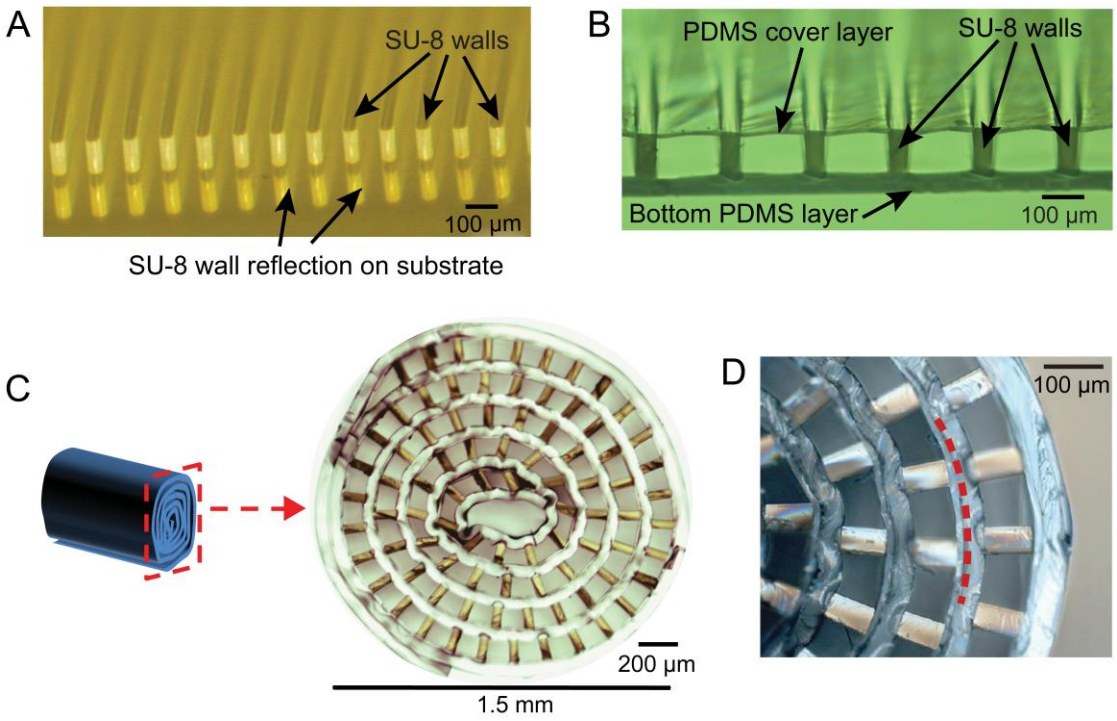

Figure 4. Microchannel scaffold images.
(A) Image of 'open' microchannels corresponding to step 5 in Figure 3. (B) Image of microchannels with the PDMS cover layer adhered to the SU-8 walls corresponding to step 10 in Figure 3. (C) Cross-sectional view of 100 µm x 100 µm microchannel scaffold rolled for implantation. (D) Close up of rolled microchannel scaffold showing neighboring microchannel layers delineated by a red line.

Overall, three distinct types of microchannel scaffolds were fabricated where each had microchannel widths of either 50 µm, 100 µm, or 150 µm for chronic *in-vivo* studies. All microchannels had heights of 100 µm and lengths of 3 mm. It was observed however, that rolling the microchannel arrays to form the scaffolds resulted in slight inconsistencies in microchannel dimensions within a scaffold. Microchannels near the interior of the scaffolds tended to be wider than the peripheral microchannels. So, while

each microchannel scaffold started with microchannel widths of 50 µm, 100 µm, or 150 µm, the rolling process created a range of widths within any given scaffold. A cross-sectional area comparison of the inner two rings of microchannels to the outer most ring of microchannels showed that this range was most apparent in the 50 µm x 100 µm microchannel scaffolds which had approximately an average 25% increase in microchannel cross-sectional area due to rolling. In contrast the 100 µm x 100 µm microchannel scaffolds and 150 µm x 100 µm microchannel scaffolds had a small increase of approximately 2.5% and 7.5%, respectively. In the end, this diversity of width provides an ability to study the effect of microchannel size in greater detail.

3.3.2 *In vitro* cytocompatibility studies

The cultured DRGs adhered well to the 'open' microchannel scaffolds. A representative DRG cultured on a scaffold with 50 µm microchannel widths stained for axons (red) and Schwann cells (green) is shown in Figure 5. The microchannels are visible as dark horizontal lines separated by the faintly auto-fluorescent SU-8 microchannel walls. Immunoreactivity to axons (NF-160, red) and Schwann cells (S100, green) is shown in the main image of the figure, while the subset images show immunoreactivity to either axons (NF-160, red) or Schwann cells (S100, green). As seen from the main image, both axons and Schwann cells grew and proliferated in a robust manner out to 4 mm in length in some cases. Both axon extension and Schwann cell migration were aligned and oriented in the direction of the microchannels (Figure 5A, B). Neurite extension and Schwann cell migration from the explanted DRGs often appeared to be preferential towards the microchannels (Figure 5C). While difficult to quantify, it was observed that more axon extension and Schwann cell growth occurred along the edges of the microchannels, on the SU-8 channel walls, as opposed to on the PDMS.

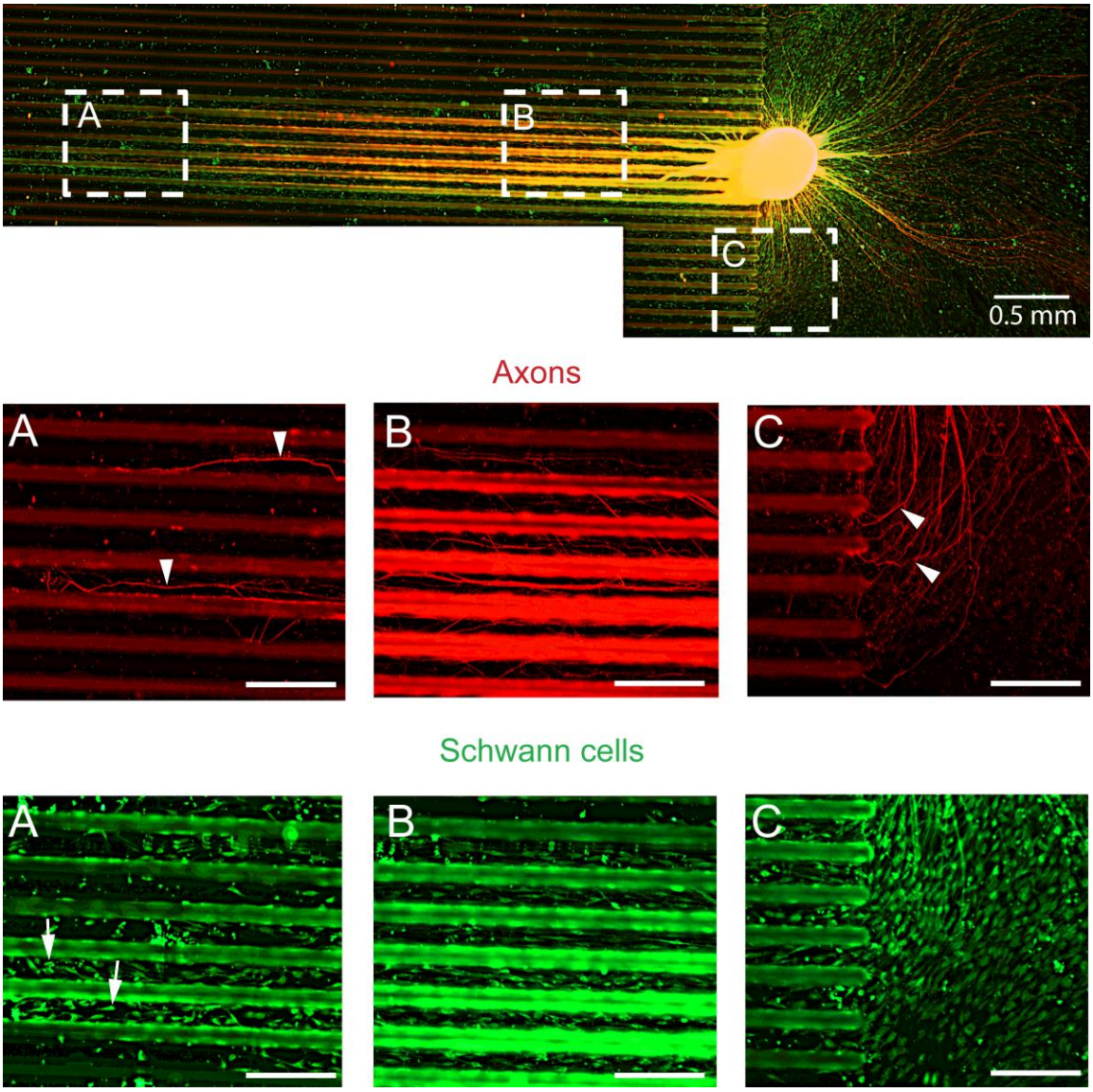

Figure 5. DRG in vitro cytocompatibility.
(Main image) DRG *in vitro* culture with axon processes and migrating Schwann cells on 'open' 50 µm wide microchannels. (A) and (B) Axons and Schwann cells were aligned and oriented in the microchannels and grew/migrated out to 4mm in some cases. (C) Growth and migration of axons and Schwann cells re-orienting towards the microchannels. Axons (red); Schwann cells (green); DRG and regions of axon/Schwann cell co-localization appear orange/yellow; Microchannels are visible as dark horizontal regions separated by auto-fluorescent SU-8 microchannel walls; Arrowheads indicate axons; Arrows indicate Schwann cells; Scale bar = 200 µm unless otherwise noted.

3.3.3 *In vivo* axon regeneration and dependence on channel cross-sectional area

Microchannel scaffolds with three different microchannel cross-sectional areas, 50 µm x 100 µm, 100 µm x 100 µm or 150 µm x 100 µm, were implanted for eight weeks to characterize the impact cross-sectional area has on nerve regeneration in a nerve amputee model. As mentioned previously the 50 µm x 100 µm, 100 µm x 100 µm, and 150 µm x 100 µm microchannel scaffolds contained 143, 84, and 59 microchannels, respectively. Among the three channel dimensions, axon regeneration inside the 50 µm x 100 µm microchannels was significantly less than that through the 100 µm x 100 µm or 150 µm x 100 µm microchannels. Representative microchannel cross-sections of all three scaffold dimensions are shown in Figure 6A. The microchannels in all three scaffold dimensions containing regenerated axons were analyzed. Fewer than half (50%) of the microchannels in the 50 µm x 100 µm microchannel scaffolds were populated with axons. On the other hand, a majority (greater than 95%) of the microchannels in both the 100 µm x 100 µm microchannel scaffolds and 150 µm x 100 µm microchannel scaffolds were populated with axons (Figure 6B). In both the 100 µm x 100 µm and 150 µm x 100 µm microchannel scaffolds, axon regeneration within the open central core of the scaffolds was observed. These axon numbers were not quantified or included in the analysis.

Further analysis focused on the 100 µm x 100 µm microchannel scaffolds. A representative cross-section of a scaffold with discernible individual axon profiles is shown at higher magnification in Figure 6C. Axon profiles per microchannel were counted up to 100 and the results are graphically depicted in Figure 6D using arbitrary bins set at 100+ axons, 11-100 axons, and 0-10 axons. On average, approximately 30% of all analyzed microchannels contained more than 100 axons, 40% microchannels contained 11 – 100 axons, and 30% of the microchannels contained fewer than 10 axons. There was no observable dependence or variation of axon regeneration to the slight

changes in microchannel cross-sectional area due to rolling or on spatial location of the microchannel within the scaffold.

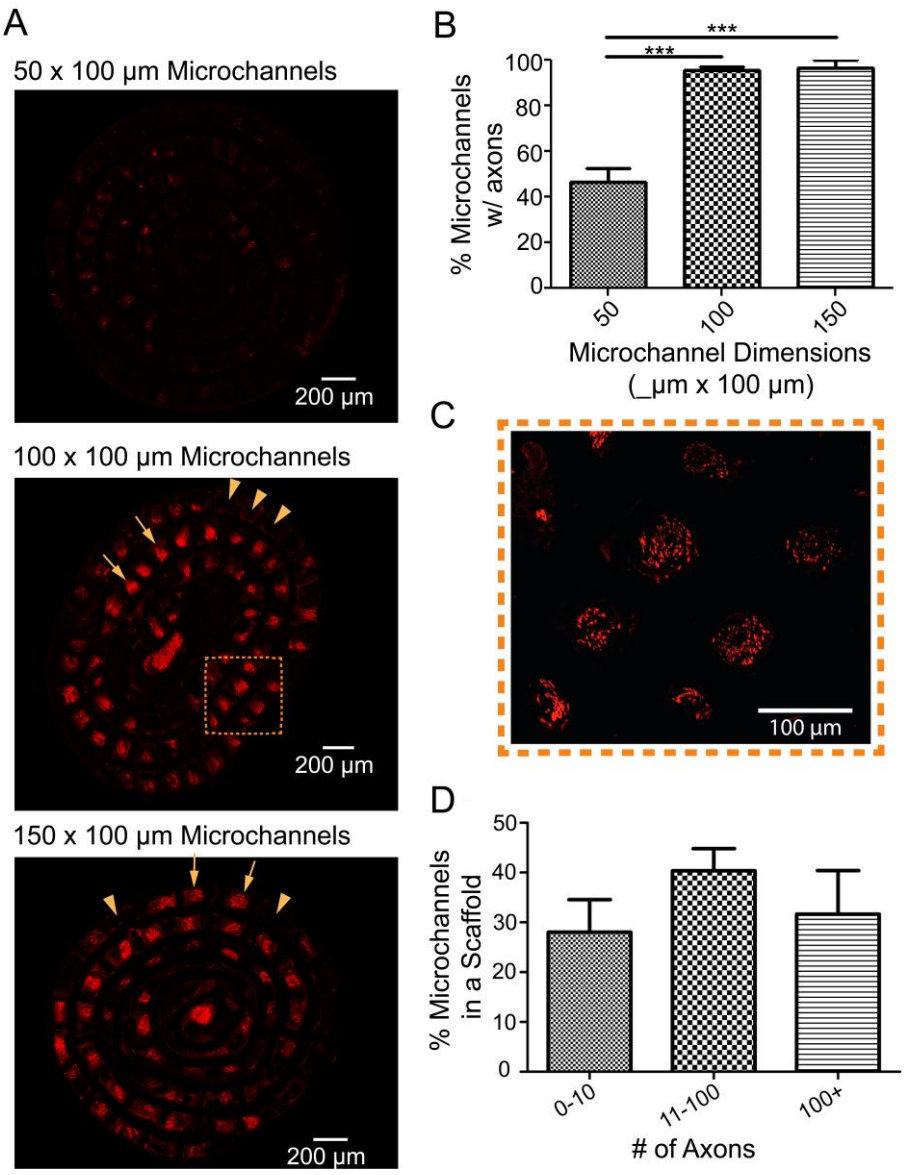

Figure 6. Axon regeneration.
(A) Representative cross-sectional comparison of axon (red) profiles through the scaffolding among the three different microchannel dimensions: 50 µm x 100 µm; 100 µm x 100 µm; 150 µm x 100 µm, respectively. Cross-sections were taken at the midpoint of each scaffold. Arrows indicate microchannels containing axons. Arrowheads indicate microchannels lacking axons. (B) Quantitative analysis on the percent of microchannels in a scaffold containing regenerated axons for each microchannel dimension. (C) Close up of 100 µm x 100 µm scaffold cross-section depicting single axons profiles within microchannels. (D) Quantitative analysis on the percent of microchannels within the 100 µm x 100 µm microchannel scaffolds containing axon populations of 0-10, 11-100, or 100+ axons. (Mean ± S.E.M., ***$p < 0.001$)

3.3.4 Space for future axon maturation

Analyses were performed to evaluate free space in the microchannels available for axon maturation over time. Accordingly, the area occupied by the regenerated tissue cable was compared to the area of the microchannels in the 100 µm x 100 µm microchannel scaffolding samples. Staining for fibroblasts was used to calculate the area of the regenerated cable (**Figure 7**A). A close up of the cross-section along with delineations of the tissue and microchannel area are shown in **Figure 7**B. Approximately 95% of all microchannels containing tissue in the 100x100 μm^2 microchannel scaffolds were observed to have at least 25% free cross-sectional area remaining (**Figure 7**C).

3.3.5 Distal nerve morphological analysis

The response of the nerve to induced guidance from the microchannel architecture was characterized using immunofluorescence for fibroblasts and basal lamina. In cross sections of the nerve tissue distal to the microchannel scaffold there was evidence of reorganization into 'microchannel fascicles', similar to typical nerve fascicles. These microchannel fascicles were characterized by defined perineurial-like sheaths of fibroblasts hosting aggregates of regenerating axons and Schwann cells (Figure 8C) and supportive extracellular matrix (Figure 8D). Additionally, an epineurial-like layer successfully reformed around the whole regenerating nerve characterized by concentric fibroblast organization (Figure 8C). The aggregates of axons and Schwann cells corresponding to the microchannel architecture were observed up to ~1 mm distal to the implant (Figure 8A). This distance coincided approximately with the end of the distal attached nerve segment. As expected, during nerve regeneration, sprouting of axons was visually observed as indicated by the evident increase of axon profiles progressively distal to the scaffolding (Figure 8A). Additionally, overall nerve regeneration was observed to be unidirectional and organized (Figure 8A). There were no signs of aberrant,

unorganized axon regeneration and/or bulbous nerve swelling distal to the microchannel scaffold.

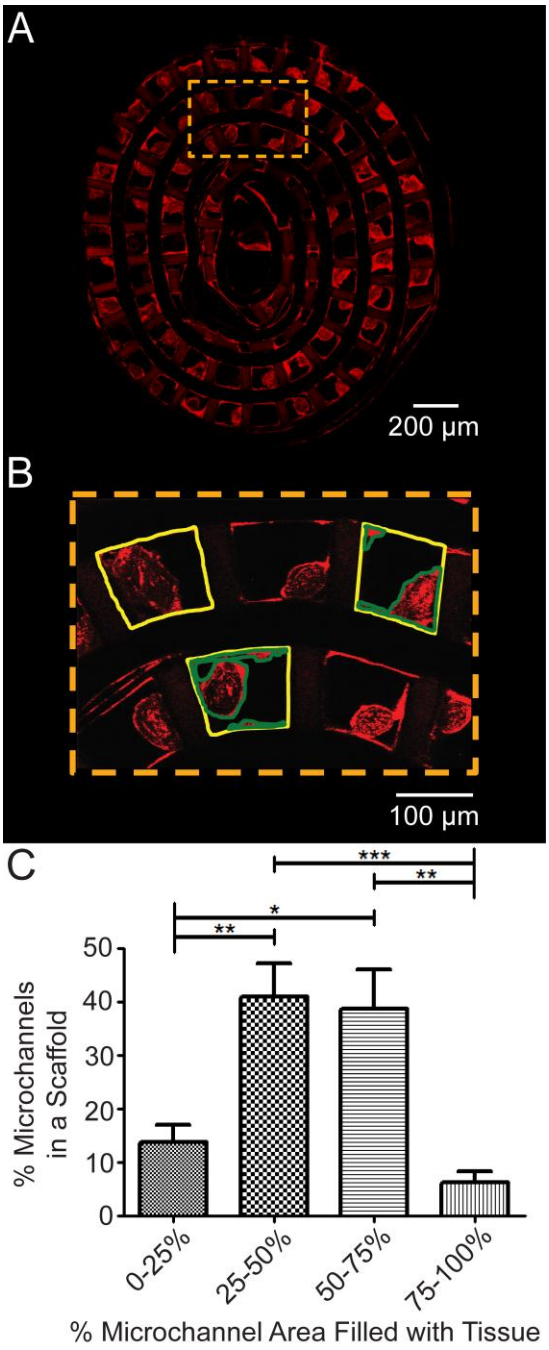

Figure 7. Characterization of area of regenerated tissue cable.
(A) Representative cross section of 100 µm x 100 µm microchannel scaffold stained for fibroblasts (red). Cross-sections were taken near the midpoint of the scaffold. (B) Close up of microchannels with delineations of microchannel area (yellow) and positive fibroblast staining used as a proxy for tissue cross-sectional area (green). (C) Quantitative analysis on the percent of microchannels within the 100 µm x 100 µm microchannel scaffolds with 0-25%, 25-50%, 50-75%, and 75-100% area filled with tissue. (Mean ± S.E.M.,*$p < 0.05$, **$p < 0.01$, ***$p < 0.001$)

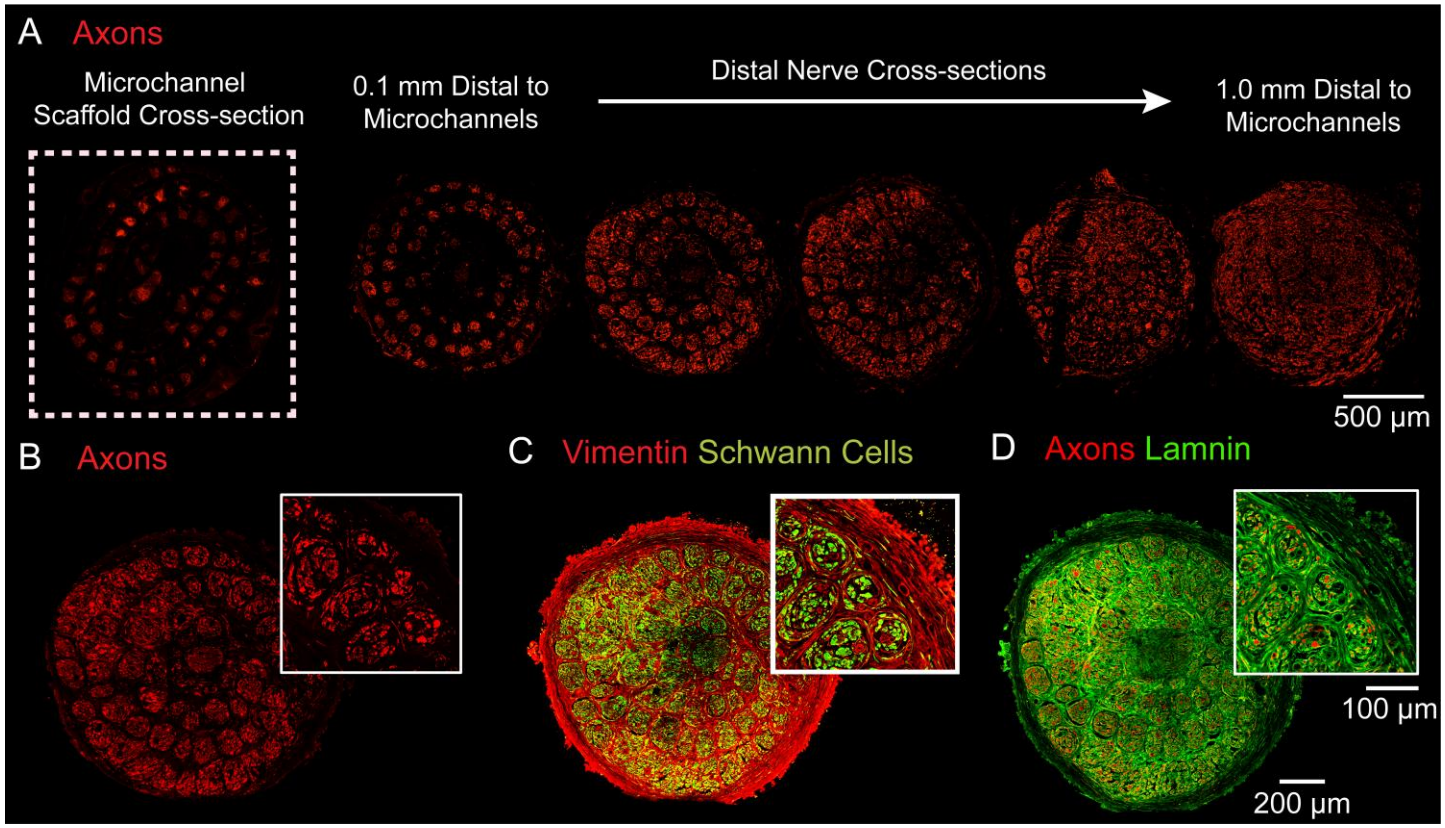

Figure 8. Distal nerve morphology.
(A) Distal nerve cross-sections stained for axons (red) at increasing distances away from the scaffold (left image is the scaffold mid-section for reference). (B-D) Nerve cross-sections distal to the scaffolding. (B) Close up of distal nerve cross-section stained for axons (red) showing aggregates of axons. (C) Distal nerve cross-section stained for fibroblasts (red) and Schwann cells (green/yellow) showing perineurial like structures. (D) Distal nerve cross-section stained for laminin (green) and axons (red) showing basal lamina and connective tissue.

3.3.6 Distal axon regeneration analysis

At a closer inspection of the extracellular matrix, evident reformation of the basal lamina and endoneurial tubes was observed tightly surrounding all the axons and accompanying Schwann cells within the distal segments of the nerve (Figure 9A). Immunofluorescence for Schwann cells identified the abundant presence of Schwann cells within the microchannel fascicles (Figure 9B) accompanying the regenerated axons. Further immunofluorescence showed at least a portion of the Schwann cells were of the myelinating phenotype and had re-deposited myelin on axons providing insulation for normal nerve conduction (Figure 9C). In general, the nerve cross-section contained a uniform distribution of tissue without large edema like voids that lack both cells and extracellular matrix within the nerve.

3.3.7 Regenerative microchannel interface

The microchannel interfaces utilized 60 μm diameter microwires as the recording electrodes. Due to the size of the microwires and based on the results from axon regeneration into the 100 μm x 100 μm microchannel scaffolds, the 150 μm x 100 μm microchannel scaffolds were chosen for interfacing. This ensured the space within the microchannels containing a microwire was close to, but not less than 100 μm x 100 μm. The recording electrodes were positioned in the middle of the microchannels and were 0.5 mm long. A proximal, distal, and side view of a representative microchannel interface is shown in Figure 10A, B, and C, respectively.

3.3.8 Spontaneous and Sensory Evoked Single Unit Action Potential Recordings

Spontaneous and/or sensory evoked single unit action potentials could be recorded from all microchannel interfaces after five months of implantation. Out of the 40 electrodes from the 5 devices, 9 were non-functional due to broken microwire leads leaving 31 electrodes that could be used for recording activity. Recordings from 8 of the

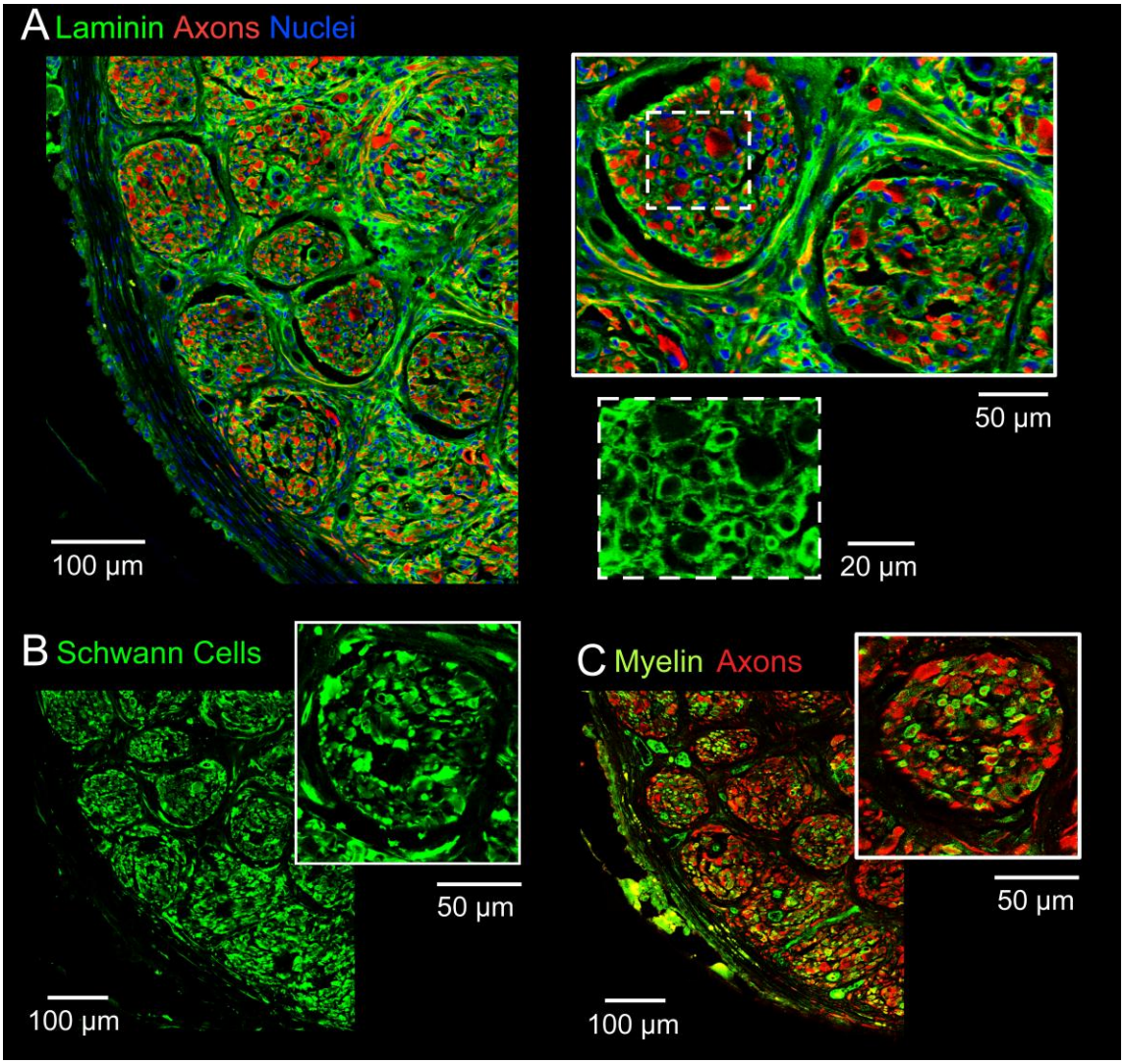

Figure 9. Distal axon characterization.
(A) Close up of distal nerve cross section stained for laminin (green), axons (red), and cell nuclei (blue). Microchannel fascicles shown in the top right insert. Bottom right insert depicts a close up of the basal laminae structure. (B) Aggregates of Schwann cells (green) and (C) re-myelinated axons, shown by co-localization of myelin (green) and axons (red), were spatially correlated within microchannel fascicles.

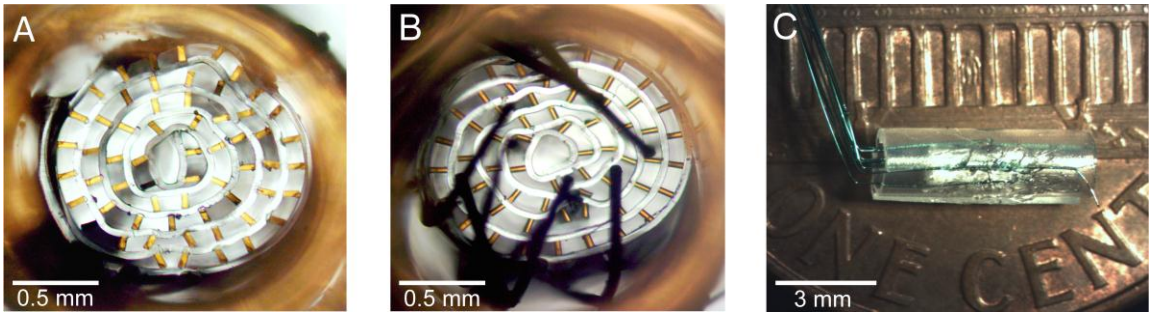

Figure 10. Regenerative microchannel interface.
Images of a representative microchannel interface with microwire electrodes. (A) Proximal view. (B) Distal view with microwire electrodes entering the microchannels. (C) Side view.

31 functioning electrodes were found to contain single unit action potentials. Peak to peak amplitudes of the action potentials ranged from approximately 30 – 80 μV. Thus regenerated axons in the microchannel interfaces were functional and had successfully innervated the most distal regions of the leg and foot. A variety of sensory stimuli were capable of producing single unit action potential activity across all animals including ankle flexion/extension, pinching and rubbing of the foot pad and toe region, and hair follicle brushing. In general, ankle flexion/extension produced the largest and most reliable action potentials across all animals.

A representative sensory evoked action potential recording from a single microchannel is shown in Figure 11. This action potential is believed to be from an afferent sensory fiber, likely a proprioceptive axon reinnervating a muscle spindle or golgi tendon organ based on responsiveness to plantar flexion. The action potential wave form, isolated using window discrimination and an automated expectation-maximization algorithm through the Plexon Offline Sorter™, is shown in Figure 11A. A typical tri-phasic appearance reported elsewhere for recordings taken within microchannels is noted in the waveform [49,59]. Figure 11B shows the raw recorded signal during plantar flexion held over 4 seconds in an 8 second time window where the flexion was released at time = 61 seconds and is denoted by a motion artifact. Figure 11C shows a plot of

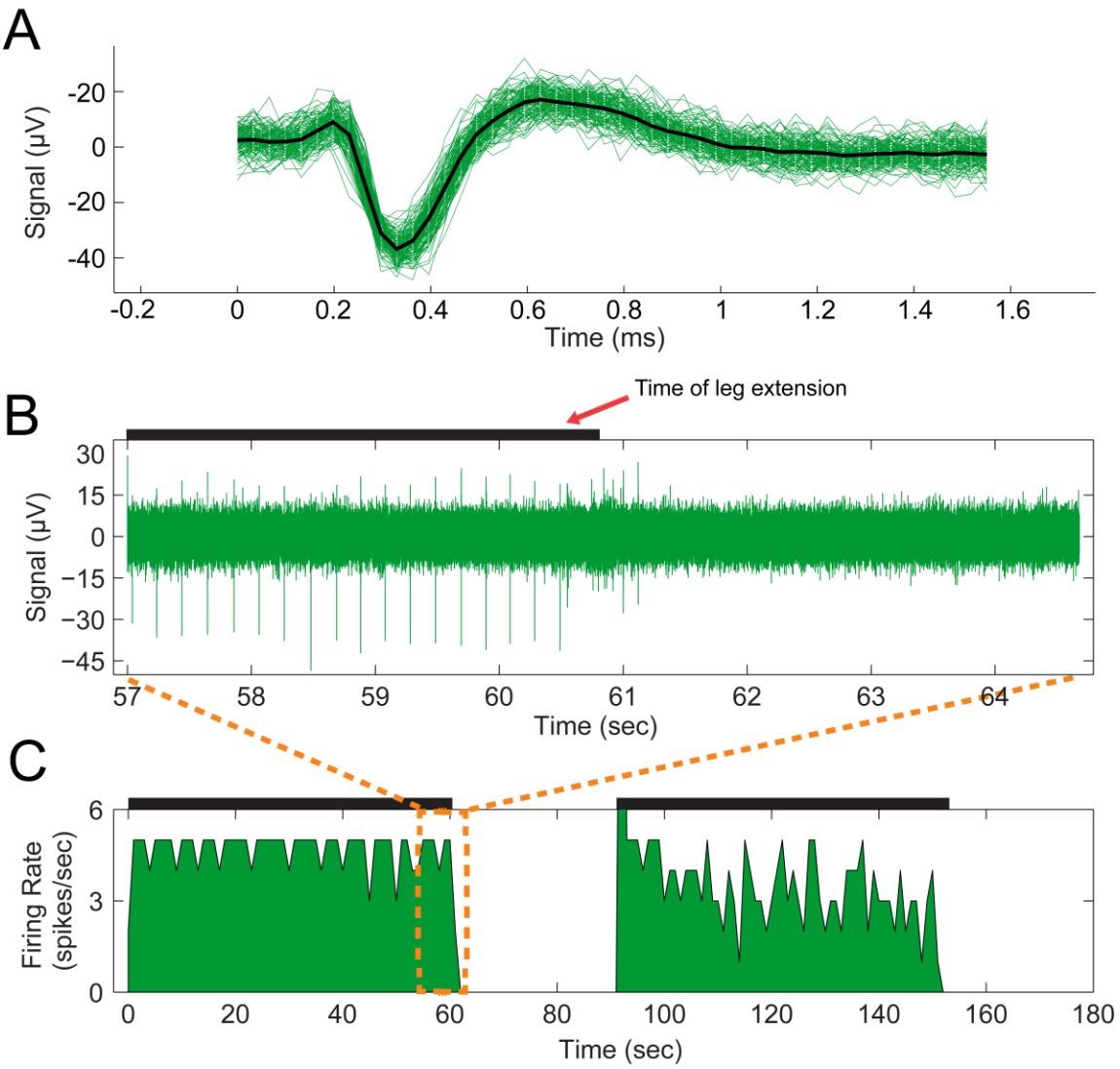

Figure 11. Sensory evoked single-unit action potential recording.
Representative sensory evoked single unit action potential recording through an electrode in a microchannel interface. (A) Action potential waveform. (B) Raw recording signal over 4 seconds of plantar flexion followed by 4 seconds lacking plantar flexion. Plantar flexion was released at time = 61 seconds and is denoted by a motion artifact during release of the ankle. (C) Spike rate of the action potential where plantar flexion was held for 60 seconds, released for 30 seconds, and repeated. A 1 second bin size was used to generate the plot.

firing rate over a longer duration where the plantar flexion was held for 60 seconds, released for 30 seconds, held for 60 seconds, and again released for 30 seconds. Robust and steady firing of action potentials was observed during the flexion periods in contrast to the lack of firing during the release periods. The average peak to peak amplitude of

this unit was measured to be 54 μV with an average SNR calculated to be 2. There was no activity in response to control sensory stimulation of the contralateral leg for this unit or any other sensory evoked unit across all animals.

3.3.9 Electrically Evoked Multi Unit Action Potential Recordings

The presence of evoked multi-unit activity recorded from the microchannel electrodes at five months was used to calculate the number of electrodes per device that could be used for successful recordings, which we have termed 'device viability'. Evoked multi-unit activity was observed on an average from 4.5/8 electrodes per device, which corresponds to a mean device viability of 56.25% (SD 12.5%) after the five months of implantation. It should be noted that this mean viability *includes* nine electrodes with broken microwire leads. These nine electrodes were deemed non-functional after the broken microwire leads were visually verified and by a lack of an electrical stimulation artifact present on all functional electrodes. In one device all of the electrodes contained evoked multi-unit activity except those which were deemed non-functional.

The ramped voltage stimulation evoked increasing levels of multi-unit activity with increasing recruitment of axons within the microchannels. The peak to peak amplitudes ranged from approximately 260 – 520 μV near the upper threshold of stimulation. The amplitudes and waveforms of the multi-unit microchannel action potentials varied between animals and microchannel interface electrodes; however, in all cases signals were clearly distinguishable and did not require averaging to detect. Furthermore, the differences in multi-unit microchannel action potential amplitudes, latencies, and waveforms across electrodes and animals indicated there were different axon populations that regenerated into each of the respective microchannels, which was expected. In all animals, electrical stimulation via hook electrodes produced visible contractions of the gastrocnemius muscles and ankle extension, indicating successful nerve regeneration and functional reinnervation of distal targets.

Representative electrically evoked multi-unit activity from three electrodes of a single microchannel interface using the 0-1 V stimulus ramp is shown in Figure 12. As just noted, different multi-unit microchannel action potentials were found in all three channels (and others not shown). Additionally, the recruitment of different units adding to the multi-unit microchannel action potentials can be seen in all three electrode recordings as the voltage stimulus was increased.

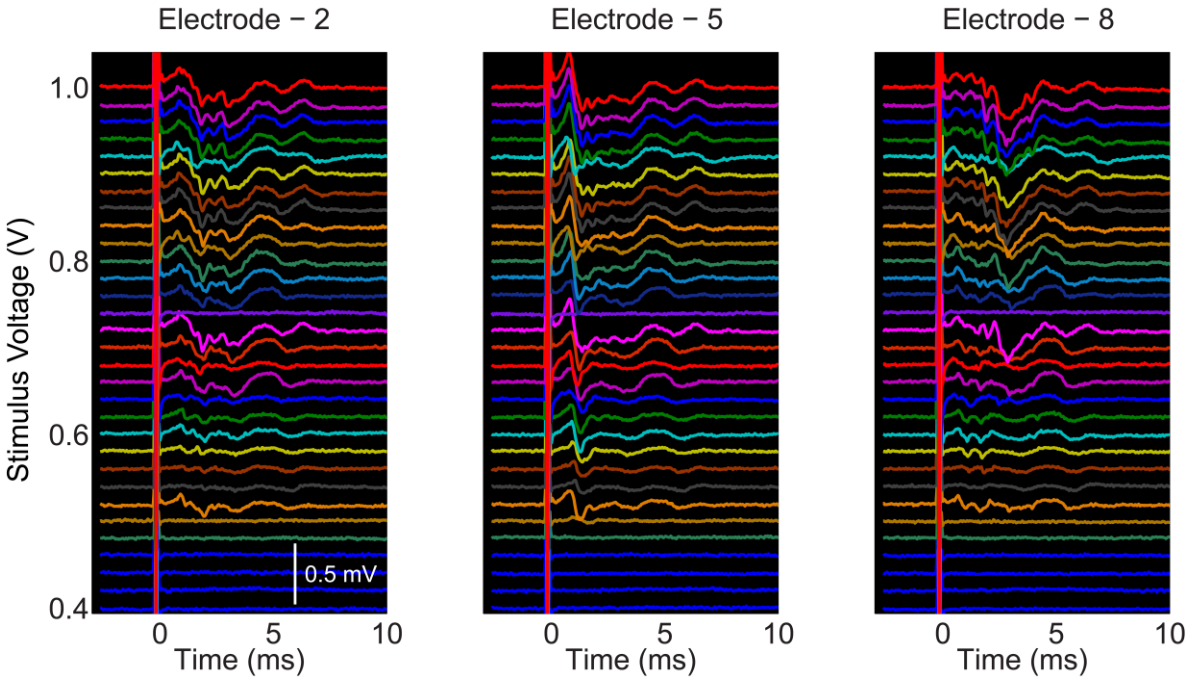

Figure 12. Electrically evoked multi-unit action potential recordings.
Representative electrically evoked multi-unit activity with different amplitudes, latencies, and waveforms from 3 representative electrodes in a microchannel interface.

3.4 Discussion

One of the major challenges in the area of neural interfacing is to develop reliable devices that establish neuronal communication for prosthetic control. There have been many efforts towards this endeavor that can be broadly categorized into central neural interfacing or peripheral nerve interfacing. The efforts in these areas to restore, at least partially, sensorimotor function predominantly hinges on developing interfaces that can restore communication through neuronal recording and stimulation. While cortical

neural interfacing is plagued by challenges of interfacing with the brain and decoding abstract signals intended for functional restoration, peripheral nerve interfacing has the potential to obtain signals that are more closely related to the intended muscle activation and are significantly less invasive. The culmination of a number of peripheral nerve interfacing studies has resulted in the development of interfaces such as cuff, penetrating and regenerative sieve electrodes [2–6,39,52]. While being helpful to some extent, these interfaces have drawbacks ranging from lack of selectivity in the case of the cuff electrode to more severe consequences in the case of the penetrating USEA where the interface implantation leads to inflammation and generation of scar tissue [2–4,6,39]. The present study was focused on development of a device that would be effective as an interface for amputees with the potential for long term utility and minimal adverse effects.

One of the key features of the design strategy was to take advantage of the regenerative approach using microchannels and materials non-toxic to the peripheral nervous system including PDMS and SU-8. A simple and common fabrication technique was developed for scaffold production and involved initially generating flat sheets of microchannels which were subsequently rolled into conduits mimicking the size and fascicular organization of the rat sciatic nerve (Figure 4). This simple fabrication methodology should tremendously help in the large scale production of these devices.

However, one of the limitations of this approach is that the procedure creates a small open core in the center of the rolled microchannel scaffold. Even though one could pursue ways to occlude this space [49], this was not initially considered because it would hinder overall regeneration. If it was found that a disproportionate number of axons regenerated through the central core instead of the microchannels, occluding the hole would have been critical. As this scenario did not occur, occluding the central core was not pursued. Another issue with the rolled approach was the inconsistency in the cross-sectional area of each microchannel from the center of the scaffold moving outwards

radially. The cross-sectional area tended to increase slightly towards the center of the scaffold. However, this change in microchannel cross-sectional area within the scaffolds (2.5% in the 100 μm x 100 μm microchannel scaffolds) did not significantly impact the performance of the device, unlike the three distinct microchannel widths evaluated, and hence was not rectified in the current study. In future modifications of the device, this issue can be resolved by decreasing the spacing of the SU-8 walls in the inner region of the device.

There are additional advantages of using the rolling approach to generate the microchannels. First, the size of the scaffold is easily scalable to nerves of different diameters. If the nerve is larger, the sheet simply needs to be longer (more microchannels) in order for the rolled scaffold to have an increased diameter. Another benefit is that the number of microchannels available for interfacing scales accordingly for larger nerves. This is especially important when dealing with upper arm or upper leg amputees where the larger amputated nerves contain significantly more relevant information needed to control a neural prosthetic.

Additionally, an important finding of this study is that the components of the microchannel device were non-toxic to both DRG neurites and Schwann cells without needing any extracellular protein coating, such as laminin. The *in vitro* experimentation also showed the microchannel design was capable of guiding and directing neurites and Schwann cells as judged by the unidirectional neurite outgrowth and Schwann cell migration along and through the microchannels (Figure 5A, B). Further, it was interesting to note that neurites and Schwann cells initially growing and migrating perpendicular to the microchannels changed their initial direction and re-oriented towards the microchannels (Figure 5C). This suggests the presence of an, at this time, unknown mechanism for preferential growth/migration towards the microchannels. However, this was not the case with neurites and Schwann cells farther away from the microchannels, suggesting probably a spatial dependence. There was also preferential growth on the SU-

8 microchannel walls. However, this was fairly inconsequential *in vivo* because the microchannels were covered with the top PDMS layer thereby containing the axons within the microchannels regardless of which surface they preferred.

In vivo experimentation with the microchannel scaffold to assess potential for chronic interfacing in amputees brought to light a number of additional significant observations. First, the implants were well tolerated in all cases with little to no scar tissue, in general. Second, robust numbers of axons were observed in the 100 µm x 100 µm and 150 µm x 100 µm microchannels showing that these microchannel scaffolds readily support nerve regeneration despite lacking distal reinnervation targets. The microchannels in the 100 µm x 100 µm microchannel scaffolds did have varying numbers of axons ranging from a handful in some cases to many hundreds in others (Figure 6D), but seldom were completely lacking axons altogether (Figure 6B). Furthermore, the 100 µm x 100 µm microchannels were at or near the lower boundary for microchannel sizes capable of supporting axon regeneration as judged by the poor regeneration in the 50 µm x 100 µm microchannels (Figure 6A, B). With regards to both the 100 µm x 100 µm and 150 µm x 100 µm microchannels, it was observed anecdotally that microchannels completely lacking axon growth tended to occur near the periphery or in the outer rings of the scaffold. This was expected based on the typical nerve regeneration pattern where preferential regeneration occurs along the Bands of Büngner which form a central cord occurring roughly near the center of scaffolds [32,72,73]. Given the robust regeneration across these scaffolds though, microchannels lacking axons were very infrequent and would be difficult to predict prior to implantation. Besides the few microchannels lacking axon regeneration, no trends of greater or lesser axon regeneration dependent on microchannel location (center vs. periphery of the scaffold) or any other discernible topographical pattern were observed. It is also important to note that these trends of regeneration and dependence on microchannel size agree well with other studies looking at non-amputee scenarios [49,57].

For the *in vivo* studies, the rationale for choosing 100 µm x 100 µm microchannels for detailed analysis was based on the need to use the smallest possible microchannel cross-section to increase the amplitude of an axon's AP while still maintaining reliable regeneration in a majority of the microchannels. In the implantations with this device, a vast majority of the microchannels had at least 25% of the original cross-sectional area remaining for future maturation of axons, Schwann cells, and the supporting tissue in general (Figure 7). A significant increase in regenerating axon numbers is not expected to occur within the microchannels given that an eight week time point was chosen for analysis. Another important point is that this analysis does not take into account the axon pruning that will occur at later time points resulting in fewer axons in the microchannels. This validated that axon constriction, as observed in the Sieve electrode [52,74], should not be a major concern when microchannel sizes similar to those in this study or larger are used in peripheral nerve interfacing applications. There was a small subset of microchannels, 5%, in which greater potential for future axon constriction might be expected, due to their being filled more than 75% with tissue when these scaffolds were explanted. However, the actual occurrence of axon constriction in this small subset would have to be assessed at significantly later time points to account for axon pruning, as previously mentioned. It is also important to note that even if axon constriction occurred in these few microchannels, it would not drastically affect the interfacing capabilities of the scaffold due to the overall number of microchannels presenting numerous opportunities to record from other axons.

Analysis of the nerve and axons distally as they regenerated out of the implanted microchannel scaffold also revealed a number of interesting details. The basic structure of the nerve stump distal to the scaffold had been reorganized in response to and matching the architecture of the proximal microchannels (Figure 8). This was first observed with the axons and Schwann cells that were grouped and organized according to the proximal microchannels (Figure 8B, C). In addition to the axon and Schwann cell

organization, connective tissue layers similar to those observed in a normal nerve had reformed. A stereotypical uninjured nerve is morphologically compartmentalized by epineurial, perineurial, and endoneurial connective tissues [11,75,76]. What was observed in this study was the reformation of all three types of connective tissue in the regenerated nerve distal to the implant. An epineurial like sheath surrounding the whole nerve cross section could be identified by concentric fibroblast arrangements. Furthermore, as a result of the re-organization within the distal nerve, multiple perineurial like sheaths forming 'microchannel fascicles' marked by concentric fibroblast arrangements around the aggregates of axons and Schwann cells was observed (Figure 8C). These ring like sheaths of fibroblasts correlated with the presence of extracellular matrix shown by the lamellae support structure (Figure 8D). This is similar in nature to the perineurium of a stereotypical nerve which has been noted for its concentric layers of flattened cells with prominent basement membranes [11,76]. In general, the microchannel architecture facilitated and encouraged parallel nerve fiber growth by directing axon regeneration through the microchannels and producing an organized microchannel fascicle morphology. The reformation of endoneurial connective tissue is discussed in a later paragraph.

It was also evident that the 'microchannel fascicles' maintained their morphology as much as 1 mm distal to the scaffolding. With distance, the fascicles gradually lost their perineurial structure and the axons gradually disassociated from the microchannel morphology to a homogeneous morphology. However, the axons still maintained a general, unidirectional growth (Figure 8A) and eventually branched out into the local muscle bed (data not shown). It is also important to consider previous work which has shown that muscle reinnervation, while a key component for functional nerve regeneration across critical gaps, is not necessary for nerve stability. In fact there has been no evidence of motoneuron death after chronic axotomy in nerves and axons lacking their reinnervation targets out to 14 weeks [28]. Furthermore, nerves and axons retain a

regenerative capability and can functionally reinnervate muscles after long periods such as 12 months of chronic axotomy, albeit a reduced number of regenerating axons over long distances, but with similar functional outcomes compared to controls [31,77,78].

While the macroscopic structure of the distal nerve changed significantly, the axons, Schwann cells, and associated connective tissue were undergoing the normal regenerative processes. Similar to the perineurium in a normal nerve, endoneurial connective tissue is heavily associated with basal lamina for structural support and cell adhesion between axons and proliferating Schwann cells. Proliferating Schwann cells are crucial for nerve regeneration by forming conduits and providing a favorable environment for subsequent axon elongation, maturation, and long term Schwann cell-axon pairing [11,32,70,75,76,79]. Such conduit like structures of connective tissue were visualized in each individual microchannel fascicle by laminin staining, as indicated by the porous texture. Accordingly, each mature Schwann cell and axon pair was invested with a tight basal lamina structure and encompassed by extracellular matrix (ECM), forming endoneurial tubes (Figure 9A). In a regenerated nerve, mature Schwann cells play a crucial role by providing aid in the conduction of nerve impulses and providing trophic support for neurons [11,32,75,79]. Further, it was revealed in the analysis of myelin and Schwann cell staining that many axons were re-myelinated and a majority were closely associated with Schwann cells, thus suggesting the presence of both myelinating and non-myelinating Schwann cell phenotypes (Figure 9B, C). With regard to the general tissue distribution, immunohistochemistry indicated that large edema filled voids lacking cell populations and extracellular matrix within regions of the nerve were absent (Figure 9A). Together these observations support the finding that microchannels are not only supportive of the proper initial microenvironment for basal lamina/ connective tissue deposition by proliferating Schwann cells but also for chronic stability of the regenerated healthy nerve.

Not only do these observations support chronic stability of the regenerated nerve with the device, but they also suggest that neuroma formation may not be a concern for use of this device in the amputee population. The regenerating nerve and axons, lacking distal reinnervation targets, displayed opposite characteristics to those most commonly associated with neuromas after being constrained to regenerate through the device. Neuromas are characterized by aberrant, random regeneration and highly disorganized axon distribution resulting in the commonly observed bulbous nerve swelling [62,63,67,70] which occurs as early as 1 week post nerve transection leading to chronic complications [63,67,70]. However, quite the opposite was observed in this study as shown by the microchannel fascicle morphology, general unidirectional growth of regenerating axons distal to the device, and lack of bulbous nerve swelling (Figure 8). Additional axonal characteristics within neuromas include a lacking Schwann cell population and myelination of axons [62,63,67], loose basal lamina structure surrounding axon/Schwann cell units [67,68], and endoneurial edema within the nerve structure [62,64]. Again, quite the opposite was observed in this study. An abundant population of Schwann cells closely associated with myelinated axons was observed. Furthermore, a tight, supportive basal lamina structure surrounded the axon/Schwann cell units and there was no presence of large voids within the nerve structure indicating an absence of edema or swelling (Figure 9).

In addition to the chronic stability of the microchannel scaffolds observed in an amputated nerve, both spontaneous and sensory evoked single unit activity were successfully recorded *in vivo* using the permanently integrated electrodes at the chronic time point a full five months after implantation. Thus indicating that the devices are both durable and that regenerating axons in them are viable over prolonged periods. The sensory evoked single unit action potentials included a multitude of activity originating from the distal foot pad region suggesting at least partial reinnervation of distal targets and potentially the recovery of proprioceptive, nocioceptive, and other sensory

perception. Additionally, multi-unit action potentials were recorded through all microchannel interfaces in response to proximal electrical stimulation (Figure 12). Observed contractions of the gastrocnemius muscles and plantar flexion in response to the electrical stimulation further suggest reinnervation of distal targets and potentially some recovery of motor function.

While it is challenging to record single unit action potentials from regenerated axons in anesthetized rats, eight of 31 functioning electrodes were successfully used towards this end. Furthermore, it is highly unlikely that all sensory afferents were stimulated even though a variety of sensory stimuli were used. So it is possible single unit action potentials could have been recorded through additional electrodes. Additional attempts were made using electrical stimuli to evoke single unit action potentials, but small levels of multi-unit activity were consistently observed even at low stimulation levels. The inability to evoke single unit action potentials is attributed to using hook electrodes which stimulate the nerve outside the epineurium and have large areas of contact. However, the presence of evoked multi-unit activity on the microchannel electrodes did allow an assessment of *overall* device viability which was found to be greater than 50% after five months of implantation, i.e. neural activity could be observed in greater than four of the eight integrated electrodes in each device. This calculation *included* nine nonfunctional electrodes with broken microwire leads. It should also be noted that the electrical stimulation ramp was performed to 1V, which was possibly submaximal to produce a full compound action potential of the entire sciatic nerve. It is therefore possible that some channels were viable but needed greater stimulation levels. The stimulation ramp also allowed the identification of multiple different axon populations within the various microchannels integrated with electrodes, which was expected based on the randomness of axon regeneration.

Overall, using the regenerative microchannel interface presented here, recordings of single and multi-unit action potentials could be made that are comparable if not better

in some aspects to what has been previously reported with regard to numbers of functional microchannel electrodes [49]. Notably, the fabrication of this interface was accomplished without the need for advanced metal deposition/patterning and insulation techniques for electrode integration. Instead simple off the shelf microwires were integrated and successfully utilized in a chronic setting. Additional work should focus on protecting the microwires from breakage though, as this was the main source of failure.

The amplitudes of the recorded action potentials also fell within ranges previously reported using a variety of peripheral nerve interfaces from LIFE electrodes to other microchannel based interfaces [1,41,50,59,80]. While these values fell within ranges reported, they were not consistently as large as reported in studies using microchannels [49,50,59]. There are a few design characteristics of the microchannel interfaces presented in this work that could contribute to the lower signal amplification. First, the microwire electrodes had a recording region that was 0.097 mm^2. This relatively large electrode/recording area would reduce the amplitude of any recorded action potential because the entire electrode surface is equipotential and therefore tends to average out signals. Furthermore, the microchannels have an amplifying effect, based on the ability to constrain the extracellular fluid surrounding an axon and, in theory, increase the amplitude of the recordable extracellular action potential [6]. The large microchannel size chosen to accommodate the 60 μm diameter microwires and the fact that the walls 'splay out' due to rolling could have reduced this overall amplifying effect (Figure 10A and B).

Another important point is much of the modeling and *in vitro* work performed to validate this theory used microchannels of either significantly smaller diameters or longer lengths [56]. While smaller diameters and longer lengths might be expected to result in larger action potential amplitudes, based on the results of this study, they may not be suitable for maintaining healthy axons over chronic periods in amputees. In other acute *in vivo* experiments, cut rootlets or portions of nerves were physically placed in microchannels [50,59]. The axons used in these experiments were freshly harvested

axons that had not undergone regeneration and are therefore not readily comparable. In a chronic terminal study, single unit action potentials were recorded through a tungsten microelectrode inserted into an implanted microchannel scaffold at the time of recording[49]. However, the electrode was not permanently integrated into nor implanted along with the microchannel scaffold. Thus completely eliminating the foreign body response to the electrode and the deposition of fibrous tissue on the electrode surface which are fundamental factors in chronic interfacing and would reduce recording capabilities. The experimental paradigm of inserting an electrode at the time of recording also provides one the ability to make multiple attempts at 'searching' for the best units and is simply not possible with integrated electrodes. In the present study, microchannel recording capabilities were evaluated using a regenerative nerve model with permanently implanted electrodes and this chronic experimental paradigm in many ways may account for the reduced amplitudes observed.

It should be noted that an additional significantly longer time point, at least one year, is needed to prove conclusively that regenerated axons from an amputated nerve remain healthy and that stable recordings can be made from them. However, based on all the nerve characteristics investigated here, the regenerative microchannel scaffold provides an environment that permits substantial axon growth and maturation within the device over a considerable time period. The regeneration occurred in a spatially orchestrated manner due to the microchannels, which induced spatial segregation into small groups of axons to the benefit of selective interfacing. Growth through the microchannels resulted in a reformation of stereotypical nerve/axon morphologies and tissue compartmentalization that contributed to chronically stable and healthy regeneration through and past the device without complications of irregular nerve regeneration characterizing a neuroma. These findings support the fundamental criteria for a regenerative peripheral nerve interface targeted towards amputees. Finally, based on the electrophysiology data presented here, action potentials can be recorded from

regenerated axons in microchannels with permanently integrated electrodes on a chronic timescale. With this the stability and viability of regenerative microchannel interfacing is established, warranting the development of advanced wiring, packaging, and wireless technologies to be utilized with large electrode count microchannel interfaces for chronic continuous behavioral studies and these are ongoing.

3.5 Conclusions

Overall the results from the current study demonstrated that the microchannel design provides an efficient platform to support regenerating axons and incorporate electronics for interfacing with small groups of axons. The simple fabrication process with biocompatible materials such as PDMS and SU-8 elevates the potential for easy scale up of production of this device. The ease with which one can incorporate microwire electrodes allows a versatile use of this device where advanced insulation and interconnect techniques are not available. The overall flexibility of the fabrication process to adapt and tailor the microchannels to the nerve size has great value in individualized customization of this device. Further, the re-organization, architecture and composition of the regenerating nerve lacking distal reinnervation targets showed numerous parallels to a normal nerve and underscores the potential for *chronic* bidirectional neuronal communication. The demonstrated capability to use microchannel interfaces to record spontaneous, sensory evoked, and electrically evoked single and multi unit action potentials on a chronic scale in the sciatic nerve after implantation for five months further supports this. These properties of the regenerated nerve when coupled with the interfacing capability of microchannels and the lack of adverse effects characteristic of neuroma formation lends this device to be a valuable element in aiding neural prosthetic control for amputees.

CHAPTER 4

Fabrication Processes for Flexible Electrode Arrays, SMT Integration, and Implantation

4.1 Introduction

While large advances have been made recently in neural prosthetics, accompanied by significant media attention, they still provide only a small fraction of the functionality of a natural limb. At the heart of the issue is the neural interface which enables control of advanced robotic limbs by the individual or patient. Advances in peripheral nerve interfacing (PNI) and specifically microchannel technology have the potential to bridge this gap through the capability to increase the extracellular resistance of the axon's action potentials (APs). This confers key unique advantages including node of Ranvier independent recordings and the mitigation of reduced AP magnitudes due to the low-impedance extracellular fluid. [6,56] These advantages make microchannel electrodes a promising peripheral nerve interfacing approach compared to current state of the art penetrating, cuff, and sieve electrode arrays. Within the last 5+ years significant work has gone towards establishing the groundwork for microchannels as a viable method for interfacing in the peripheral nervous system with the largest success seen in a non-regenerative implementation for the bladder system. [58,59] However there still remains room for significant development with more complicated peripheral nerve systems such as that of the limbs. This is especially true in scenarios where a chronic regenerative implementation is practical.

Furthermore, there is a need to develop advanced microchannel interfacing technology capable of performing in chronic interfacing applications. Inherent challenges to the peripheral nerve system include soft nerve tissue that can be easily damaged by rigid electronics such as those based on silicon technology and the fact that it is a hostile

aqueous environment. Initial attempts with flexible and elastomeric PDMS based devices have been made to assess microchannel interfacing in an acute scenario. [50,58,59] However these either do not contain large micro-electrode arrays (MEA), capability to easily integrate surface mount technology (SMT) for multiplexing and amplification, or are not applicable for implantation and awake behavioral animal evaluation as needed for clinical translation.

Patterning MEAs and photolithography in general on PDMS has been notoriously challenging and it is incredibly difficult to produce high-density small features on the substrate. For that reason devices will utilize other substrates such as polyimide that, while not elastomeric in nature, are still flexible. [49] However, an elastomeric substrate for electronics enables a new class of *stretchable* electronics with significant advantages that can find numerous applications ranging from *in vivo* sensors to skin based diagnostics to consumer electronics. Metal patterning for sensors and/or interconnects on PDMS is often accomplished utilizing shadow masks where one accepts larger features instead of going through the difficulty of attempting to pattern a photoresist lift-off mask directly on the PDMS. [50,59] A lift-off approach to patterning metal is preferred to etching away excess metal because metal etchants are highly toxic and are absorbed into the PDMS substrate making them difficult to implement in *in vivo* applications. Other approaches have utilized permanently cross-linked photoresists such as SU-8 because of the strength of the photoresist and its resistance to cracking. [81,82] The disadvantage being it is permanently cross-linked so removal of the mask is achieved through physical means by pulling it off the PDMS substrate. None of these approaches however directly address the inherent underlying issues plaguing photolithography on PDMS. Here we have developed five processing solutions targeting the underlying issues preventing widespread photolithography on PDMS.

The ability to easily integrate micro-chips and other electronics is incredibly important to the overall utility of a peripheral nerve interface as well as any general

device meant for diagnostics, sensors, or consumer oriented applications. It affords one the option to ‘upgrade’ or switch out components of the device at later stages as they become available or needs of the device change. For instance, with the GT-RE a large channel wireless chip that can be implanted is currently not available. Work is actively being pursued to develop these technologies [83] and it is prudent to design the GT-RE for eventual integration with technologies such as these. Currently, the vast majority of electronic components including resistors, capacitors, transistors, batteries, microchips, etc. are available in surface mount packaging. This packaging places flat connection terminals for the components at the base of the component so it can merely be placed in contact on top of other terminals and soldered together. This allows a significant reduction in component size and the smallest components on the market are only available as surface mount devices. However, integrating these devices with stretchable and flexible substrates has been difficult as soldering is not applicable due to heat induced failure of the substrates. Other approaches have centered on direct integration of the SMDs during fabrication, stiffening the substrate to prevent flexibility/stretchability in the region of integration, thermosonic ball bumping process to produce rivet-like connections, or through-holes and connector pins. [82,84–90] These techniques require additional fabrication steps which are challenging and complex, specialized equipment in the case of the ball bumping process and/or lose the advantages of small SMD component size. Furthermore, none of these approaches are easily streamlined with industry’s standard SMD integration processes. The easiest method is to utilize the surface mount approach originally intended for these components and PCB’s.

Hermetic packaging is another challenge implantable devices must overcome especially when microchips and other electrical components have been integrated. Parylene C has seen much use in this application as a vapor deposited polymer which is deposited at room temperature. Parylene C has a long standing history of use with medical devices and has been FDA approved in a variety of applications. It also functions

as an electrical insulator and the lifetime of Parylene C insulated circuits has even been shown to be 20+ years using accelerated failure testing and the Arrhenius relationship. Finally deposition as a thin-film, for example 10 µm, allows it to be highly flexible making it a good first choice for a flexible peripheral nerve interface. [91–94] Encapsulants based on silicone derivatives are another approach that has seen wide use with devices for both mechanical potting as well as insulation. These silicones come in a variety of commercially available forms including room temperature vulcanizing (RTV) and often contain additives aiding with adhesion to a variety of substrates including metals, ceramics, and other polymers. Furthermore, they are flexible and elastomeric making them ideally suited for devices with the same properties. It should be noted however, that these silicones are not impermeable to water vapor. So, it is important that they not contain air bubbles in contact with electronic components as water will eventually penetrate the silicone and accumulate in the bubble leading to a short. If there are no bubbles or voids, then there is no room for moisture to accumulate making the silicone an effective encapsulant. [39,95–98]

Here we report on flexible and elastomeric regenerative microchannel interfaces with large micro-electrode counts and easy integration of SMT for high-throughput peripheral nerve interfacing in awake and ambulatory rats. This is depicted schematically in Figure 13. First a design and fabrication approach for flexible (Parylene C) and elastomeric (PDMS) micro-electrode arrays (MEA) with large numbers of high-density microelectrodes is discussed. In particular we have developed five processing solutions targeting the underlying issues preventing widespread patterning and photolithography on PDMS. Microchannels walls are then patterned onto the surface of the MEAs along with a capping PDMS layer to enable microchannel interfacing with peripheral nerves. Second, a simple and broadly applicable SMT integration strategy is examined. Finally, flexible and elastomeric polymer based hermetic insulation and encapsulation strategies are utilized enabling implantation and electrophysiology in awake and freely moving rats.

Of importance, these design and fabrication techniques are applicable to a broad range of flexible devices and sensors benefiting from stretchable and/or flexible interconnects, SMD integration, and/or operation in hostile aqueous environments. Examples of devices benefitting from the techniques and technology reported here include flexible sensors such a continuous glucose monitors, flexible diagnostics such as recent skin based health monitors, and the burgeoning flexible wearable technology industry. [99–108]

4.2 Materials and Methods

4.2.1 GT-RE Design

The basic concept of the GT-RE microchannel interface (Figure 13) has been discussed previously [71,109]. Briefly, an MEA is patterned onto a base polymer layer. Two different devices were developed where the polymer utilized was either polydimethylsiloxane (PDMS) or Parylene C. The metal traces were then passivated with PDMS or Parylene C forming a flexible, and elastomeric in the case of PDMS, MEA. SU-8 microchannel walls were patterned on top of the MEA and a capping PDMS layer was adhered on top forming a sheet of microchannels with electrode sites housed in the base of the microchannels. This sheet was rolled perpendicularly to the direction of the microchannels forming a cylinder matching the shape and size of a nerve, in this case the sciatic nerve of a rat. Importantly the rolling took place along the base polymer layer forcing the capping PDMS layer to stretch. If the sheet were to be rolled around the top PDMS layer, it would buckle and block the microchannels. The microchannels were 100 µm wide, 100 µm tall, and 3.5mm long with 20 µm wide microchannels walls. These dimensions were based on previous work that in part investigated microchannel sizes and the relationship to nerve regeneration in a clinically translatable amputee animal model. [109] Metal traces connected to the electrodes in the microchannels ended at a series of bonding pads intended for connection to surface mount devices (SMDs) utilizing a SMT

integration methodology detailed further on. Importantly, a*ny* SMD or surface mount printed circuit board (PCB) can be integrated with the GT-RE or other flexible and/or elastomeric based device using this method.

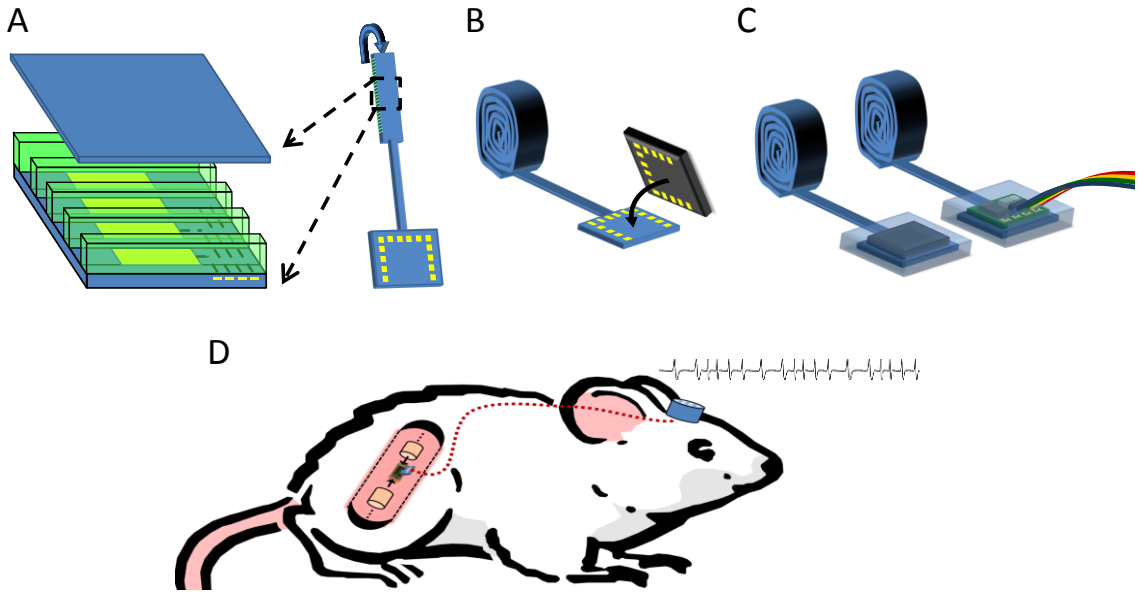

Figure 13. Schematic of fully integrated microchannel interface – The Georgia Tech Regenerative Electrode (GT-RE).
(A) Microchannel architecture showing a blue polymer substrate with integrated gold microelectrodes and traces leading to bonding pads, green SU-8 microchannel walls, and a blue top capping polymer layer forming a sheet of microchannels with integrated electrodes. The sheet of microchannels is rolled forming a cylinder of microchannels. (B) Integration of surface mount device (SMD) components for a variety of capabilities including potentially multiplexing, amplification, and wireless communication. (C) Encapsulation of the SMD region enabling operation in aqueous environments such as the body. Instead of a wireless SMD microchip, signal extraction wires are also shown. (D) Implantation of the GT-RE in the rat sciatic nerve model where signal extraction wires are burrowed subcutaneously to a percutaneous headcap mounted on the skull to enable neural signal recordings.

In this study two different PCB's (Sierra Circuits, Inc.) were integrated utilizing the surface mount approach. One PCB was pre-assembled by Sierra Circuits, Inc. and contained Intan Technologies 32-channel micro-chip (RHA2132) and off-components for on-board multiplexing and amplification. The PCB design is depicted in Figure A 1 and was utilized in *in vitro* validation. The micro-chip and components could have been directly integrated onto the bonding pads of the GT-RE. However, this was not pursued for the sake of simplicity gained by outsourcing assembly on a PCB which allowed integration of just one item with the GT-RE as opposed to the many components associated with the microchip. The second PCB (6 mm x 9 mm) integrated with the GT-RE was intended for *in vivo* applications. It was used as a wire attachment hub and had 34 wires (0.001" Stainless Steel 7 strand PFA, A-M Systems) soldered accounting for the electrodes, references, and a local ground which allowed eventual connection to a separate off-board amplifier for electrophysiology experimentation. The off-board amplifier was connected directly to a computer for analysis and did not utilize any multiplexing. The 34 wires coming off the PCB were divided into separate groups of 17 wires and utilized a 3 braid bundle with sets of 3, 4, and 4 wires for mechanical reinforcement and to prevent breakage *in vivo*. Each braid was fed into a silicone tube (Standard Silicone Tubing, Helix Medical, LLC) to act as an extra layer of insulation and mechanical protection. The ends of these wires were connected by Omnetics Connector Corp. to a 36-pin Male Nano Strip Omnetics connector. This connector was eventually utilized as a percutaneous connector on a rat's skull enabling awake and freely moving electrophysiology experimentation.

4.2.2 Electrode Design

Electrodes were patterned to be 100 µm x 70 µm. Accounting for a slight overlap of the passivation layer to help prevent delamination of the metal from the polymer substrate led to an effective electrode area of 80 µm x 40 µm. Metal traces leading from

the electrodes to the bonding pads for SMD integration were 30 µm wide with 70 µm spacing. The bonding pads were 105 µm x 190 µm. The electrodes were spaced once every third microchannel to allow for an equal distribution of electrodes throughout the cross-section of the GT-RE post rolling. A common bipolar reference was placed near the bonding pads and a common pseudo-tripolar reference was designed with electrode sites at the entrance and exit of every microchannel containing an electrode. The photolithography mask dictating the referencing design along with the electrodes, traces, and bonding pads can be seen in Figure 14. Of importance, seemingly extraneous features were placed surrounding the GT-RE features on the mask designs. While not having any direct implications to the design of the GT-RE, these features served the incredibly important purpose of stress relief and are discussed later in the discussion.

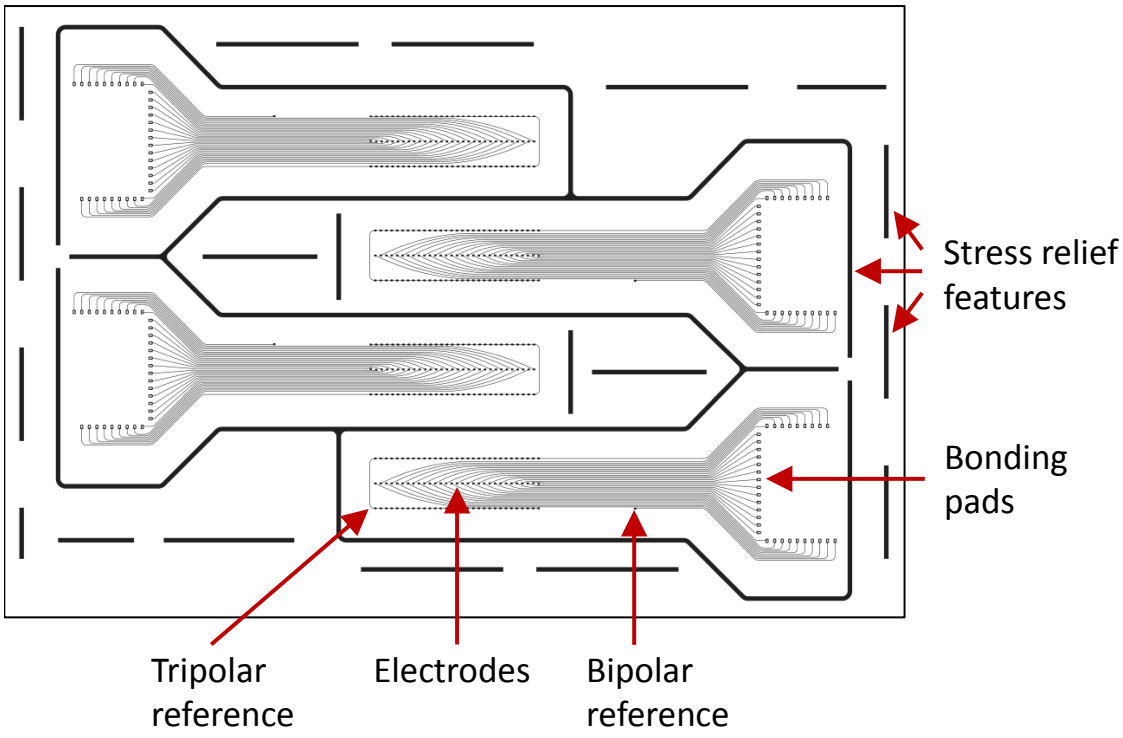

Figure 14. Photolithography mask design.
Mask design of electrodes, traces, bonding pads, references and stress relief features. Four devices are included in this design enabling batch production of 4 GT-RE's at a time.

4.2.3 Flexible and Elastomeric PDMS based MEA Fabrication

The fabrication steps for patterning the metal electrodes, traces, and bonding pads are represented schematically in Figure 15A with the general steps numbered accordingly. To fabricate the flexible and elastomeric PDMS based MEAs a 40 μm PDMS base layer (1:10 weight ratio Sylgard 184, Dow Corning) was first spun and cured on glass coated in titanium (50 Å) and gold (350 Å) for anti-adhesion using a hot plate. This was followed by lift-off patterning to define titanium and gold electrodes, traces, and bonding pads on the PDMS substrate. Of importance, thick-film photoresist layers were used for these photolithography steps and all general patterning steps on PDMS. Detailed reasoning for doing so is left for the discussion.

After curing the PDMS base substrate, the sample was briefly treated with oxygen plasma to increase adhesion and enable wetting of the PDMS with the photoresist NR4-8000P (Futurrex, Inc.). A lift-off approach was used to pattern metal electrodes, traces/interconnects, and bonding pads next. A 30 μm layer (thick-film) of NR4-8000P was spun immediately after oxygen plasma treatment and cured in an oven at 120 °C for 9 min, not on a hotplate. All photoresist baking (pre and post-exposure baking) for the MEA fabrication was performed in an oven with a slow ramp down to room temperature for post-exposure baking and is another important factor in the thick-film photolithography approach described. The reasoning is again left for the discussion. The NR4-8000P was exposed using an experimentally determined exposure dose of 590 mJ/cm^2. Exposures for all subsequent photolithography steps took place under the same filter. Post-exposure baking took place in an oven at 90 °C for 25 min with at least a 1 hour cool down to room temperature. Development was performed with the sample inverted at an angle in a beaker to allow dissolved photoresist to sink to the bottom maintaining a fresh supply of developer at the interface with the photoresist. This enables

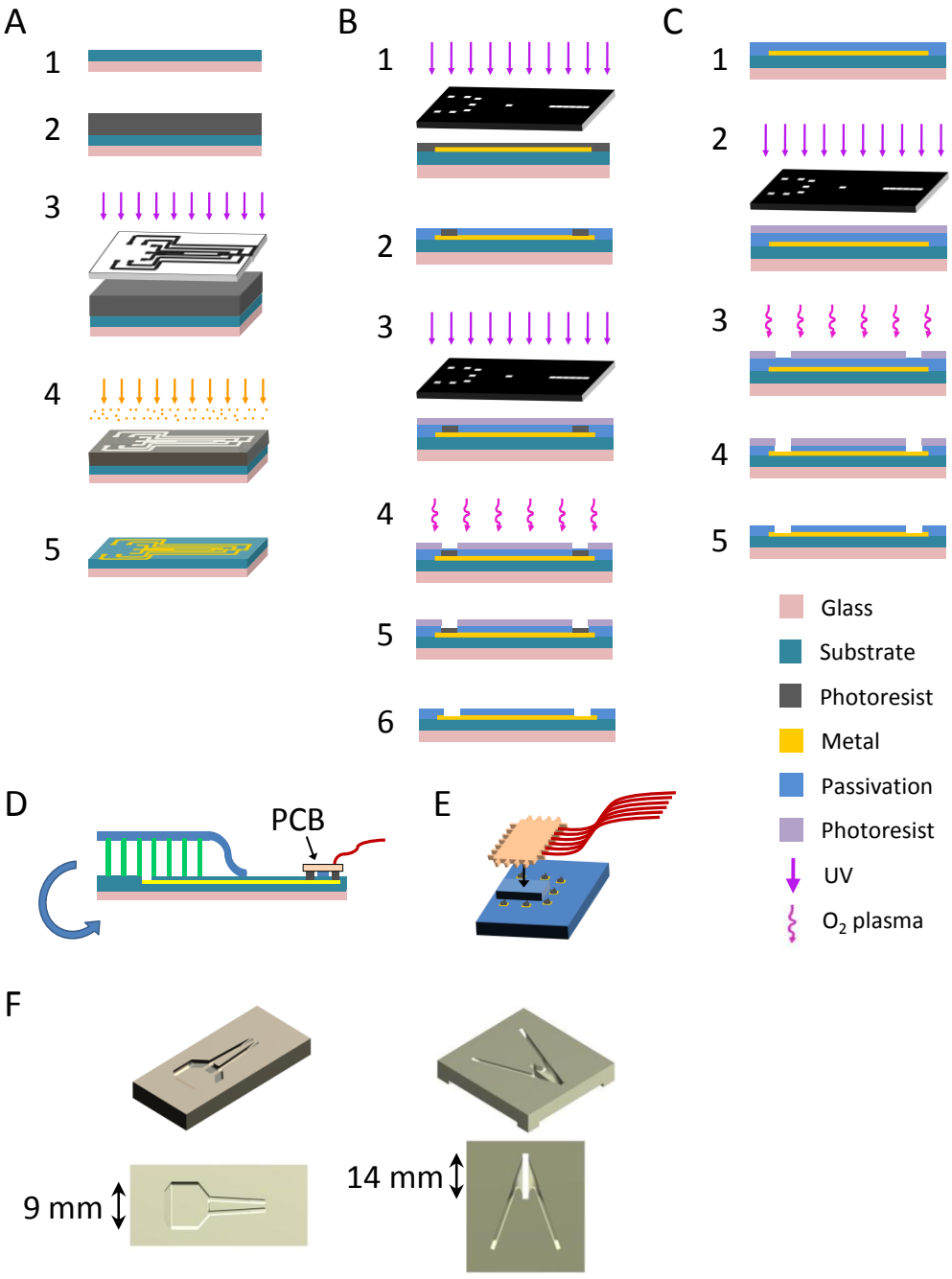

Figure 15. GT-RE fabrication.
(A) Metal patterning using a lift-off approach to define electrodes, traces, and bonding pads. (B) PDMS passivation using a sacrificial post approach. (C) Parylene C passivation using a bulk etching approach. (D) Addition of microchannels and rolling of the microchannel region along the base substrate layer. An integrated surface mount PCB with signal extraction wires is also shown. (E) SMT integration technique using conductive epoxy placed on bonding pads and a spacer to define a minimum bondline. (F) Molds for silicone adhesive encapsulation of the PCB region and headcap region. The PCB mold is depicted on the left and the headcap mold on the right.

faster development times without the need for agitation which consistently results in delamination of the cross-linked photoresist from the PDMS substrate. A final careful dip in fresh developer followed by gentle rinsing in DI water and passive air drying was performed. Etching residual photoresist in the developed areas, also known as descumming, was performed with oxygen plasma anywhere from 30 sec to 3 min depending on the degree of photoresist remaining. In general it is preferred to etch over developing longer periods of time due to the propensity for the photoresist to delaminate from PDMS during development.

Prior to metal deposition, brief oxygen plasma treatment was again used to activate the exposed regions of the PDMS surface. Titanium (100 Å) and gold (1000 Å) were deposited using an e-beam evaporator and lift-off was performed again with the sample inverted at an angle in the beaker. Mild stirring of the resist remover solution was performed to enable faster lift-off. Afterwards, the sample was air dried and baked at 90 °C for 30 min to evaporate any absorbed solvent.

A sacrificial-post approach [82] was used in order to passivate the metal traces with PDMS while leaving the electrodes and bonding pads exposed. These fabrication steps are represented schematically in Figure 15B with the general steps numbered accordingly. This was thought to be preferable over bulk plasma etching to pattern PDMS as plasma etching PDMS is notoriously difficult and tends to be more of a ‘dirty’ physical bombardment process as opposed to chemical etching. First, another 30 µm layer of NR4-8000P was spun on the substrate immediately after oxygen plasma treatment and cured in an oven at 127 °C for 9 min. The NR4-8000P, while the same thickness as previously used for metal patterning was exposed using an experimentally determined exposure dose of 1575 mJ/cm^2. This large difference in exposure dose is a function of feature size and is an important aspect for photolithography on PDMS discussed later in the discussion. Post-exposure baking took place again in an oven at 90 °C for 30 min with at least a 1 hour cool down to room temperature. Development of the

photoresist film leaving behind the sacrificial posts on the electrodes and bonding pads was performed in the same manner as that for metal patterning. However, extra care was taken during development to avoid agitation and samples were defaulted to extra oxygen plasma etching to avoid over development of the sacrificial posts and subsequent delamination from the substrate. Edges of the substrate were also developed separately as they took additional time due to typical edge bead formation from spinning. Developing the edges at the same time as the sacrificial posts results in over development and delamination as just mentioned.

After sacrificial post development and etching, the sample was briefly treated again with oxygen plasma in an attempt to increase adhesion and enable the formation of stable bonds between the PDMS passivation layer and the PDMS substrate with metal traces. Immediately after plasma treatment a 10 μm layer of PDMS was spun on. The sacrificial posts cause ripples to form in the passivation layer during spinning. In order to allow these ripples to dissipate, the sample was allowed to sit at room temperature, before curing, on a level surface for 1.5 hours. The PDMS passivation layer was then cured on a hotplate at 65 °C for 1 hour followed by an oven bake at 75 °C for 4 hours to ensure a full cure.

While the sacrificial posts were 30 μm in height and the PDMS passivation was only 10 μm, a thin residual film of PDMS invariably coats the posts during the spinning process. This thin residual film of PDMS prevents solvent from accessing the posts during sacrificial post removal necessitating etching of the residual PDMS to expose the sacrificial posts. An etching mask was next patterned onto the substrate to protect the passivation layer from the effects of etching. The necessity of this etching mask, while not used elsewhere [82,90], is validated and explained in the results and discussion. After curing of the PDMS passivation layer, the substrate was briefly treated with oxygen plasma for adhesion. A 13 μm layer of the photoresist SPR 220-7.0 (Shipley Company, L.L.C.) was immediately spun on and baked at 90 °C for 10 min with a 1 hour minimum

cool down to room temperature. The SPR 220-7.0 was exposed using an experimentally determined exposure dose of 150 mJ/cm^2. A 1 hour hold time was used after exposure to allow water to diffuse back into the photoresist film, which is necessary to complete the cross-linking reaction. Importantly, a post-exposure bake is not necessary with SPR 220-7.0 before development and helps eliminate the risk of cracking in the photoresist film during the following processing steps. After the hold time, the SPR 220-7.0 was developed and allowed to air dry exposing only the residual PDMS film covering the NR4-8000P sacrificial posts. The substrate was then hard baked in an over at 70 °C for 30 min to anneal the SPR 220-7.0 photoresist film, strengthening it prior to etching of the residual PDMS film. The substrate was subject to SF_6 and O_2 plasma for 6 min to etch the residual PDMS film on the sacrificial posts. Following etching, the SPR 220-7.0 etch mask and NR4-8000P sacrificial post photoresists were stripped from the substrate together. The sample was then baked in an oven at 75 °C for 45 min to evaporate any solvent absorbed by the PDMS substrate during the stripping process. Thus, completed the fabrication of the flexible and elastomeric PDMS based MEAs.

4.2.4 Flexible Parylene C Base MEA Fabrication

Fabrication of flexible Parylene C based MEAs followed a similar process with a few differences. First a 10 µm base layer of Parylene C was deposited on glass coated in 2% Micro-Clean solution to aid in removal of the Parylene C from the glass post-fabrication. For the sake of simplicity, the same lift-off approach utilized for the PDMS based MEAs was used to pattern the Au/Ti electrodes, traces/interconnects, and bonding pads. It should be noted that this approach is not *necessary* to pattern metal on Parylene C based devices as it is with PDMS based devices because Parylene C does not have a high coefficient of thermal expansion (35.5 ppm [110]) relative to photoresists. This is in stark contrast to PDMS (310 ppm [111]).

The sacrificial post method was not used to pattern the Parylene C passivation layer as Parylene C is not deposited in a liquid form, but through a vapor deposition polymerization process. Additionally it is relatively easy to bulk plasma etch Parylene C compared to the difficult in doing so with PDMS as stated previously. The following fabrication steps are represented schematically in Figure 15C with the general steps numbered accordingly. First, the Parylene C substrate with patterned Au/Ti was briefly treated with oxygen plasma in an attempt to increase adhesion and enable the formation of stable bonds to the Parylene C passivation layer. A 5 µm passivation layer of Parylene C was then deposited on the substrate. The same SPR 220-7.0 etch mask as described for PDMS etching was utilized to expose the electrodes and bonding pads of the Parylene C based MEAs. However, etching of the Parylene C passivation layer was performed using only O_2 plasma for 25 min with 90° rotations of the substrate every 5 min to ensure an even and complete etch. The gold electrodes and bonding pads served as an etch stop layer. The remaining photoresist was stripped and MEA baked as described before. Two of the devices tested *in vivo* utilized 15 µm and 10 µm Parylene C base layer and passivation layers respectively to aid in physical handling and Parylene C – Parylene C layer adhesion. These changes were implemented based on personal recommendations from research groups with long standing expertise in Parylene C based MEAs. In these MEA's the SPR 220-7.0 etch mask and annealing step were increased to 15 µm and 80 °C for 2 hours, respectively to ensure the masks' presence during the Parylene C passivation etching process. Additionally the etch time of the Parylene C passivation layer was increased to 45 min with 90° rotations of the substrate every 11 min and a final etch of 4 min to ensure an even and complete etch.

4.2.5 Microchannel Fabrication

First, microchannel walls were patterned onto the MEA's. Adding the SU-8 microchannel walls has been reported previously. (Biomaterials Paper) Briefly, a 100 µm

layer of SU-8 is spun on the MEA's after O_2 plasma treatment to aid in adhesion in the case of the PDMS based MEAs. O_2 plasma was not utilized with the Parylene C based MEAs because delamination was not an issue and due to incomplete development of SU-8 in unexposed regions likely stemming from the significantly increased adhesion. After spinning, the MEAs underwent pre-exposure baking, exposure, post-exposure baking and finally development resulting in microchannel walls patterned on top of the MEAs.

After the microchannel wall fabrication, the capping PDMS layer was adhered. First a 40 μm PDMS layer was spun on clean glass forming the 'top PDMS substrate'. This was a permanent PDMS layer not part of the GT-RE. Its purpose was to account for slight variability in SU-8 microchannel wall heights ensuring contact between the PDMS cover layer and the entire surface area of every microchannel wall. This was then briefly treated with O_2 plasma to aid in 'wetability' after which polyacrylic acid (PAA), a water resorbable layer, was immediately spun on and dried on a hotplate at 65° for 5 min. Next a 5 μm PDMS layer was spun on and cured using a hotplate at 90° for 20 min without allowing the PAA to cool or absorb ambient moisture. After curing, the top PDMS substrate was briefly subject to O_2 plasma again to aid adhesion and a second 5 μm PDMS layer was immediately spun on. During this time, the MEA with SU-8 microchannel walls facing upwards was placed on a hotplate set to 90° in preparation for the top PDMS substrate. After the second 5 μm PDMS layer finished spinning, the top PDMS substrate was immediately placed on the MEA substrate under weight with the uncured 5 μm PDMS layer and SU-8 microchannel walls in contact with each other. The two substrates (MEA and top PDMS layer) were cured together on the hotplate at 90° for 20 min. After cooling the substrates were soaked in water until the PAA dissolved and the top PDMS glass substrate slid easily off leaving the capping 10 μm PDMS layer securely adhered to the SU-8 microchannel walls. The capping 10 μm PDMS layer was formed through the two 5 μm PDMS layers spun on top of each other. Finally the MEAs with complete microchannels were peeled off the glass substrate and the microchannel

region rolled. Importantly, the rolling took place along the substrate base layer forcing the capping PDMS layer to stretch. If the sheet were to be rolled around the top PDMS layer, it would buckle and block the microchannels. To aid in the rolling process, silicone adhesive was applied to the midline of the microchannel region on top of the PDMS capping layer. The silicone adhesive was used to adhere each consecutively rolled layer to the previous to prevent unrolling. The concept of these fabrication steps is represented schematically in Figure 15D.

4.2.6 SMT Integration

Bonding pads on the GT-RE were designed to match those on a PCB to be connected using a surface mount technique similar and translatable to industry standard practices. Silver based conductive epoxy (H20E, Epoxy Technology, Inc.) was used as the junction between the two sets of bonding pads. A small amount of conductive epoxy was first applied to the bonding pads of the GT-RE using the extreme tip of an insulin needle (3/10 cc Insulin Syringe 28G1/2", BD). This was then placed under vacuum to ensure there were no bubbles in the bonding pad region as it was recessed compared to the level of the passivation layer. An 80 µm PDMS spacer, formed by spinning the layer on a separate substrate and cutting samples, was next applied to the bottom of the PCB taking care not to cover any of the PCB bonding pads. The goal of the PDMS spacer was to create an 80 µm bond line between the GT-RE bonding pads and the PCB bonding pads. This bond line is *crucial* to enabling conductivity between the incredibly small bonding pads of the GT-RE and those of the smallest SMDs commercially available. The reasoning for this is explained later in the discussion. Conductive epoxy was then applied to the PCB bonding pads. The clear nature of the PDMS GT-RE and Parylene-C GT-RE made it easy to align the bonding pads by looking through the GT-RE bonding pad region at the PCB bonding pads and align both visually before matting the two by hand. Care was taken to apply only a limited volume of the liquid conductive epoxy to ensure

neighboring bonding pads on the GT-RE or PCB did not short due to inadvertent flow. After mating, the GT-RE and PCB were placed in an oven at 120° C for 20 min to cure the conductive epoxy. The general concept of this approach for SMT integration is shown schematically in Figure 15D and E.

4.2.7 Hermetic Insulation and Encapsulation (Device, Silicone Tubing, & Headcap)

Molds for insulating and encapsulating the PCB region (PCB mold) and headcap (headcap mold) of the GT-RE's were first 3-D printed using an Objet Eden 250 (Stratasys Ltd.). CAD renderings of the two molds utilized are shown in Figure 15F. A uniform 10 μm layer of the AZ P4620 photoresist (MicroChemicals) was then spray coated on all surfaces of the molds using a Suss MicroTec AltaSpray coater, baked, and exposed. The photoresist served as an eventual dissolvable release layer to release the GT-RE PCB region and headcap from the molds.

Prior to insulation and encapsulation in the molds, the GT-RE's were treated briefly with plasma using ambient air as the source to enhance adhesion. Silicone adhesive (40076, Applied Silicone Corporation) was then applied to the cable region between the microchannels and the bonding pads for mechanical protection to aid in handling. The silicone adhesive was applied uniformly over the top, bottom, and sides of the cable region and also served as an encapsulating layer to help with insulation in the body.

Dilute silicone adhesive for use with the PCB mold was prepared by adding 1.5 mL of xylene to 1 g of silicone adhesive in a sealed tube and subjecting it to sonication for approximately 6 hours until the silicone adhesive was completely dissolved. The GT-RE's were again briefly treated with plasma using ambient air to enhance adhesion. The PCB region of the GT-RE's was placed immediately in the PCB mold, immersed in dilute silicone adhesive, and subject to vacuum for approximately 1 hour to ensure all air

bubbles were removed. During the course of vacuuming additional layers of dilute silicone adhesive were added to the PCB mold to account for the shrinking volume of dilute silicone adhesive as the xylene was removed. The dilute silicone adhesive would also shrink during the curing process and was an advantage creating a more robust mechanical seal around protruding components of the GT-RE from the PCB region. The dilute silicone adhesive was allowed to cure for a minimum of 24 hours before the PCB molds were immersed in ethanol. The ethanol dissolved the photoresist release layer and with slight mechanical force, allowed easy removal of the insulated and encapsulated PCB region of the GT-RE. Prior to encapsulating the PCB region, some of the GT-RE's were first briefly treated with O_2 plasma to enhance adhesion and coated with a 10um layer of Parylene C. Later devices avoided this step as adhesion between the GT-RE regardless of PDMS or Parylene C substrate was observed to be strongest with silicone adhesive. In order to protect the exposed microchannel electrodes from being coated in Parylene C, the microchannel region was temporarily enclosed in a Parafilm envelope. Similarly the gold pin connector region of the headcap was enclosed in Parafilm.

The silicone tubes with signal extraction wires were also filled with dilute silicone adhesive aiding in mechanical protection of the signal extraction wires and providing an extra layer of insulation. Silicone adhesive (non-dilute) was also applied to the exterior of the silicone tubes in a ring shape approximately 3 cm away from the PCB region providing a tethering point during implantation as discussed later.

Insulation of the signal extraction wires as they entered the Omnetics headcap followed a similar procedure as the PCB region of the GT-RE. The GT-RE was again treated with plasma using ambient air to increase adhesion. The headcap was immediately placed in the headcap mold, immersed in silicone adhesive (non-dilute) and allowed to cure for a minimum of 24 hours. The headcap mold was immersed in ethanol which dissolved the photoresist release layer and with slight mechanical force, allowed easy removal of the insulated and encapsulated headcap of the GT-RE. It should be

noted, the ends of the signal extraction wires connected to the headcap were already insulated using a proprietary process and epoxy by the Omnetics Connector Corp. As it was not known how effective their process and epoxy would be, in-house insulation and encapsulation of the headcap was necessitated. As a final measure of insulation the GT-RE's were briefly subject to O_2 plasma to enhance adhesion and coated with a final 5um layer of Parylene C. The parafilm enclosures around the microchannel region and gold pins of the headcap were removed and the junction protected with silicone adhesive.

4.3 Results and Discussion

4.3.1 Photolithography on PDMS for Flexible/Elastomeric MEAs and Interconnects

The following details the results of attempts to perform photolithography and photoresist patterning on PDMS. A detailed discussion of the issues preventing success and the theory behind five processing solutions and why they circumvent the issues commonly observed is also present.

Much of the underlying issues with performing photolithography on PDMS stem from the large coefficient of thermal expansion of PDMS (310 ppm [111]). As a result, the PDMS substrate expands and contracts during the various curing steps of the photoresists films. Photoresist films in general do not expand or contract at the same rate however and are subject to extreme stress resulting in the cracking commonly observed. Furthermore, poor adhesion to PDMS requires higher curing temperatures to facilitate adhesion when the photoresists are first applied to the PDMS surface. This is in addition to pre-treatment of the PDMS with O_2 plasma to enhance adhesion. Figure 16A shows the initial results of attempts to pattern the photoresist lift-off mask for metal deposition. As can be clearly seen, there were a combination of cracking and delamination issues commonly observed when performing photolithography on PDMS. Attempts to reduce cracking by reducing the curing temperature resulted in increased delamination. Attempts

to facilitate adhesion to the PDMS substrate by increase curing temperatures, while helping mitigate delamination, resulted in increased cracking. There was no curing temperature found at which both the cracking and delamination could be circumvented as shown by the presence of both in Figure 16A. Figure 16B shows the initial results of attempts to pattern the sacrificial posts for PDMS passivation after metal deposition on the PDMS substrate. Here also there existed a combination of issues including

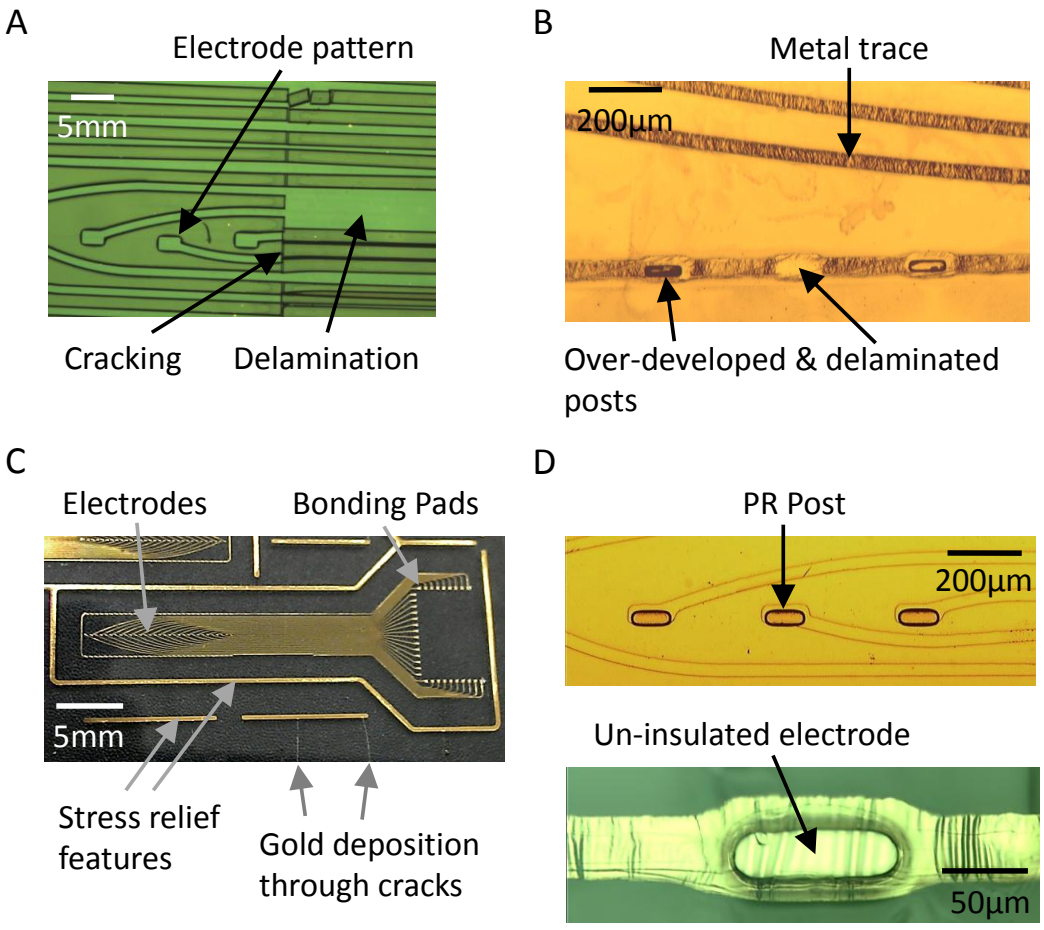

Figure 16. Photolithography, metal patterning and passivation with elastomeric substrates (PDMS).
(A) Traditional photolithography for the photoresist lift-off pattern on PDMS resulting in cracks and delamination. (B) Traditional photolithography for the photoresist sacrificial posts on PDMS resulting in overdevelopment and delamination. (C) Successful metal patterning using the 5 processing solutions enabling patterning on PDMS. Stress relief features can also be observed along with the successful mitigation of crack propagation across the sample. (D) Successful sacrificial post patterning and PDMS passivation using the 5 processing solutions enabling patterning on PDMS.

over-development of the bulk feature and at the photoresist/PDMS interface resulting in structural adhesion failure during washing steps and delamination. As mentioned with the lift-off mask, attempts to increase curing temperatures to reduce development rates resulted in photoresist cracking. Attempts to maintain the correct feature size and prevent delamination by reducing development time resulted in residual photoresist remaining in un-crosslinked areas of the substrate.

A combination of five different novel processing solutions were implemented to circumvent the issues commonly observed with high-density, small feature size photolithography on PDMS. These included first, novel stress relief features observed in the initial lift-off mask design from Figure 14 as well as in Figure 16C after successful Au/Ti metal patterning for the electrodes, traces, and bonding pads. While not having any direct implications to the design of the GT-RE, this novel design incorporation is a crucial design criterion for successful high-resolution photolithography and patterning on PDMS substrates. The stress relief features served to not only significantly decrease the extent of cracking observed in the photoresist films, but also prevent crack propagation through the sample. This is denoted in Figure 16C by the arrow showing gold deposition in a photoresist crack ending at a stress relief feature. Instead of preventing PDMS expansion and contraction during the curing steps of the photoresist the stress relief features *allow* this to occur but in areas away from the device features. This helps reduce the overall stress the photoresist films are subject to. In addition the stress relief features form a protective boundary around the device features helping mitigate crack propagation as previously mentioned. It should be noted, the stress relief features utilized in this study were not optimized and were in fact a first attempt at the design. The success, in combination with the other four processing changes was so large that further optimization was not needed for this study's purposes. The logical next step however would be to optimize the stress relief features for size and shape and understand the interplay this has with device feature design through a finite element analysis and modeling exercise.

Second, thick-film photolithography was used where the photoresist used for both the lift-off mask and sacrificial posts were 30 µm thick as opposed to the 1 µm – 5 µm films commonly used. This increased the inherent strength of the photoresist film and helped further reduce the propensity to crack during the various curing steps. The reduced propensity to crack allowed an increase in curing temperature which helped mitigate delamination. The increased film thickness also enables both the third processing solution following in the next paragraph and the fifth processing solution shortly thereafter. This is an example of how the five processing changes are intertwined and depend on one another.

Third, an oven was utilized for all curing steps for the photoresist films instead of the traditional hot plate. This enabled more controllable curing as well as a differential cure profile of the photoresist film. Heat provided by a hotplate comes from beneath the sample via conduction causing solvent within the photoresist film to rise within the film and eventually leave the film from the surface. In contrast, heat provided by an oven comes from the ambient air inside the oven via convection which uniformly covers the photoresist. As a result the surface of the photoresist cures first creating a skin layer. This skin layer in turn resists the evolution of solvent from the bulk of the photoresist films. [112–114] As a result this dramatically increases curing times needed to obtain a full even cure through the bulk of the photoresist film in comparison to a hot plate. This is usually considered a disadvantage and is a reason why hot plates are the chosen method for photoresist curing. In the case of photolithography on PDMS, this actually provides an advantage. The increased cure time allows for more controllable curing. Of significance, the formation of the skin layer enables the differential cure profile mentioned previously where the skin layer of the photoresist is fully cured as needed for feature definition in photolithography. In contrast the layer of photoresist in contact with the PDMS substrate retains more solvent and is therefore less brittle and less likely to crack during future processing steps. The formation of the differential cure however is

dependent on the photoresist film thickness and is enabled by the second processing solution as mentioned previously. It should also be noted that with small feature sizes the reduced curing of the base of the photoresist film would result in delamination due to poor cross-linking and resulting over-development. Larger feature sizes like those used in the lift-off mask are resistant to this because of the increased surface area in contact with the PDMS substrate and the extra development time needed for delamination to occur.

Fourth, exposure times for small photoresist features, such as the sacrificial posts, were increased by 250% to account for the reduced curing of the features stemming from the third processing solution. The increased exposure resulted in increased crosslinking of the features despite the reduce curing and dramatically reduced the subsequent rate of development. In turn, the reduce rate of development prevented issues with poor feature definition stemming from over-development. The tendency for delamination was also reduced as the interface between the PDMS and photoresist was more resistant to over-development and adhesion failure. It should be noted that the increased exposure time would make defining an undercut at the edge of the photoresist feature difficult. An undercut was not necessary for the sacrificial posts and therefore this limitation did not adversely affect the fabrication of the GT-RE. Increasing the feature size however would prevent the tendency for delamination and allow a reduction of the exposure time enabling the formation of an undercut if it is desired. An example of this is with the photoresist lift-off mask where an undercut was required for adequate lift-off during metal patterning.

Fifth, the method of un-crosslinked photoresist removal was altered from purely development to development and bulk etching, also known as descumming. As mentioned a few times previously developing the photoresist for long periods of time risks bulk over-development of the features generating incorrect feature sizes and shapes. It also drastically increases the likelihood of feature delamination from the PDMS substrate. However, it was found that in order to mitigate these issues the resulting

reduction in development time resulted in residual photoresist left across the surface of the PDMS in non-feature regions. To combat this, the samples were etched using O_2 plasma as part of a prolonged descumming step. Normally this would be an ill-advised processing step as longer periods of etching would also etch the photoresist features generating incorrect feature sizes and shapes similar to over development, in some ways. The interplay with the third and fourth processing changes however prevented this from occurring. The generation of the skin layer during the oven curing steps enabled the surface of the photoresist to be more resistant to etching than the bulk layers of the photoresist, especially those immediately in contact with the PDMS substrate. Furthermore, the significantly extended exposure times in the fourth processing step led to significantly increased crosslinking of the features and as a result, increased resistance to etching compared to non-feature regions.

These five processing solutions directly address the underlying issues faced when attempting photolithography on PDMS. When enacted together they enable successful photolithography on PDMS which can be used for lift-off in metal patterning and sacrificial posts in PDMS passivation patterning. As noted earlier, Figure 16C depicts the results of successful lift-off and metal patterning for the Au/Ti electrodes, traces, and bonding pads. Figure 16D depicts the results of successful sacrificial post patterning and subsequent PDMS passivation patterning after sacrificial post removal. Overall these patterning successes enabled the fabrication of a PDMS based micro-electrode array that was then integrated with microchannels and SMT for peripheral nerve interfacing.

4.3.2 Parylene C MEAs

In contrast to the fabrication of the PDMS MEAs, fabrication of the Parylene C MEAs for the Parylene C GT-RE's was incredibly straightforward and without complication. As mentioned in the methods, the fabrication process used for the Parylene C MEAs was similar in nature to that of the PDMS MEAs. However this was not

necessary because Parylene C is not elastomeric and does not have a large thermal coefficient of expansion (35.5 ppm [110]). The original process for the PDMS MEAs was used merely for the sake of simplicity. That being said, the fact that the fabrication techniques developed for the PDMS MEAs could be used outright for the Parylene C MEAs is an indication of the broad applicability of the fabrication techniques and the five processing solutions. An oven annealing process was also attempted with the Parylene C GT-RE's post MEA fabrication as it has been reported to aid in adhesion between Parylene C layers. [91–93,115] The protocols previously reported were replicated. Unfortunately the increased crystallinity of the Parylene C post-annealing was so high it could no longer be rolled without substantial cracking. Rampant cracking was also observed in the cable region between the microchannels region and bonding pads just over the course of additional fabrication even with significant attempts to handle the device with care. Accordingly the annealing steps were abandoned. It appears that while annealing Parylene C layers is reported to provide advantages in adhesion and water permeation, this can only be utilized in relatively immobilized applications such as retinal or cortical interfacing. [91,115–117] This is likely due to the reduced need for flexible devices and the lack of large mechanical motion with the brain and retina compared to the limbs of an individual or animal.

4.3.3 Microchannel Patterning & 3-D Configuration

While patterning SU-8 microchannel walls on PDMS has been previously reported [109], significant challenges were initially encountered when attempting this on the PDMS MEA's. Initial attempts resulted in tunnels present at the bottom of the SU-8 microchannel walls. This can be observed in Figure 17A where a top down view depicts the tunnels running through the entire width of the microchannel walls and a side view of

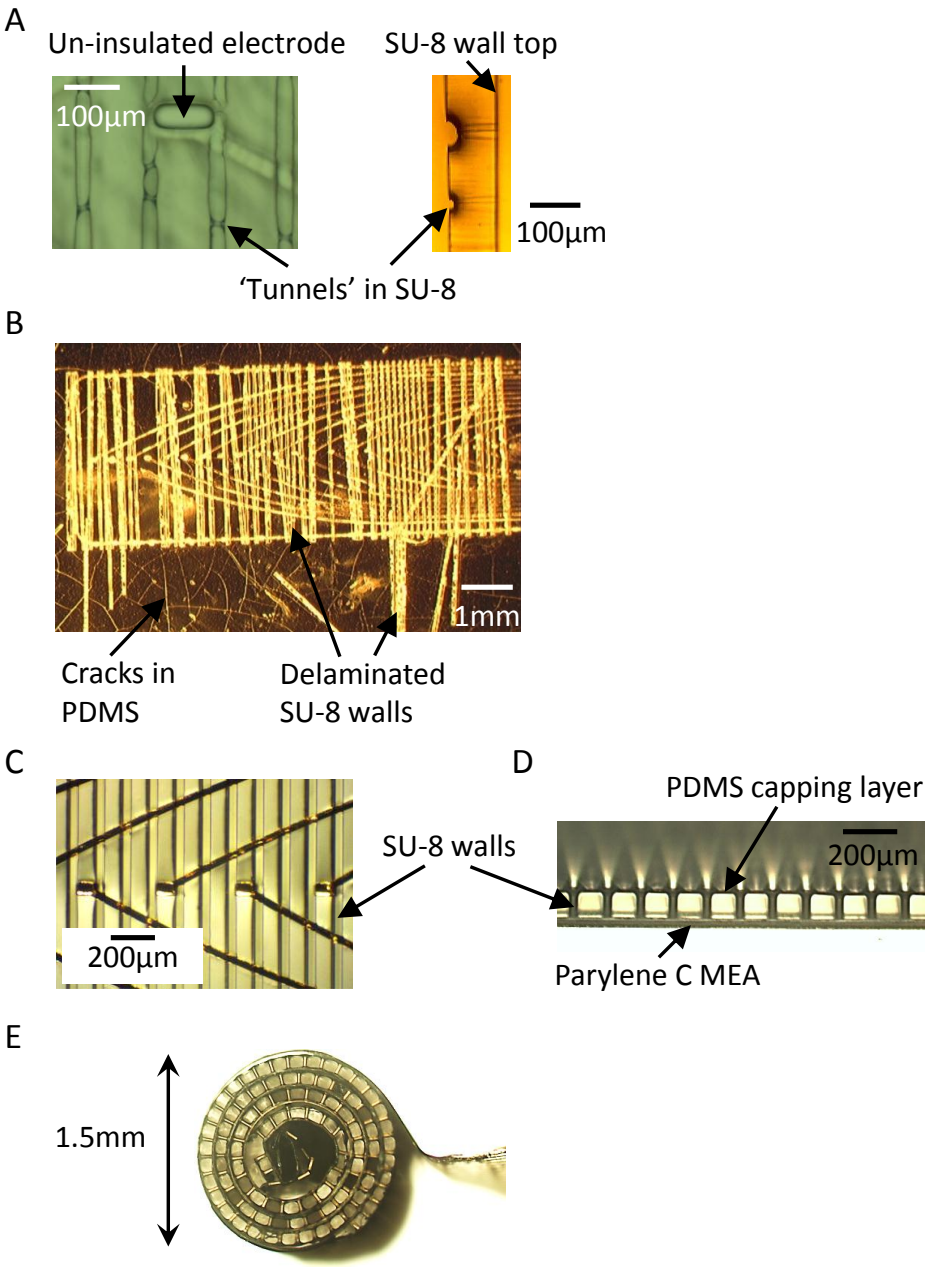

Figure 17. Microchannel patterning and 3-D configuration.
(A) Tunnels in SU-8 microchannel walls stemming from cracks in the PDMS passivation layer shown through a top down and side view of the SU-8 walls. (B) Cracking of the PDMS passivation layer stemming from the previous PDMS etching step and mass delamination of the SU-8 microchannel walls. Tunnels are present within the SU-8 walls, but are not visible at this magnification. (C) Successful patterning of SU-8 microchannel walls after utilizing an etching mask during the PDMS passivation fabrication. (D) Addition of the PDMS capping layer to the top of the SU-8 microchannel walls forming a sheet of microchannels. (E) Rolled sheet of microchannels forming a cylinder of microchannels matching the dimensions of a nerve. The electrode trace cable connecting to bonding pads (out of image) can be seen on the right.

the microchannel walls depicts the cavity at the bottom of the SU-8 microchannel wall. These tunnels were present on almost every microchannel across every sample fabricated. After investigation it was found these tunnels corresponded to cracks in the PDMS passivation layer. These cracks were present across the entire surface of the PDMS passivation, even in non-device regions. It was hypothesized that the cracks were enlarged during the SU-8 curing steps and as a result created a non-uniform heat profile at the bottom of the SU-8 microchannel walls. This resulted in poor crosslinking directly above the cracks and tunnel formation during development. Attempts to reduce the curing temperatures to reduce the crack enlargement not only did not reduce the presence of cracks, but also resulted in mass delamination of the SU-8 feature due to poor adhesion. This can be observed in Figure 17B where cracks in the PDMS passivation are widely present and SU-8 delamination is also easily visible. The lighting was held at an angle to emphasize the cracks in the passivation layer.

Given that the cracking was only present in the passivation layer, it was hypothesized that they were a result of the etching the PDMS passivation layer during the sacrificial post patterning. It should be noted that cracks running over gold traces did not result in cracks within the gold traces thereby indicating the cracks were only present in the passivation layer. As described in the methods, a PDMS passivation layer etching mask was patterned prior to etching to protect all regions of the PDMS. As a result of the presence of the etching mask, all cracking in the passivation layer was mitigated. Furthermore, there was no evidence of tunnel formation with the SU-8 microchannel walls. Successful patterning of the SU-8 microchannel walls on the PDMS MEA can be observed in Figure 17C along with the lack of cracks and tunnels. The microelectrodes were positioned every third microchannel in the middle of the microchannels. Based on these results it was concluded that the cracking observed in the PDMS passivation layer stemmed from the etching of the PDMS passivation to undercover the sacrificial posts. Cracking was also observed when etched with CF_4 instead of SF_6. While this has not

been reported previously using a similar etching processes, prior studies did not attempt to pattern on top of etched PDMS and would not have encountered this issue. [82,90,118,119]

Patterning SU-8 microchannel walls on the Parylene C MEAs for the Parylene C GT-RE's was in contrast fairly straightforward again and proceeded according to previously published work as mentioned in the methods. However, it is worth noting that initial attempts included a brief O_2 plasma treatment which resulted in residual SU-8 remaining post development in un-exposed regions. This was predominantly the case on the gold electrodes and bonding pads and is thought to be due to significantly enhanced adhesion to the gold. Accordingly the O_2 plasma treatment was avoided. Delamination in either case was never observed.

After successful patterning of the SU-8 microchannel walls on both the PDMS and Parylene C MEAs, the capping 10 μm PDMS layer was adhered on top of the walls as shown in Figure 17D for an example Parylene C MEA. The methodology reported here for accomplishing this, while similar, was significantly less complicated and intricate than previously reported. [109] There were a total of 97 microchannels and when this sheet of microchannels was rolled, it formed a cylinder of microchannels approximately 1.5 mm in total diameter (Figure 17E). The use of silicone adhesive to prevent unrolling of the microchannel layers in the Parylene C GT-RE's proved highly effective as unrolling was never an issue. However, if silicone adhesive was not used, it was found to be impossible to keep the microchannel sheet rolled long enough to enable placing the nerve cuff around it. Silicone adhesive was not necessary with the PDMS GT-RE's as the various PDMS layers adhered well to each other and prevented unrolling. A consequence of rolling the microchannel sheet by hand was the tendency to obtain more of an oval cross-section as opposed to perfectly circular. This however was an inconsequential result and did not affect device performance. Additionally, there was a small open core through the center of the rolled microchannels. This has been reported

previously and does not adversely affect regeneration through the microchannels themselves. [109]

4.3.4 SMT Integration

Easily integrating micro-chips and other electronics is incredibly important to the overall utility of any flexible/elastomeric device, not just the GT-RE or a peripheral nerve interface. As mentioned previously it provides the opportunity to integrate components into the device, such as a high channel wireless data transmission chip, which may not exist yet. The vast majority of electronic components commercially available come in surface mount packaging necessitating surface mount integration techniques which have traditionally been challenging and complex.

The methodology reported here directly addresses this need, is incredibly simply to implement and is translatable to industry practices. As mentioned in the methods a spacer was used to set an 80 μm bond line between the surface mount bonding pads of the PCB and those of the GT-RE. This bond line is crucial and is what enables the surface mount approach to provide stable conductivity. Due to the incredibly small bonding pads and proximity between the pads of the GT-RE and those on commercial components available, an incredibly small volume of conductive epoxy is necessitated to avoid shorting neighboring bonding pads. Initial attempts to merely place a small volume of conductive epoxy between the sets of bonding pads without the spacer yielded an open circuit despite the presence of conductive epoxy.

The conductive epoxy is a two part solution consisting of an epoxy base and silver particles. It was observed that application of small volumes led to a reduced ratio of silver particles to epoxy. This was believed to be the inherent issue behind the poor conductivity. Furthermore, upon curing the epoxy shrinks and with the reduced number of silver particles this led to an open circuit. This was validated experimentally by drawing straight conductive epoxy traces of different thicknesses/widths on glass. As the

volume of the trace was reduced, conductivity from one end of the trace to the other also disappeared. Based on these observations, the devised solution became to ensure a larger presence of silver particles in the volume of applied conductive epoxy. As the conductive epoxy was supplied by the manufacturer at a standard ratio of silver particles to epoxy, reducing the epoxy content was not feasible. Furthermore, reducing the epoxy content would have increased the viscosity of the conductive epoxy making it extremely challenging to deliver small volumes on the order of a single nanoliter.

Instead a spacer was introduced between the sets of bonding pads to enable a larger volume of conductive epoxy (2 – 3 nanoliters) to be applied without concern of shorting neighboring bonding pads. This volume was calculated based on the size of the bonding pads and the thickness of the spacer. The spacer created an 80 µm bond line which provided a larger z-axis for the conductive epoxy to occupy. This can be observed in Figure 18A where a side view of the GT-RE bonding pads and PCB ponding pads is shown with a 'column' of conductive epoxy providing the electrical connection. In this image a 120 µm bond line was used to aid in visualization. A top down view is also shown where both sets of bonding pads can be seen along with conductive epoxy and another set of bonding pads lacking conductive epoxy. The slight increase in volume of conductive epoxy determined by the bond line ensured a higher silver particle to epoxy ratio which resulted in a closed circuit between the sets of bonding pads. Of note, the GT-RE bonding pads were 190 µm x 105 µm which is comparable to the terminals of the smallest commercially available chip resistors (01005: 200 µm x 100 µm terminals) and components used in today's electronics. The 'column' of conductive epoxy proved to be mechanically stable as failure due to the GT-RE – PCB junction was *never* observed during the fabrication process or after implantation. Attempts to physically remove the PCBs from the PDMS substrate resulted in failure and tearing of the PDMS substrate, not the PDMS-conductive epoxy interface indicating a high bond strength. Furthermore, the bond line mandates only a *modest* increase in device footprint (thickness) by 80 µm and

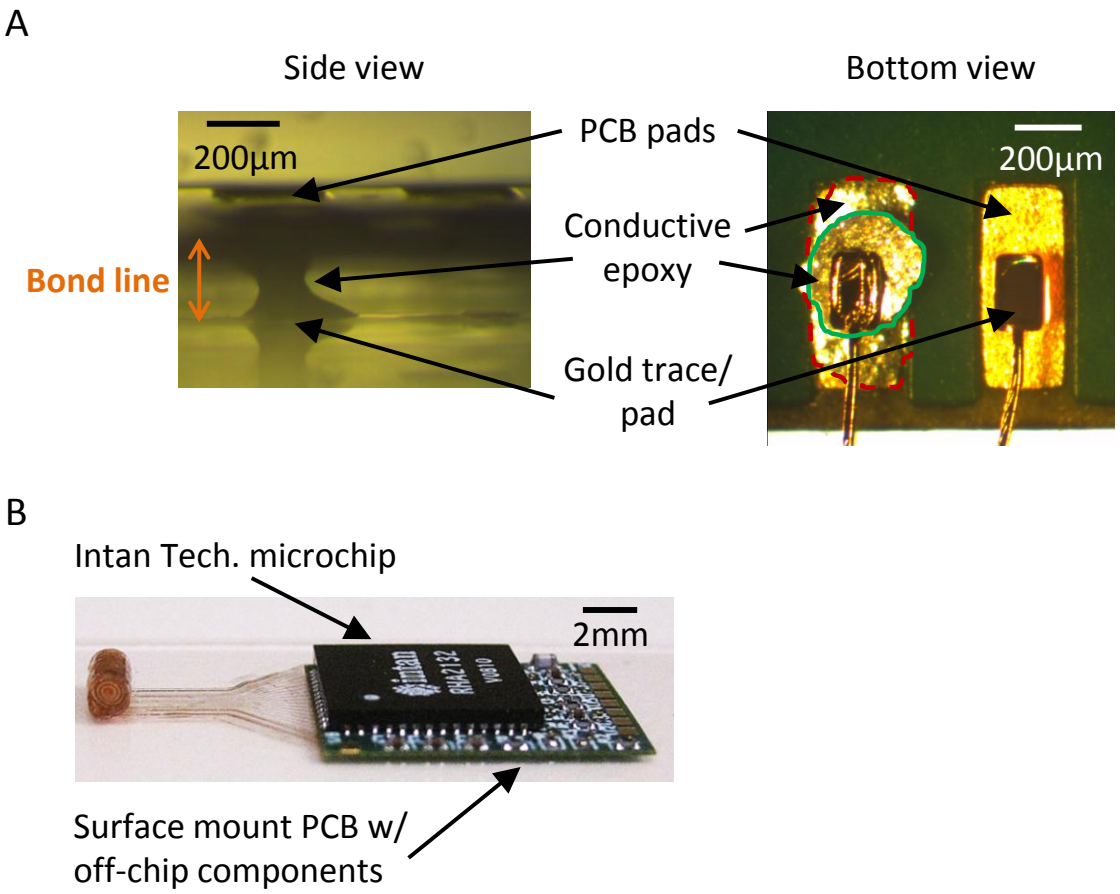

Figure 18. Surface mount technology (SMT) integration.
(A) Side view and bottom up view of a surface mount PCB attached using a column of conductive epoxy. The bondline resulting from the spacer (out of image) between the substrate MEA and PCB is identified in the side view. Two layers of conductive epoxy pertaining to two connected sets of bonding pads are shown in the bottom up view. (B) Integration of the Intan Technologies microchip and off-chip components with the GT-RE.

is unlikely to affect any application utilizing this approach. In fact, a bond line of 40 µm was validated for conductivity but was not utilized due to difficulties with hand application of such small conductive epoxy volumes. Industry grade dispensers would likely not have this issue. This approach is therefore widely applicable to the integration of the smallest surface mount devices commercially available with flexible and elastomeric substrates for a wide range of applications.

The goal of developing this SMT integration approach was to allow the easy integration of both the Intan Technologies 32 channel multiplexer amplifier chip (including off-chip components) and a PCB hub with signal extraction wires. The Intan Technologies chip was integrated with the PDMS GT-RE (Figure 18B) and was utilized only in an *in vitro* setting for reasons detailed later. The PCB wire hub with signal extraction wires was integrated with the Parylene C GT-RE and was utilized in an *in vivo* setting.

4.3.5 Hermetic Packaging

To enable operation of the PDMS GT-RE with the Intan Technologies chip and the Parylene C GT-RE with the PCB wire hub in aqueous based environments such as peripheral nerve interfacing, hermetic packaging techniques were developed. These techniques centered on the use of Parylene C for insulation and silicone adhesive for mechanical protection and insulation. While Parylene C was deposited using vapor deposition polymerization, the silicone adhesive was supplied as a viscous liquid requiring the development of molds for encapsulation and a release layer from the molds. The release layer utilized was a positive photoresist which was spray coated uniformly over the mold. This was a highly effective release layer allowing easy removal of the encapsulated parts. It is important that a positive photoresist was used because exposure to light allowed the photoresist to become soluble in developers. Negative photoresists on the other hand would have undergone crosslinking when exposed to light making them insoluble and necessitated that the mold be utilized in a dark room devoid of light to avoid crosslinking.

In addition to the insulation and encapsulation of the PCB hub with the Parylene C GT-RE's, the signal extraction wires were divided up, braided and threaded through two silicone tubes for mechanical protection and further insulation. This can be seen in Figure 19. The dimensions of the PCB hub were 6 mm x 9 mm and after encapsulation

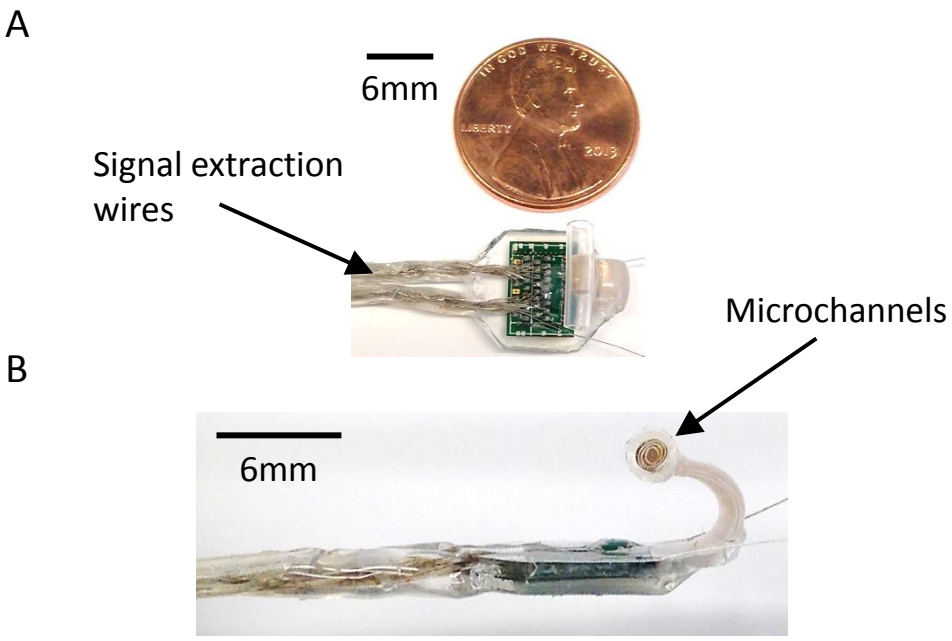

Figure 19. Hermetically encapsulated Parylene C GT-RE integrated with signal extraction wires for in vivo implantation.
(A) Top down view showing the surface mount PCB with signal extraction wires. (B) Side view where the microchannel region is visible.

the total footprint of the GT-RE was approximately 9 mm x 12 mm. The cable connecting the microchannel micro-electrodes to the bonding pads was kept at an angle during silicone adhesive encapsulation which forced it to cure in the angle observed. This allowed the microchannel region to be placed over the PCB and reduce the overall footprint of the GT-RE. A local ground wire can also be observed near the PCB region.

In these images, the stainless steel wrap around the microchannels has been omitted to enable better visualization of the microchannel region and nerve cuff. The encapsulated PDMS GT-RE with the Intan Technologies chip can be observed in Figure 20. Here the microchannel region was left unrolled and lacked the SU-8 microchannel walls to demonstrate the potential flexibility and stretchability of the PDMS MEA.

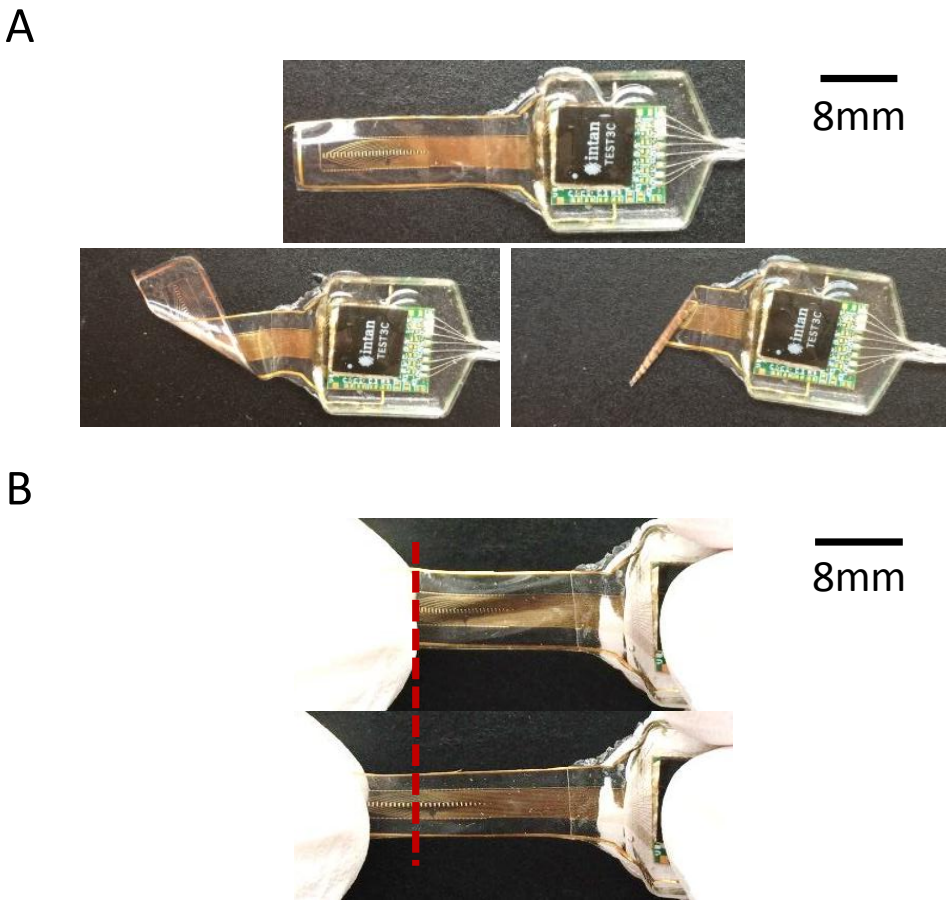

Figure 20. Hermetically encapsulated PDMS GT-RE integrated with Intan Technologies microchip for multiplexing and amplification.
(A) Examples of the PDMS GT-RE flexibility. (B) Example of PDMS GT-RE stretchability. Note that in these images the GT-RE lacked the SU-8 microchannel walls for demonstration purposes.

The hermetic packaging for the PCB region and headcap was the most challenging aspect of the entire fabrication process as the silicone adhesive steps were largely done by hand application or utilized molds for encapsulation. During the silicone adhesive encapsulation small air bubbles would occasionally remain within the silicone adhesive during the curing process. These were not a concern however as they were not in contact with the PCBs, signal extraction wires or any other electrical connection. So while silicone adhesive is an imperfect moisture barrier and moisture /water would eventually accumulate within the air bubbles, this would not adversely affect the function

of the GT-RE's. Regarding the signal extraction wires, braiding and filling the silicone tubes with silicone adhesive proved to be a mechanically robust method of protecting them from mechanical forces during fabrication and implantation. Due to the braiding and presence of the silicone adhesive, any forces applied to a single wire would get distributed across the 16 other wires within the silicone tube. Breakage of wires was never observed.

4.4 Conclusions

Taken together, the five processing solutions for photolithography on PDMS, SMT integration technique, and hermetic packaging approaches enabled the fabrication of flexible and elastomeric GT-RE's with PDMS or Parylene C as the substrate material for use as an implantable peripheral nerve interface. Besides applicability to peripheral nerve interfacing, the five processing solutions developed enable the patterning of high-density MEAs and interconnects using industry translatable processes for flexible and stretchable electronics. The novel stress relief features provide a new avenue of investigation for mask design criteria when patterning on materials with large thermal coefficients of expansion. Furthermore, the interplay between thick-film photolithography, oven curing processes, exposure time, feature size, and development vs. etching are all important considerations which need to be evaluated together. Any one of these alone is unlikely to enable mass development of PDMS based electronics. However together, they drastically increase the viable processing window one can utilize for fabrication. The SMT integration technique developed addresses the critical need for an easy, industry translatable technique for incorporating off the shelf commercial components necessary for advanced flexible/elastomeric electronics, including neural interfaces. The hermetic packaging approach utilized two established methods for insulating and encapsulating the GT-RE enabling evaluation in an aqueous environment, a fundamental criterion for awake and freely moving electrophysiology in animals.

CHAPTER 5

Evaluation of the Georgia Tech Regenerative Electrode (GT-RE) for Single Unit Action Potential Recordings

5.1 Introduction

Today, neural prosthetics provide a small fraction of the functionality of the natural limb they are meant to replace. However, compelling evidence in the last decade has shown that amputees retain significant motor and sensory function in peripheral nerves post-amputation which has paved the way for bidirectional sensorimotor prosthetics. [1] A bidirectional sensorimotor prosthetic aims to record volitional motor commands from peripheral nerves to control a robotic limb, while sensors on the device produce direct stimulation of peripheral nerves to deliver sensory feedback. Advances in robotics have led to high dimensionality robotic limbs, but the peripheral nerve interface (PNI) remains the "weak-link" due to the lack of reliable, specific engagement of large numbers of independent electrodes with the peripheral nerve. It is imperative for a fully functional peripheral interface to communicate with the nerve in a highly specific and reliable manner so to deliver and receive discrete information relevant for natural sensation and movement.

Penetrating peripheral nerve interfaces, such as the Utah Slanted Electrode Array, must penetrate the nerve in order to place its electrode tips near axon profiles and provide the specificity needed. [39,41,120] Cuff electrodes have seen some clinical translation and mitigate this injury to the nerve, but do so at the expense of recording and stimulation specificity. [36–38] The cuff electrodes reside outside the nerves epineurium where the distance from axons is too great to record single unit action potentials. [6,39] Accordingly, while being helpful in a number of clinical applications, their overall utility is limited. Regenerative peripheral nerve interfaces, including the traditional Sieve

electrode, seek to provide a balance of specificity without nerve injury by allowing nerves and axons to regenerate close to integrated electrodes. [48,51,54,121,122] It is important to note that this in many ways necessitates a target clinical population of amputees or individuals with a nerve injury where the device can be implanted at the time of surgery. Unfortunately all of these hallmark peripheral nerve interfaces, while significant engineering accomplishments, fail to record large numbers of single unit action potentials from axons chronically and cannot enable the full functionality of a robotic limb. [4–6,39,40,53,54]

Microchannels are a relatively new approach to peripheral nerve interfacing and offer some unique and significant advantages over these previous approaches. One of the fundamental issues with peripheral nerve interfacing is the low impedance extracellular fluid surrounding axons. This low impedance fluid significantly reduces the extracellular amplitude of action potentials (APs) by effectively shunting them to ground and as a result reduces the viability of all previous PNI approaches. [6] Another important consideration is the node of Ranvier placement which occurs at least every 2 mm along the length of an axon. [7,55] Nodes of Ranvier are locations of an axon where the AP is largest in amplitude due to a gap in myelin insulation. This forces a spatial requirement on peripheral nerve interfacing where electrodes need to be as close to the nodes as possible. Previous peripheral nerve interfacing approaches are unable to take this spatial requirement into account, again reducing overall electrode viability. [6,39,46,53] In contrast, axons can be placed or forced to regenerate through small microchannels on the order 100 μm. Doing so effectively constrains the low impedance extracellular fluid thereby increasing the extracellular resistance and preventing the AP signal from dissipating as easily. As a result the extracellular amplitudes of the APs are significantly larger enabling higher signal to noise recordings. [6] Furthermore, making the microchannels longer than 2 mm effectively guarantees the presence of a node of Ranvier within the microchannel. This coupled with the increased extracellular resistance enables

node of Ranvier independent recordings because the amplitude of the AP signal is relatively constant throughout the microchannel. [6] This theory has been modeled and well validated in previous *in vitro* studies. [6,56]

Microchannel *in vivo* studies have focused on evaluating the efficacy of recording single unit action potentials using electrodes contained within the microchannels. These rodent studies have ranged from acute recordings where axons have been placed within microchannels to terminal recordings after chronic implantation where axons have regenerated through microchannels. [49,50,58,59,109] Significant work has also gone into validating the chronic stability of nerves and axons after they have regenerated into and through microchannels with an eye towards clinical translation to an amputee population. [109] However, none of these previous studies have evaluated a fully integrated microchannel interface with large numbers of microelectrodes and signal extraction capabilities enabling recordings in awake and freely moving rodents. This is a needed next step on the path towards clinical translation.

Here we have developed and evaluated a microchannel interface, the Georgia Tech – Regenerative Electrode (GT-RE), and its ability to be utilized for challenging single unit action potential recordings in awake and freely moving rodents. First, *in vitro* functionality of the GT-RE's was explored using artificial neural signals. Secondly, *in vitro* dorsal root ganglia (DRG) studies were utilized to validate cytocompatibility after microfabrication of the GT-RE's which involved a number of toxic solvents and processes. Finally, *in vivo* the large electrode count GT-RE's were implanted in the rat sciatic nerve transection model. *In vivo* recordings were performed while the rats were awake and ambulating to evaluate the capability to record single unit action potentials through microchannel interfaces.

5.2 Materials and Methods

5.2.1 GT-RE Design

The basic concept of the GT-RE microchannel interface was shown previously in Figure 13. A micro-electrode array (MEA) was integrated into a flexible polymer layer, either PDMS or Parylene C. The electrodes were 80 µm x 40 µm and spaced once every third microchannel to allow for an equal distribution of electrodes throughout the cross-section of the GT-RE post rolling. A common bipolar reference was placed near the bonding pads and a common pseudo-tripolar reference was designed with electrode sites at the entrance and exit of every microchannel containing an electrode. In some cases during *in vivo* testing a local low impedance wire was used as a bipolar reference instead. The referencing design along with the electrodes, traces, and bonding pads was shown previously in Figure 14. SU-8 microchannel walls were patterned on top of the flexible MEA and a capping PDMS layer was then adhered on top of the SU-8 microchannel walls. This formed a sheet of 97 microchannels with electrode sites housed in the base of the microchannels. This sheet was rolled perpendicularly to the direction of the microchannels forming a cylinder matching the shape and size of the rat sciatic nerve. The microchannels were 100 µm wide, 100 µm tall, and 3.5mm long with 20 µm wide microchannels walls. These dimensions were based on previous work that in part investigated microchannel sizes and the relationship to nerve regeneration in a clinically translatable amputee animal model. [109]

Metal traces connected to the micro-electrodes in the microchannels ended at a series of bonding pads intended for surface mount connection to a PCB. The PCB integrated with the PDMS GT-RE's contained the Intan Technologies 32-channel amplifier multiplexer micro-chip (RHA2132) and associated components. The PDMS GT-RE's were utilized in *in vitro* functional testing. The PCB integrated with the Parylene C GT-RE's was used as a wire attachment hub and had 34 multi-stranded

stainless steel wires soldered accounting for the electrodes, references, and a local ground. These signal extraction wires were connected to an Omnetics 36 channel percutaneous connector which allowed eventual connection to a separate off-board amplifier for electrophysiology experimentation. The Parylene C GT-RE's were used in both *in-vitro* and *in vivo* functional testing.

5.2.2 *In Vitro* Functionality

Previously recorded neural signals were used as an artificial signal source to evaluate the GT-RE functionality. The GT-RE's were placed with the electrode/microchannel region submerged in PBS. The previously recorded neural signals were output from a computer as an audio signal and, using a stripped audio cable submerged into the PBS, played into the PBS. It was attempted to then record the artificial neural signals through the PDMS GT-RE electrodes integrated with the Intan Technologies micro-chip or the Parylene C GT-RE electrodes integrated with the PCB hub for signal extraction wires.

5.2.3 *In Vitro* Cytocompatibility

In vitro cultures of lumbar dorsal root ganglia (DRGs) were used to assess the cytocompatibility of the GT-RE's post fabrication accounting for the fabrication process and various solvents used. Given the similarity between the fabrication process for the PDMS and Parylene C GT-RE's and the fact that cytcompatibility was previously evaluated for PDMS/SU-8 microchannels [109], only Parylene C GT-RE's were utilized in this experiment. The culture methodology has been previously reported [109]. Briefly, unrolled GT-RE's lacking the PDMS cover layer were placed at the bottom of tissue culture wells. No protein coatings of any kind, such as laminin, were used to help with cell adhesion or overall cytocompatibility. DRG's were explanted from P0 rat pups, the nerve roots were dissected away and the DRG's were placed on the unrolled GT-RE's at the entrance to the microchannels. During the first several hours of incubation a thin layer

of DMEM/F12 media with 10% fetal bovine serum and 50 ng/mL nerve growth factor (NGF) (Roche) was applied prevent the DRG's from floating and allow adhesion to take place. Following this the culture wells were filled with the same media which was replaced every two days including the NGF.

The DRG cultures spanned a total of two weeks at which point they were fixed with 4% paraformaldehyde in PBS for 20 min and washed three times with 1X PBS. To allow visual assessment of neurite outgrowth, Schwann cell migration, and overall cytocompatibility, the cultures were reacted with antibodies to the 160 kDa neurofilament protein (1:500, mouse IgG1 NF160, Sigma) and S-100 (1:250, rabbit IgG S100, Dako) overnight at 4° C. This was followed by the secondary antibodies goat anti-mouse IgG1 Alexa 594 (1:220, Invitrogen) and goat anti-rabbit IgG Alexa 488 (1:220, Invitrogen). Finally, cell nuclei were marked by incubating in DAPI diluted to a concentration of 10 mM in PBS for 15 min at room temperature. The fluorescently labeled cells and nuclei were visualized using a Zeiss upright microscope and the images were captured with an Olympus digital camera.

5.2.4 GT-RE Implantation, Electrophysiology and Signal Analysis

To prepare the GT-RE's for implantation, a silicone tube was placed around the rolled microchannels acting as a nerve cuff for suturing. Stainless steel foil (Multipurpose 304 Stainless Steel Foil .002" thick, McMaster-Carr) was then wrapped around the nerve cuff and connected to a ground wire acting as an implantable electrical shield for the GT-RE. The stainless steel wrap served as a large ground and pseudo-faraday cage to help shunt EMG and other electrical artifact to ground. There was also another short 2 cm wire emanating from the headcap which was wrapped around a stainless steel screw using to secure the headcap to the skull. This served as another ground in the case of wire breakage. For sterilization purposes, the GT-RE's were immersed in ethanol for 24 hours. A vacuum line was used to ensure ethanol was drawn into and through the microchannels

and to prevent bubbles from remaining. After 24 hours the GT-RE's were transferred to sterile PBS and incubated for another 24 hours to remove all traces of ethanol prior to implantation. The transfer took place without breaking a liquid environment ensuring air was not introduced to the microchannels.

The GT-RE's were implanted in the rat sciatic nerve transection animal model. In isoflurane anesthetized rats, the sciatic nerve was transected at the mid-thigh and the GT-RE was sutured to the proximal and distal segments of the cut nerve. The musculature was then reapposed with the two silicone tubes containing the 34 signal extraction wires emerging from between the muscle flaps. The silicone tubes and attached headcap were burrowed subcutaneously to a midline incision at the top of the skull. Importantly, the silicone tubing was tethered using non-resorbable 5-0 sutures to the underlying musculature along its path to the skull in order to provide strain relief during normal rat movement. These tethering points occurred near the upper thigh and then again above the spinal cord by the pelvis creating a large S-shaped curve. At the midline incision, the periostium was retracted with a periostium scraper. 40% phosphoric etch gel (Henry Schein) was applied to clean the skull surface and six stainless steel screws were drilled into the skull. Screws were placed anterior to bregma, posterior to bregma and posterior to lambda, on both sides of the midline. Next, the burrowed head stage was situated onto the skull and affixed using UV curable dental cement (Henry Schein) which was applied to the screws and the head stage. The skin was then wound clipped around the head cap forming a percutaneous connector for the electrophysiology experiments.

Electrophysiology experiments were performed 3 weeks after the GT-RE implantation. Recordings using the GT-RE were taken while the implanted rats were ambulating on a treadmill in order to record 'naturally occurring' single unit action potentials. This is in contrast to electrically evoked multi-unit activity which requires stimulation of the nerve and is not nearly as challenging or translatable in terms of assessing neural interfacing capability. The general electrophysiology methodology has

been reported previously. [123,124] Briefly, the rats were placed on a level, single lane Plexiglas-enclosed treadmill (53 cm x 10 cm x 14 cm; Columbus Instruments, Columbus, OH, USA) set to a modest speed of 10 m/min. The implanted GT-REs were connected to an amplifier through the percutaneous headcap connector. 100 seconds of recordings were taken, amplified by 1000x using a bandpass of 300 – 3000 Hz and digitized for off-line analysis. Additional filtering was performed in software from 400 Hz to 3200 Hz using a 4 pole Butterworth filter. All recorded signals were sampled at 10KHz. Single unit action potentials were identified and sorted using the publicly available semi-automated spike sorting algorithm Wave_clus. [125]

The number of microelectrodes that recorded single unit action potentials was used to determine the overall electrode yield of the GT-RE. To ensure that the identified single unit action potentials were not double counted across two or more electrodes, a cross-talk screen was performed. One millisecond time windows centered on the timestamps of an AP recorded using a given electrode in a device were compared to the timestamps of all other APs identified across all other electrodes of the same device. If there was more than 50% overlap between the occurrence/timestamps of multiple APs, the waveforms were visually analyzed for similarity in shape, excluding differences in amplitude and numbers of occurrence. Similarity in amplitude was not used as determinant criteria of cross-talk due to the fact that if an action potential acquired from a given electrode also appeared on another through cross-talk, it would likely appear reduced. The number of occurrences of the single unit action potentials was also not used as a determinant criteria based on similar logic. The number of occurrences of an AP could at most be the same, if not likely fewer on the receptive electrode than the source electrode conducting the true signal. If it was determined that across two or more electrodes the waveform shapes were visually identical, the action potential was then assigned to the electrode which recorded the largest average amplitude and greatest number of occurrences of that waveform.

5.3 Results

5.3.1 *In vitro* Functionality

The GT-RE's microelectrodes were functionally tested *in vitro* for their ability to be used to appropriately detect neural signals. The microelectrodes had a mean impedance of 640 kΩ measured at 1 kHz. Evaluating the ability to record neural signals was accomplished by recording an audio neural signal played into PBS containing the GT-RE. A schematic of the setup is shown in Figure 21A. An example of the recorded audio neural signals, along with a magnified portion showing single unit action potentials, taken using the Parylene C GT-RE integrated with the PCB hub for signal extraction wires is shown in Figure 21B. This recording was obtained from a single microelectrode of the Parylene C GT-RE. Single unit APs as small as approximately 30 μV in amplitude were successfully recorded. A similar recording taken using the PDMS GT-RE integrated with the Intan Technologies 32 channel multiplexer amplifier chip is shown in Figure 21C. Microelectrodes with traces that were physically cut on purpose in both the Parylene C and PDMS GT-RE's did *not* result in successful recordings of the audio neural signals, as expected.

5.3.2 *In vitro* Cytocompatibility

DRGs were cultured on unrolled GT-RE's lacking the capping PDMS layer to assess overall cytocompatibility for a peripheral nerve interfacing application. In general the DRGs adhered well to the Parylene C where they were initially placed at the entrance to the SU-8 microchannels. A representative DRG culture stained for axons (red) and Schwann cells (green) is shown in Figure 22A. The electrodes and traces are the curved darker vertical lines and the SU-8 microchannel walls are the faintly fluorescent horizontal lines. The DRG is located on the left side of the microchannels. Portions of the image appear overexposed due to the high degree of cellular growth. Despite the intense fabrication process and exposure to toxic chemicals, the GT-RE's were readily capable of

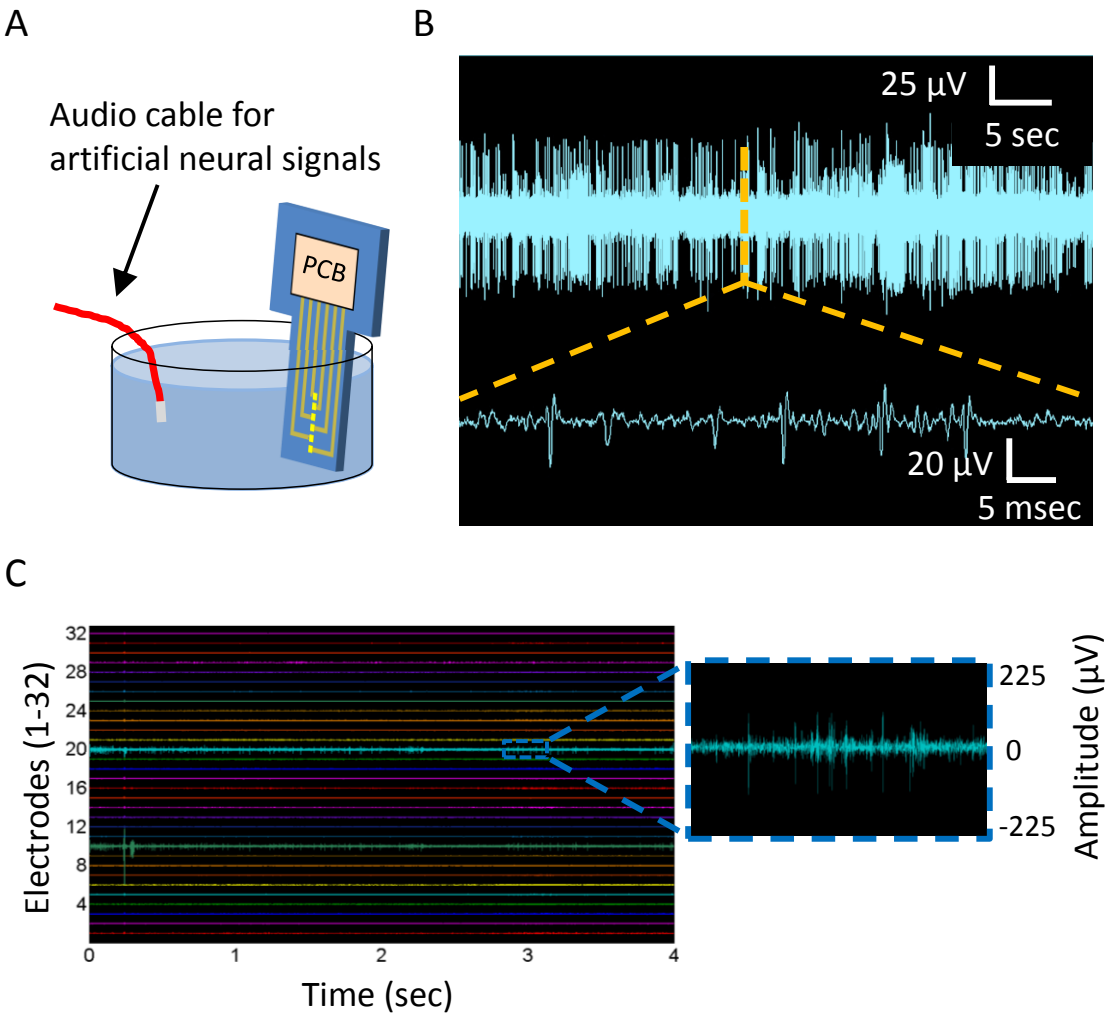

Figure 21. In vitro functional testing using artificial neural signals.
(A) Schematic of *in vitro* setup where an audio cable was used to play artificial neural signals into PBS containing the GT-RE. (B) Example recording of the artificial neural signal taken using the Parylene C GT-RE integrated with a PCB hub for signal extraction wires validating functionality. (C) Example recording of the artificial neural signals taken using the PDMS GT-RE integrated with the Intan Technologies microchip validating functionality.

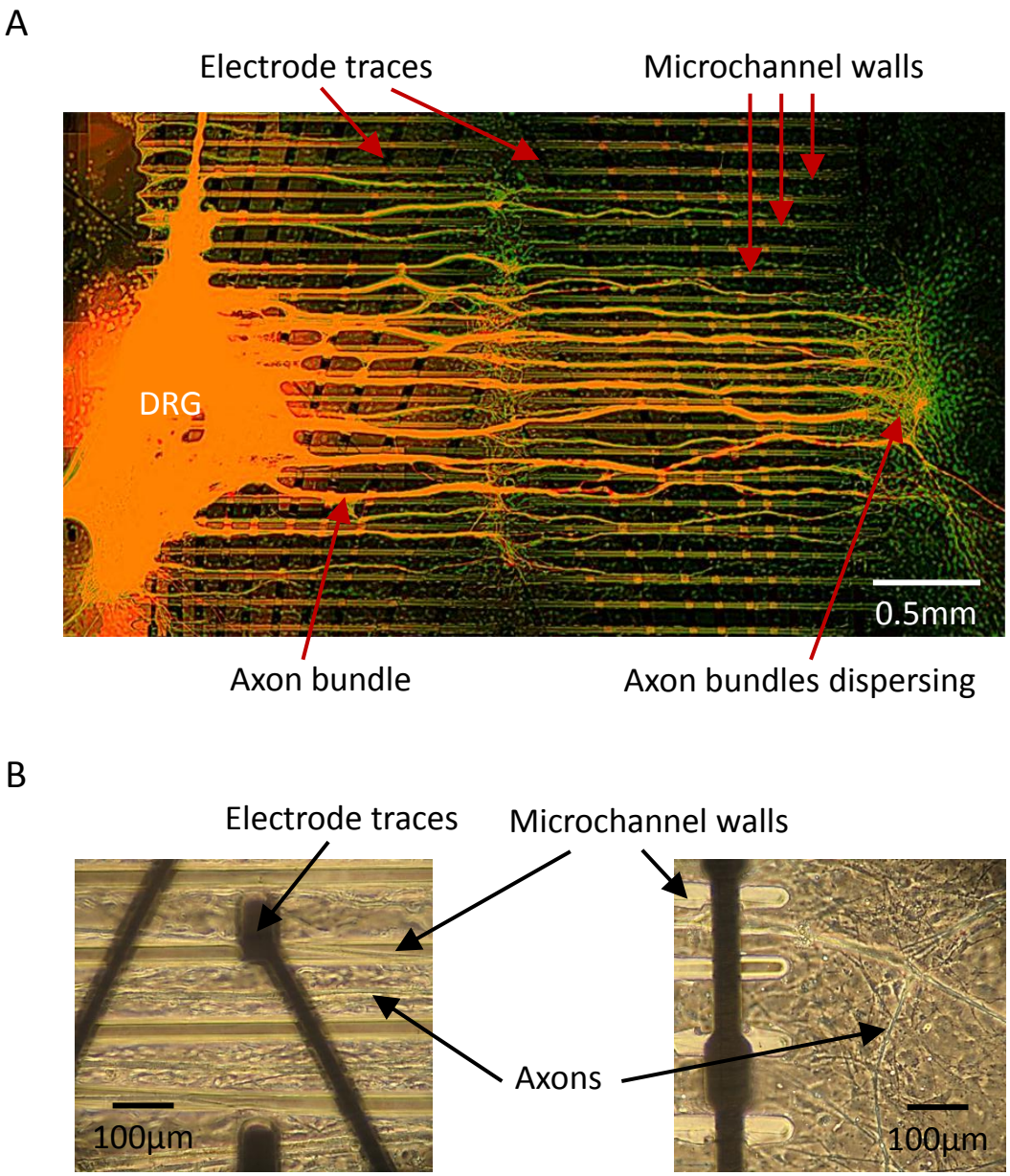

Figure 22. In vitro cytocompatibility studies of the GT-RE.
(A) DRG *in vitro* culture with axon processes and migrating Schwann cells on 'open' 100 µm wide microchannels. Axons bundles and Schwann cells observed emanating from the DRG were aligned and oriented in the microchannels. The axons and Schwann cells grew/migrated out past the 3.5 mm long microchannels where the axons bundles appear to disperse. Axons (red); Schwann cells (green); DRG and regions of axon/Schwann cell co-localization appear orange; Microchannels are visible as dark horizontal regions separated by faintly auto-fluorescent SU-8 walls; Electrode traces are visible as vertically curving lines. (B) Bright field images of axons and Schwann cells at the electrode region of the microchannels and at the end of the microchannels. A sheet of Schwann cells is present over the entire substrate making it difficult for individual cell identification.

supporting multi-cellular growth emanating from the DRGs. Both axons and Schwann cells grew and proliferated in a highly robust manner past the end of the microchannels in under 2 weeks. In general, axon extension and Schwann cell migration were aligned and oriented in the direction of the microchannels. Axon extension and Schwann cell migration from the explanted DRGs also appeared to be preferential towards the microchannels. The degree of extension and migration towards the microchannels was so extreme that the bulk mass of the DRGs actually *moved* onto the microchannels from their original location at the entrance of the microchannels.

Axons emanating from the DRG's formed bundles of axons similar in nature to fascicles found in nerves *in vivo*. For the most part these bundles stayed within a single microchannel, but at times can be observed growing over the microchannel wall into a neighboring microchannel. However, the growth continued in a general unidirectional manner. Regardless of the microchannel, the axons, and Schwann cells, seemed equally likely to grow on the Parylene C substrate as the SU-8 microchannel walls. It was also observed that the axon bundles tended to disperse at the end of the microchannels (Figure 22A). It was difficult to fluorescently image the Schwann cells due to the large degree of proliferation and resulting fluorescence intensity. The exposure time had to be significantly reduced as a result making the degree to which Schwann cells are present seem significantly less than in reality. Bright field images of the microchannel region and exit side of the microchannels have been included in Figure 22B to illustrate the striking degree of proliferation. A 'sheet' of Schwann cells was present on the surface of the GT-RE.

5.3.3 *In vivo* Electrophysiology

All 4 Parylene C GT-RE's, with an average of 19 electrodes (63.33 %) ± 3.9 standard deviation, successfully recorded a multitude of unique single unit action potentials 3 weeks after implantation in an awake and freely ambulating scenario. As

noted in the Methods, single unit APs were deemed unique based first on a comparison of the timestamps of the APs. If the occurrence of different APs overlapped more than 50% the waveforms were visually assessed for similarity in shape. If deemed similar, the AP was assigned to a single electrode to prevent double counting the AP across two or more microelectrodes. The average peak-to-peak amplitude of the APs was approximately 125 μV with a 77 μV standard deviation. The average signal-to-noise ratio (SNR) was calculated by dividing the peak-to-peak amplitude of each AP by the peak-to-peak noise band (2 times the standard deviation) and averaging the resulting individual SNRs. This was found to be 2.98 with a 1.4 standard deviation. Note that the APs were not subtracted out or removed from the raw signal for noise band calculation. In some cases the presence of large artifacts during a given trial would affect the noise band calculation. These trials were not included in the analysis. Figure 23 depicts a stereotypical raw signal recorded using an electrode from a single GT-RE. Identified single unit APs from the raw signal along with the respective spike raster plots are shown as well. In many cases, multiple single unit APs could be identified in a recording from a single electrode. However, extensive spike sorting to identify all possible single unit APs recorded using every electrode was not performed due to the time intensive nature of the analysis. Figure 24 depicts an example GT-RE and all the micro-electrodes integrated in the microchannels that were successfully used to record single unit APs. Examples of the APs from all of the micro-electrodes are shown alongside the MEA image.

An evaluation of the success of each microelectrode in recording an AP based on spatial location within the cross-section of the GT-RE was also performed. Each microelectrode position was taken, and out of the four GT-RE's, evaluated for the % success in recording an AP. This is depicted as a color map in Figure 25A where solid green, light green, light red, and solid red indicate the given microelectrode recorded an AP in 100%, 75%, 50%, and 25% of the GT-RE's, respectively. A statistical analysis was performed comparing the average percent success of recording an AP using the innermost

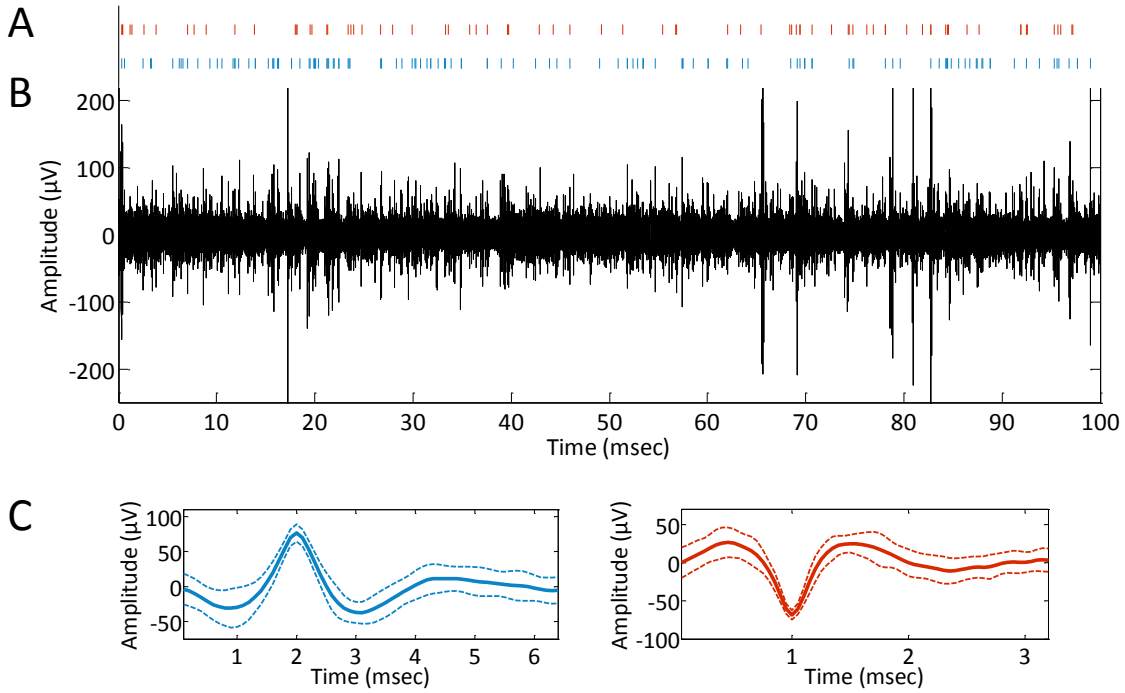

Figure 23. GT-RE in vivo stereotypical recording in awake and ambulating rats. (A) Spike raster plots of two identified APs from the raw signal shown in (B). (B) Raw recording signal over 100 seconds. (C) Waveforms of two single unit action potentials identified in the raw signal. Dotted lines signify 1 standard deviation from the mean. Colors correspond to the raster plots in (A).

15 microelectrodes vs. the outermost 15 microelectrodes. This is depicted in Figure 25B where the inner half of the microelectrodes in the GT-RE were on average 15% more successful at recording APs compared to the outer half of the microelectrodes.

While the Parylene C GT-RE's were all successful in recording a multitude of single unit action potentials at week 3, by week 6 the Parylene C insulation exhibited signs of delamination from the Parylene C base layer in the cable region of the GT-RE. This is shown in Figure 26 where forceps have been inserted between two previously adhered Parylene C layers after they were physically separated. As such, recordings were not analyzed at the 6 week time point. However, it is important to note that while the Parylene C GT-RE's were eventually non-viable and the Parylene C exhibited signs of delamination, the silicone adhesive used for encapsulation did not exhibit any signs of

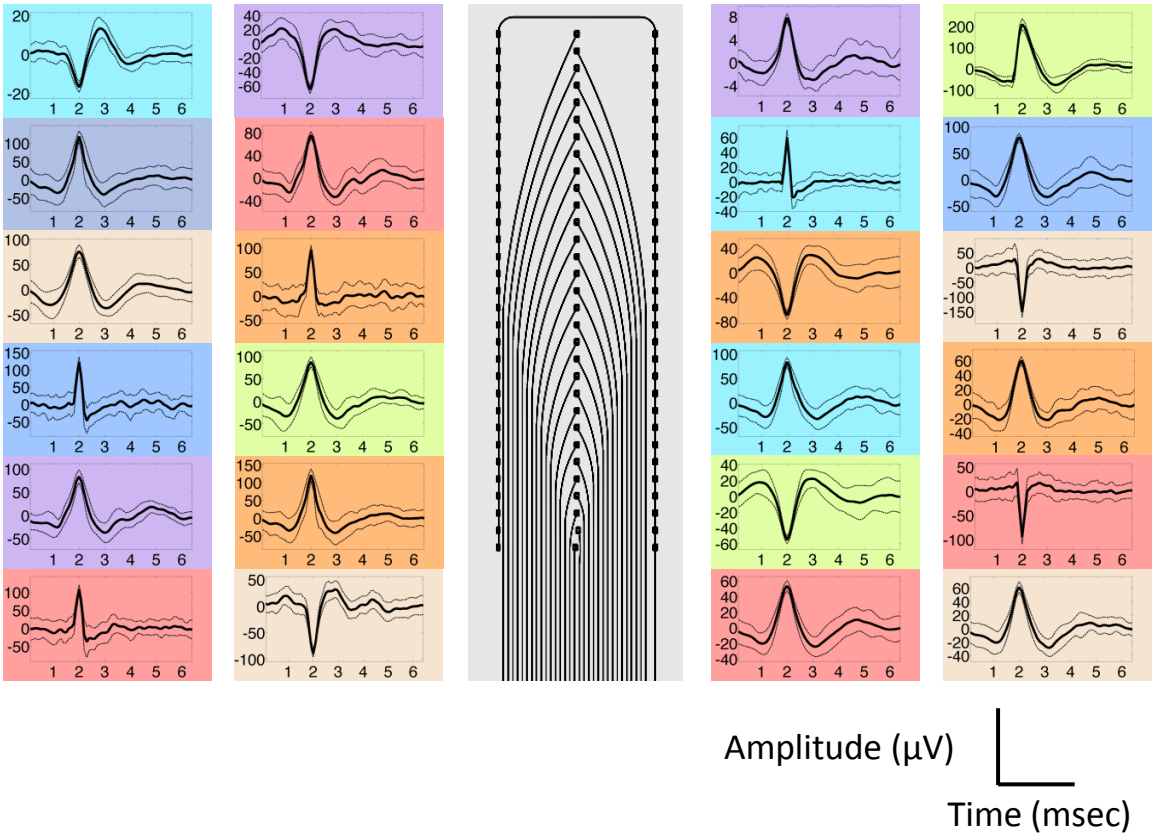

Figure 24. Collage of AP waveforms from a GT-RE.
Example waveforms recorded using a single GT-RE. Dotted lines signify 1 standard deviation from the mean. The microelectrode schematic is shown in the middle for reference.

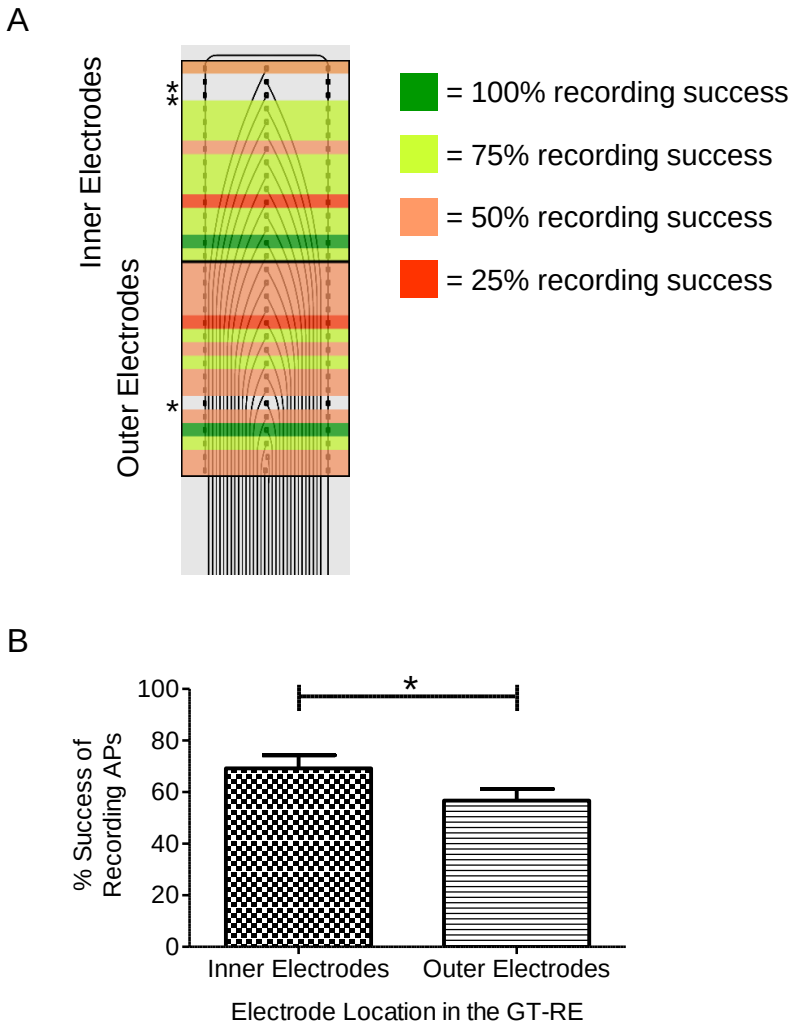

Figure 25. Recording success of inner microelectrodes compared to outer microelectrodes across all GT-RE's.
(A) Color map of percent success of recording an AP for each microelectrode across all GT-RE's. Solid green indicates the given microelectrode successfully recorded an AP in all GT-RE's. Light green indicates the given microelectrode recorded an AP in 75% of the GT-RE's. Following from this, light red indicates 50% of the GT-RE's and solid red indicates 25% of the GT-RE's. * indicates microelectrodes that were not connected during recordings and therefore not included in the analysis. (B) Quantitative analysis of the average percent success of recording an AP using the inner electrodes of the GT-RE compared to the outer electrodes of the GT-RE. On average, the inner half of the microelectrodes in the GT-RE were statistically more successful at recording an AP compared to the outer half of the microelectrodes. (Mean ± S.E.M., * $p < 0.05$)

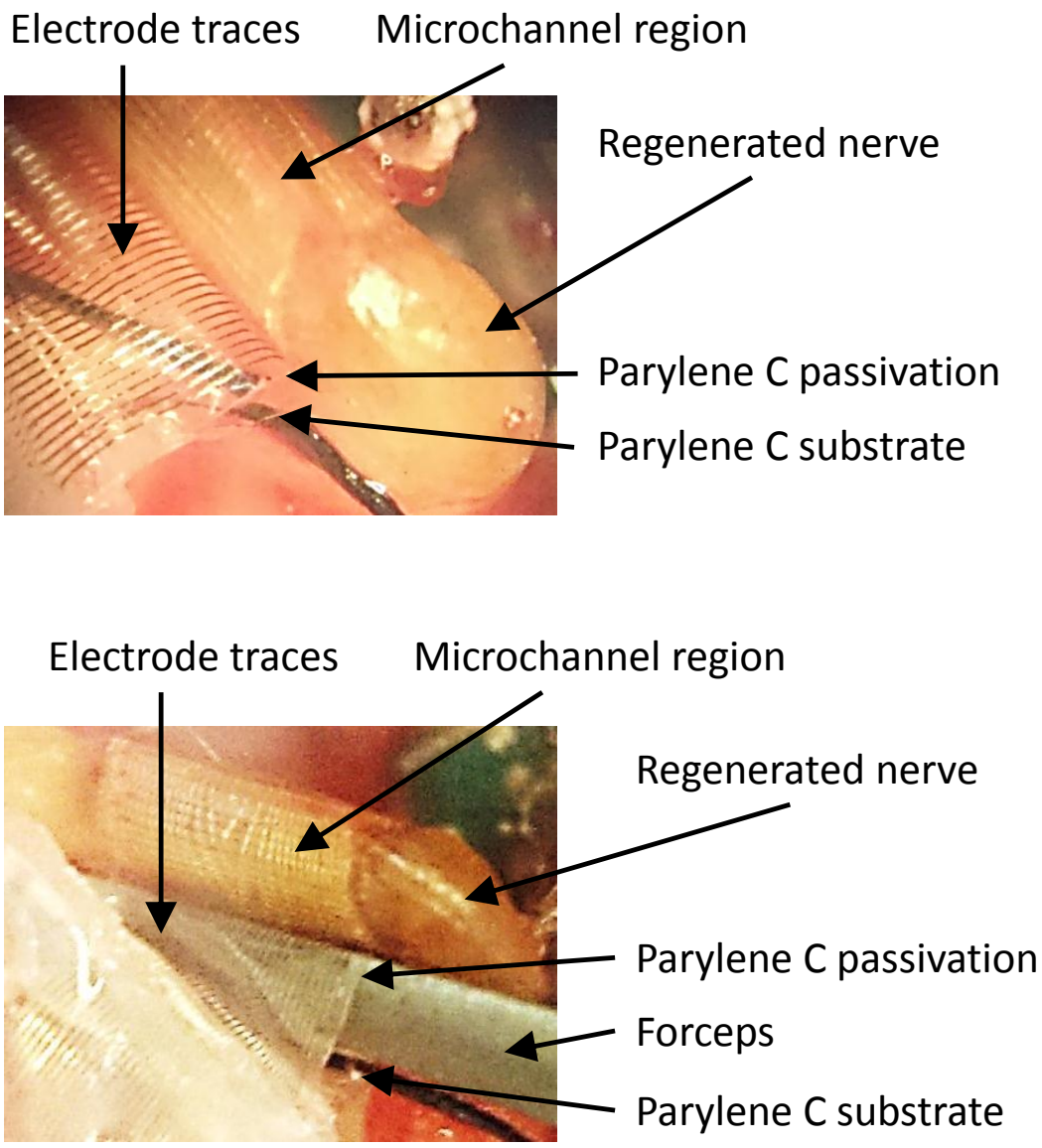

Figure 26. Parylene C GT-RE delamination.
(A) Example of delamination in the Parylene C cable between the passivation and substrate layers after 6 weeks of implantation. The rolled microchannel region with the regenerated nerve is clearly visible. Gold traces in the Parylene C cable leading from the microchannel region to bonding pads (out of image) are also clearly visible. (B) Forceps have been inserted between the Parylene C passivation layer and Parylene C substrate layer to aid in identifying the region of delamination.

delamination from the Parylene C it was initially adhered to or itself. This is despite extensive physical attempts to cause visible delamination of the silicone adhesive. The PDMS GT-RE's, utilizing the PCB wire hub, were also implanted and recordings attempted at the 3 week time point. However the recordings lacked identifiable waveforms and had a peak-to-peak noise band of approximately 4 μV indicative again of delamination and a short to ground. This was immediately validated upon explantation where the various PDMS layers had separated exposing the microelectrode traces and conductive epoxy junctions to the body.

5.4 Discussion

The vast majority of commercially available advanced prosthetic limbs provide only a fraction of the functionality of the natural limb they are meant to replace. This short coming largely stems from an individual's inability to 'control' the advance prosthetic. As a result, there remains a great need to design technology that enables seamless integration between conscious thought and resulting prosthetic limb movement for amputees. Peripheral nerve interfacing has the potential to provide such integration by obtaining neural signals from an amputated nerve which are intended for muscle activation and natural limb movement. These biological signals can then be translated into digital input for robotic limb control. Furthermore, there is the opportunity to implant a peripheral nerve interface at the time of surgery in the cases of amputation or nerve repair.

In the last 5+ years, there have been significant advancements in establishing the groundwork for microchannels as a viable avenue to chronic peripheral nerve interfacing. Acute non-regenerative implementations of microchannels have been evaluated where dissected nerves strands were placed in microchannels and recordings performed. [50,58,59] These studies validated the potential for microchannels to be used *in vivo* for single unit AP recordings. Other studies implanted microchannel interfaces and

performed terminal evaluations post-regeneration of transected nerves through the microchannels. [49,109,126] These studies validated the potential for microchannels to be implemented chronically and the potential to record single unit action potentials after chronic implantation. To date however, fully integrated – large electrode count microchannel interfaces have not been implemented and evaluated in awake and freely moving rodents. While such an accomplishment is arguably the most challenging experimentation model for evaluating a peripheral nerve interface, it is a necessary step towards clinical translation.

Here we have developed and evaluated a high micro-electrode count peripheral nerve interface, the GT-RE, for the ability to record single unit action potentials in awake and ambulating rodents. First the functionality of the devices was validated *in vitro* through functional testing as well as DRG cytocompatibility studies. Finally the GT-RE was evaluated *in vivo* to assess the potential for chronic peripheral nerve interfacing in the rat sciatic nerve animal model. Two GT-RE's were developed with different substrate materials, either PDMS or Parylene C. In general however, the GT-RE's were designed as a sheet of 97 microchannels with gold microelectrodes integrated into the base of the microchannels. The microelectrodes were placed in the center of every third microchannel. The sheet of microchannels was rolled to form a spiral conduit that matched the shape and size of the rat sciatic nerve. This design allows standard microfabrication and lithography techniques to be used to fabricate the device which is eventually rolled into a 3-dimentional structure. The microelectrodes themselves were connected to bonding pads via small gold traces in a cable which was then connected to a surface mount PCB containing either the Intan Technologies 32 channel multiplexer amplifier microchip (RHA2132) or basic signal extraction wires. The goal of integrating the Intan Technologies microchip was to evaluate the ability to integrate commercial off the shelf components into the GT-RE as they become available. An example might be an

implantable large channel wireless chip. Examples of the GT-RE prior to implantation were previously shown in Figure 19.

In vitro functional testing was utilized to assess the capability of the GT-RE's to record single unit action potentials similar in size and nature to what would be encounter *in vivo*. Both types of GT-RE's were successful in this regard, recording artificial neural signals injected into PBS on the order of 30 μV. Recordings from the PDMS GT-RE with the integrated Intan Technologies chip can be seen in Figure 21C. *In vitro* functionality testing of the Parylene C GT-RE utilized the PCB hub for signal extraction wires. An example recording from a single electrode of the Parylene C GT-RE is shown in Figure 21B. The ability to record the artificial neural signals through both the PDMS and Parylene C GT-RE's validated that the microelectrodes integrated in the GT-RE's were functional. Additionally, the GT-RE's could be used for neural recordings of some of the smallest AP's commonly observed *in vivo*. It is also significant that the artificial neural recordings were accomplished using the Intan Technologies chip and PCB hub integrated via the novel SMT integration technique discussed earlier. These results validated the SMT integration technique, the applicability of the technique to flexible *and* elastomeric substrates, and the ability to integrate various commercially available components into the GT-RE as needed.

Despite *in vitro* functional success with GT-RE's utilizing the Intan Technologies microchip, the microchip itself was not continued forward in later experiments. This was in part because the microchip and accompanying data transmission cable were physically too large to implant as they were not designed for implantation. Furthermore, many difficulties were encountered when attempting to build a custom LabVIEW program to interrogate the chip and custom miniaturized PCB with off-chip components shown previously in Figure 18B. These attempts faced numerous physical limitations associated with the transmission of high speed digital signals over long distances. Due to these limitations, transmission of data could only be achieved over shorter distances (1-2 feet),

which was not sufficient for use in freely moving animals. The use of lower sampling frequencies and acquisition rates was also explored, however proved to be insufficient for the intended application. Since the Intan Technologies chip was not necessary to evaluate the GT-RE as a microchannel interface, the PCB acting as a hub for signal extraction wires was utilized in all later *in vivo* experiments.

Cytocompatibility studies revealed that the toxic fabrication processes used to produce the GT-RE's are not retained with the devices and that the GT-RE's are suitable for implantation. Results were obtained without any surface coatings or treatments of any kind including plasma treating to increase hydrophilicity or protein coating such as laminin to facilitate adhesion and cytocompatibility. In fact the axon growth and Schwann cell proliferation was so robust that imaging became extremely challenging due to the overall levels of fluorescence and resulting appearance of overexposure (Figure 22A). The Schwann cells in particular proliferated to a degree that was largely unexpected as they formed a sheet of cells across the substrate (Figure 22B). The axons interestingly formed bundles similar to fascicles observed *in vivo* and reminiscent to those observed in a previous regeneration study where microchannel fascicles were described (Figure 22A). [109] These axon bundles grew out past the 3.5 mm long microchannels and likely would have continued if the microchannels were longer. This was previously observed in terms of axon length where growth occurred out to 4 mm in just seven days even though the axon bundles were not present. [109] It does appear though, that without the presence of the microchannel topography the axon bundles did not continue growing farther but instead disassembled and the axons congregated near the exit of the microchannels (Figure 22A). This suggests that the formation of the axon bundles is inherently tied to the presence of the microchannels. Furthermore, the formation of axon bundles in this study as compared to the lack thereof in the previous studies is attributed to the 100 µm wide microchannels used here as opposed to the 50 µm or 75 µm wide microchannels used previously. [71,109] The 100 µm wide microchannels

used here also matches those used *in vivo* in the previous study where uniform fascicular growth characterizing 'microchannel fascicles' was observed. [109] This further supports the hypothesis that *in vitro* axon bundle formation is a microchannel structure based phenomena. In contrast, axon bundle formation is unlikely to be a material based phenomenon of Parylene C vs. PDMS as both have been establish as cytocompatible in general and with DRGs in particular. Adhesion of DRGs and associated proliferating/migrating cells types was also observed on both substrates further indicating a lack of differences stemming from material selection.

It was also interesting to observe that the mass of the DRG's cultured on the GT-RE's in all cases actually migrated from their original position closer to or even onto the microchannels. Specific attraction to the SU-8 microchannel walls does not appear to explain this however, as it was noted earlier that the axon bundles did not seem particularly inclined to grow there versus on the Parylene C. Despite the lack of material preference for growth or proliferation, the axons and Schwann cells were aligned and oriented to the direction of the microchannels, as expected. It is also worth noting any axon growth and Schwann cell proliferation on top of the microchannel walls is inconsequential to the *in vivo* application as there would be a capping PDMS layer forcing the axons and Schwann cells to remain within the microchannels.

The GT-RE implants were tolerated well by the rats with no additional discomfort other than that stemming from the initial surgery. The size of the GT-RE however did in many ways fill the cavity below the biceps femoris muscle and significant increases in PCB size would be difficult to accommodate, at least in a rat animal model. Placing the microchannels over the middle of the PCB was a significant advantage as it allowed the PCB to be placed deeper into the leg of the rat and is recommended for future experiments. Both the PDMS and Parylene C GT-RE's were tested *in vivo* at a 3 week time point. This time point was chosen to allow enough time for axons from the proximal end to regenerate into and likely through the microchannels. Data from an unpublished 4

week study showed ample regeneration in similarly sized microchannels. Unfortunately, no useful data was recorded using the PDMS GT-RE at the 3 week time point. Recordings only showed incredibly low noise bands on the order of 4 μV indicating a short to ground and likely delamination. Upon explantation at the 3 week time point, this was confirmed visually with delamination of the PDMS passivation and PDMS substrate layers. It is unknown when during the 3 week implantation the delamination occurred.

Recordings using the Parylene C GT-RE's however were quite successful at the 3 week time point. An example of a raw signal from a stereotypical microelectrode within a microchannel is shown in Figure 23B. A multitude of single unit APs was identified within this and other raw signals across the many electrodes from the GT-RE's. Examples are depicted in both Figure 23 and Figure 24. Overall 63% of the microelectrodes integrated into the microchannels of the GT-RE were successfully used to record single unit APs. This is a significant finding considering previously reported success rates with other microchannel interfaces and especially given that the GT-RE is a large electrode count microchannel interface with 30 integrated microelectrodes. [49,50,58,59,109] The single unit AP amplitudes and SNRs reported here also fell within ranges previously reported in studies using microchannels in acute scenarios or terminally after implantation. [49,50,58,59,109] Furthermore, the GT-RE enabled successful recordings in awake and ambulating animals building significantly on these previous acute and terminal experiments. The ability to record and identify single unit APs is the paramount criteria peripheral nerve interfaces are judged by when considering a host of clinical applications from bladder control to robotic limb control. Accordingly, the findings reported here give significant credence to further work developing these technologies which target eventual clinical application.

Interestingly, it was found that the inner microelectrodes of the GT-RE were on average more successful at recording single unit APs when compared to the outer microelectrodes as shown in Figure 25A and B. A previous study evaluating regeneration

of axons through microchannel scaffolds noted that microchannels lacking axon regeneration tended to reside near the periphery of the device. [109] Given the early 3 week time point used in this study compared to the 8 week time point in the previous study, this effect could have been exacerbated here as regeneration would not yet have stabilized and could still be occurring in the outer microchannels. Myelination would also be ongoing and may be lagging in the outer microchannels. The net effect would be reduced AP recording success with the outer microelectrodes. That being noted, it is expected that the difference in AP recording success between the inner and outer microelectrodes would diminish over the following weeks and months as the regeneration stabilizes. These findings are also important from a design perspective as researchers performing microchannel interfacing at earlier time points such as 3 weeks should bias microelectrode placement towards the center of the device.

Given the 3 week time point used for these electrophysiology recordings and the fact that the axons had to traverse a 3.5 mm gap before reaching the distal segment, it is highly unlikely these axons reinnervated their distal targets. Therefore, this early recording time point is in some ways similar to a nerve amputee animal model where the amputated nerve permanently lacks it distal reinnervation targets. As such, the success of recording a multitude of single unit APs at this early time point can be used as an indicator that microchannel interfacing in an amputee scenario would also likely be successful. This is especially true given previous work which has investigated and shown the regenerative capacity and stability of amputated nerves once they have grown into and through microchannel devices. [109] It can also be surmised that a majority of the single unit APs recorded were likely motor units due to the fact that the input for most sensory units would be in the distal targets which had yet to be reinnervated. Therefore, the total number of APs recorded was likely significantly lower than what could be recorded at future time points once reinnervation occurs and sensory input generates additional APs. This may in part account for the electrodes which did not successfully

record single unit APs. Of course recording sensory APs is only relevant to scenarios where sensory input is of value. For advanced prosthetic control in particular, the number of reliably recordable motor APs is the first primary concern. However, recording sensory APs and utilizing conduction blocking techniques holds significant value for mitigating the chronic and often debilitating pain individuals experience post-amputation in addition to providing sensory feedback through prosthetics.

While there was significant success at the 3 week time point with Parylene C GT-RE's, delamination issues in the cable region were observed similar to that of the PDMS GT-RE's at a 6 week time point. An example of the delamination in the cable region can be observed in Figure 26. The rolled microchannel region with the regenerated sciatic nerve and the microelectrode traces leading to the bonding pads (out of image area) can also be visualized in the figure. The fact that delamination occurred in the Parylene C GT-RE was unexpected given previous reports indicating the utility of Parylene C as a viable chronic substrate and insulator for *in vivo* applications with flexible cortical and retinal interfacing devices. [98,117,127–129] It has even been reported through multiple studies using accelerated failure testing that Parylene C should perform as a viable insulator on the order of years, out to more than 20 years, of implantation. [91–93,130] It seems evident that these accelerated failure tests must be viewed with significant precaution. One possible reason for the large discrepancy is the accelerated failure tests are most often performed in saline baths. This does not accurately represent the blood filled environment where numerous immune cells and components of the blood play active roles in attempting to degrade an implant. These processes are integral parts of device failure, in this case delamination. Another potential cause for the major discrepancy is the lack of mechanical or physical stress/movement during the accelerated failure tests. In these tests, the devices are stationary and not subject to motions typical of an *in vivo* environment, especially that of the limbs. This is also relatively true of cortical and retinal interfacing which occur in less movement prone regions and therefore subject

the devices to less physical or mechanical stress. In fact inspection of the Parylene C GT-RE's showed numerous areas of buckling and plastic deformation of the Parylene C in areas of high movement along with delamination occurring in those regions indicating physically/mechanically induced failure played a role in overall device failure.

While Parylene C – Parylene C delamination was observed at the 6 week time point, adhesion of the silicone adhesive used as an encapsulant to the GT-RE seemed incredibly robust. Attempts to *physically* remove the silicone adhesive were unsuccessful indicating strong bonding and resistance to delamination. It is recommended that future work investigate utilizing dilute forms of the silicone adhesive as a substrate for device fabrication in addition to being utilized for encapsulation purposes. The fabrication of such devices should not be significantly different from fabrication on PDMS as previously described and seem likely to solve the delamination issues encountered here.

In the end, the fact that both the PDMS and Parylene C GT-RE's eventually suffered from delamination issues indicates a need for further materials development with regard to hostile *in vivo* environments. It is worth mentioning, that while the PDMS GT-RE suffered from delamination well before the Parylene C GT-RE, the benefit of stretchability makes PDMS or silicone based devices far more attractive for future development. Parylene C is fundamentally only flexible as a 2-dimensional film. Application over a 3-dimentional object that can flex, for example a tube, causes buckling of the Parylene C at the region of bending and/or plastic deformation on the opposite side due to its inability to stretch. Both result in stress points within the Parylene C film and will eventually cause failure of the Parylene C after repeated motion. PDMS and silicone derivatives do not suffer from this disadvantage and therefore hold significantly more promise with devices that are subject to mechanical stress and/or trauma during their lifetime. Once these adhesion issues are mitigated in the *in vivo* environment, future work will need to investigate truly chronic AP recording capabilities using the GT-RE or other microchannel interfaces. While the 3-week time point shows

significant promise, additional failure mechanisms stemming from chronic implantation will need to be elucidated. These may be a combination of biotic and abiotic issues and solutions will need to be developed that directly target them. This however, does not take away from the significant promise shown by recording single unit APs from a large number of integrated microelectrodes at the 3-week time point. The capability of using a fully integrated microchannel interface, the GT-RE, for regenerative peripheral nerve interfacing in awake and ambulating rodents has been established. Future work will continue building upon these findings bringing microchannel interfacing closer to clinical translation.

5.5 Conclusions

In this study a novel microchannel interface, the GT-RE, with large numbers of integrated microelectrodes was evaluated in a challenging, awake and freely moving rat animal model. Two different GT-REs were developed where one was composed of a PDMS substrate and the other of a Parylene C substrate. The GT-RE's were integrated with either Intan Technologies 32 channel multiplexer amplifier chip or a PCB acting as a hub for signal extraction wires utilizing a novel surface mount technology (SMT) integration technique. *In vitro* functional testing validated the capability of both types of GT-RE's to record single unit APs similar in size to those found *in vivo* as well as the SMT integration technique. DRG *in vitro* cultures revealed striking cytocompatibility of the GT-RE post-cleanroom processing with large degrees of axon growth and Schwann cell proliferation. Characteristics of the growth even resembled nerve fascicles normally found *in vivo*. Finally *in vivo* implantation of the GT-RE's revealed the capability of microchannel interfacing to be utilized for high-throughput single unit AP recording in awake and ambulating rats. On average 63% of the 30 microelectrodes per device were successfully utilized towards this end as early as 3 weeks post-implantation marking a significant advancement in microchannel interfacing. At 6 weeks delamination of the

substrate materials for the GT-RE was observed indicating a need for future material development to enable chronic recordings. *In vivo* observations indicate silicone derivatives as a substrate material, in addition to an encapsulant, may be the path forward. In the end, the findings of this study help direct future technology development and enable truly chronic, pre-clinical testing of peripheral nerve interfacing using the relatively new microchannel approach.

CHAPTER 6 CONCLUSIONS AND FUTURE DIRECTIONS

6.1 Conclusions

In the 2005, 1.6 million persons were living with a limb amputation (one in 190 Americans) and it has been projected that by 2050 this number will more than double to 3.6 million in the United States alone [8]. While these numbers do not compare to those of cancer or heart disease, they are still quite staggering when one considers the drastic loss in function and quality of life these individuals are forced to endure for their remaining years. Current day prosthetics do not adequately replace the function of the lost limb. While substantial progress during the last decade has occurred with regard to revolutionizing these prosthetics, most of it has focused on the robotics side. However, the ability to control and 'feel' through these advanced prosthetics lags behind. Inherently this stems from the lack of a seamless *interface* between the robotic limb and the individual. Amputees retain significant function in their nerves post-amputation, which offers a unique opportunity to establish this interface with the peripheral nerve. [1]

Traditional approaches to peripheral nerve interfacing have centered on penetrating the nerve with electrodes, wrapping electrodes around the outside of the nerve, or encouraging axons within the nerve to grow past electrodes in a regenerative model. While all of these approaches have shown the *potential* to record neural signals they fail to do so chronically or cannot record single unit APs and thereby fail to enable the full functionality of advanced prosthetics. These traditional approaches inflict nerve trauma and suffer from chronic scar formation, are not near axons to enable single unit AP recordings and/or fall victim to the incredibly small amplitudes of single unit APs which are largest only at the nodes of Ranvier. [4–6,36–41,53,54,120]

Here we evaluated a relatively new approach to peripheral nerve interfacing by using microchannel technology. It has been shown through modeling and *in vitro* studies that single unit APs from axons inside a microchannel are significantly larger in

amplitude and remain relatively constant throughout the length of the microchannel regardless of the node of Ranvier position. [6,56] These inherent characteristics of microchannels make them a promising approach to circumvent the challenges faced by previous approaches. Additional studies with microchannels have shown *in vivo* the capability of axons to regenerative through microchannels in a transection/non-amputee animal model. [57] Attempts to record from regenerated axons were also made using non-implanted electrodes inserted into the microchannels post-regeneration at the time of experimentation/recording. While only a handful of single unit APs were recorded, this suggests that these axons are in fact functional. [49] Other *in vivo* studies have investigated non-regenerative scenarios where nerves have been teased and rootlets placed within microchannels. Acute recordings have been performed in these scenarios further supporting the viability and potential for microchannel interfacing. [50,58,59]

This work builds upon these promising studies with the goal of bringing microchannel interfacing closer to clinical translation for amputees. The chronic integration of amputated nerves with microchannels and the ability to record APs after chronic implantation of microchannels permanently integrated with electrodes was first investigated. PDMS and SU-8 based microchannel scaffolds were developed towards this end and utilized permanent microwire electrodes for interfacing purposes. *In vivo* studies showed that at least at 8 weeks post amputation, 100 µm x 100 µm microchannels were able to sustain robust regeneration of axons in nearly 100% of the microchannels with space remaining within the microchannels for future tissue and axon maturation. Further analysis of the axons and nerve as it grew out the distal end of the microchannels showed a striking degree of spatially orchestrated regeneration matching the microchannel architecture forming ‘microchannel fascicles’ in the distal nerve stump. These microchannel fascicles were characterized by axon and Schwann cell groupings as well as the reformation of epineurial-like and perineurial-like sheaths of fibroblast arrangements all supported by a reorganized extracellular matrix. In general, the

microchannel architecture facilitated and encouraged parallel nerve fiber growth by directing axon regeneration through the microchannels and producing an organized microchannel fascicle morphology. Furthermore, the axons, Schwann cells, and endoneurial support structure immediately surrounding these cell types appeared to all be undergoing the normal regenerative process. Together these characteristics *strongly* suggest that microchannels are not only supportive of the proper initial microenvironment for regeneration but also for chronic stability of an amputated nerve. Additional evidence for this lies in the aforementioned display of characteristics being completely *opposite* to those commonly associated with neuropathic complications such as neuroma formation; one of the largest clinical concerns with implanting a device into an amputated nerve. These findings support the fundamental criteria of *safety* for a regenerative peripheral nerve interface targeted towards amputees.

In addition to the chronic stability of the amputated nerve with microchannel scaffolds, both spontaneous and sensory evoked single unit APs were successfully recorded *in vivo*. Additionally, multi-unit APs were recorded in response to electrical stimulation proximal to the microchannel implant. These recordings were accomplished using electrodes permanently integrated within the microchannels at a chronic time point a full five months after implantation. An assessment using the evoked multi-unit activity found overall device viability to be greater than 50% at this chronic time point. This calculation included all nonfunctional electrodes with broken leads. The stimulation ramp used during electrical stimulation also allowed the identification of multiple different axon populations within the various microchannels integrated with electrodes. Importantly, this could be used for mapping the distribution of different axon types within the microchannel interface to enable more selective and axon specific interfacing capabilities. This is discussed further in the following Future Directions section. Overall, the recordings of single and multi-unit action potentials were comparable if not better in some aspects to what has been previously reported with regard to numbers of functional

microchannel electrodes [13]. Notably, this was accomplished with a ‘simple’ device that lacked integrated MEAs and/or electrode passivation techniques. Instead simple off the shelf microwires were integrated and successfully used in a chronic setting. This is significant, because this microwire electrode based device could hold substantial utility for applications that do not require high-throughput peripheral nerve interfacing and large numbers of recorded APs. Finally, based on the electrophysiology data presented in Aim 1, action potentials can be recorded from regenerated axons in microchannels with permanently integrated electrodes on a chronic timescale.

With this the stability and viability of regenerative microchannel interfacing was established, warranting the development of fully integrated microchannel interfacing technology to be utilized for awake and freely moving animal studies. Accordingly, this work focused next on developing these technologies which included A) integration of MEAs and interconnects into flexible and elastomeric substrates; B) integration of SMT onto flexible and elastomeric MEAs; and C) flexible and elastomeric polymer based hermetic insulation and encapsulation strategies enabling implantation. Integration of MEAs into elastomeric substrates such as PDMS has been a significant challenge that has prevented the wide spread use of PDMS as a substrate for high-density large count microelectrode arrays. Here we developed five processing solutions targeting the fundamental issues preventing successful patterning and photolithography on PDMS. These included 1) novel stress features, 2) thick film photolithography, 3) differential curing profiles in an oven, 4) large increases in exposure times to account for reduce photoresist crosslinking at the substrate interface, and 5) the addition of bulk etching as a method for photoresist removal in addition to standard development. Together these 5 processing solutions drastically increase the processing window one has to design and fabricate high-density patterns on substrates with large coefficients of thermal expansion like PDMS. While in this work these five solutions have been used to develop flexible and stretchable MEAs, the number of applications for these solutions is extremely large.

One example of the utility for these solutions is the ability to effectively create a flexible and stretchable PCB. This could drastically change the form factor of today's electronics from laptops to cell phones as they are all inherently tied to their mechanically rigid PCB or motherboard connecting the various electrical components.

Following the successful integration of MEAs into flexible and elastomeric substrates, an approach for SMT integration was developed to allow the easy addition of off the shelf electronics such as microchips and/or PCBs containing other components. This approach involved defining a minimum bondline to enable stable conductivity between sets of surface mount bonding pads. The bondline is necessary due to the nanoliter volumes of conductive epoxy needed to form an electrical junction with the incredibly small bonding pads of the smallest commercially available components used in today's electronics. The resulting 'column' of conductive epoxy proved to not only provide stable conductivity but was mechanically robust through the entire fabrication process and following *in vivo* implantation/testing. Furthermore, this approach was successfully demonstrated *in vitro* and *in vivo* through the integration of two different surface mount PCBs containing either Intan Technologies microchip or signal extraction wires for AP recordings. In the end, this SMT integration technique is widely applicable to the incorporation of the smallest SMDs available with flexible and elastomeric substrates for a wide range of applications. Furthermore, it is incredibly simple to implement as all that is needed is a 40 μm spacer and is translatable to standard industry practices.

The third major area of technology development centered on polymeric based hermetic insulation and encapsulation approaches to enable implantation of the GT-RE's. Two approaches were used in conjunction with Parylene C deposition for insulation and silicone adhesive encapsulation for mechanical protection as well as extra insulation. While the Parylene C failed due to delamination at the 6 week time point after *in vivo* implantation, the silicone adhesive displayed adhesion characteristics suggesting viability

for significantly longer periods of time. It is also important to note that the PDMS substrate and insulation layers of the PDMS GT-RE's also suffered from delamination at an even earlier time point. This author feels it is due to the use of the sacrificial post technique for patterning the PDMS passivation layer. In this technique, the PDMS passivation layer is spun around sacrificial posts. This results in ripples within the PDMS film which was then allowed to rest for approximately 4 hours before curing giving time for these ripples to relax. During this time, it is believed the adhesion of the PDMS passivation layer to the PDMS substrate was lost. However, it is unknown whether avoiding the 4 hour rest period would solve this problem. The fact that the silicone adhesive did not have an adhesion failure *in vivo* and that the processing solutions for PDMS can likely be used with silicone adhesives suggests that future devices ought to explore silicone adhesives as a substrate material.

Overall the three major phases of technology development allowed the fabrication of advanced microchannel interfacing technology capable of being implanted and used for AP recording in the challenging awake and freely moving rodent animal model. Perhaps most importantly, these fabrication techniques are applicable to a broach range of next-generation devices spanning healthcare sensors, to diagnostics, to even consumer electronics.

Given that fully integrated microchannel technology was developed, the final aspect of this work focused on evaluating these devices for the ability to record single unit APs in awake and freely moving rodents as the next step towards clinical translation. As detailed previously, two types of GT-RE's were developed where one type had a substrate materials of PDMS and the other type had Parylene C. Both types of GT-RE's showed *in vitro* the capability to record artificial neural signals similar to the single unit APs that would be encountered *in vivo*. *In vitro* cytocompability studies showed the extensive cleanroom processing needed to fabricate the GT-RE's did *not* result in toxic devices and did *not* induce cell death of the cell types prominent to a nerve.

When both GT-RE's were evaluated *in vivo*, the PDMS based GT-RE's failed due to delamination before AP recordings could be performed at the 3 week time point. However, the Parylene C GT-RE's were successfully utilized for recording a multitude of single unit APs across the 30 integrated microelectrodes. In fact 63% of the electrodes were successfully used towards this end, a significant milestone in microchannel interfacing. It was also found that the 15 innermost electrodes were more successful at recording single unit APs when compared to the 15 outermost microelectrodes. This difference, while significant, is likely to be temporary and may stem from the early time point used for recordings when regeneration is unlikely to be robust across the entire cross-section of the device. Instead at these early time points regeneration is typically most pronounced in the center agreeing with the findings of greater AP recording success with the innermost electrodes. This finding however, provides design criteria for researchers developing microchannel interfaces based on the timeline of their studies. If the study has a short timeline on the order of a few weeks, it would be prudent to bias the placement of electrodes towards the center of the device's cross-section instead of having a uniform distribution.

While at 6 weeks delamination was again encountered with the Parylene C GT-RE's, once this issue is overcome these devices will likely be highly successful peripheral nerve interfaces. This is especially true given these results showing APs can be recorded from significantly large numbers of electrodes in the challenging awake and ambulating rat animal model. Finally, this is an important step towards clinical translation as the ability to record and identify single unit APs is the paramount criteria peripheral nerve interfaces are judged by when considering efficacy for robotic limb control. In the end, the findings of this work as a whole help direct and give significant credence to future technology development enabling eventual clinical application of microchannels for peripheral nerve interfacing.

6.2 Future Work

What follows is not only directions for specific future work regarding this thesis and microchannel technology, but also some thoughts regarding the field of peripheral nerve interfacing in general and future directions needed to enable translation of the many technologies being developed.

6.2.1 Nerve – Microchannel Interface Chronic Stability

With an eye toward clinical translation, there remains significant work to be performed before microchannels can be used for peripheral nerve interfacing. First and foremost the regenerated nerve – interface stability needs to be further investigated. While the studies presented in this thesis suggest chronic stability of the amputated nerve, this needs to be validated at a significantly longer time point of at least 1 year. The major concern is that axon numbers would decrease during the many months following implantation. This being said, it is important to remember that the goal of a regenerative peripheral nerve interface is not to regenerate the nerve in its entirety. In contrast, it is to regenerate and maintain enough 'normally' functioning axons to enable peripheral nerve interfacing. Given the robust regeneration observed at 8 months it is unlikely to see a truly drastic reduction in axon numbers. Even if a 25% reduction in axon numbers were to be observed after 1 year of implantation, there would likely still remain enough axons to enable interfacing applications. It is also worth noting that quantification of axon numbers within microchannels needs to be normalized to the numbers of axons significantly proximal to the nerve. This will guard against skewing the data based on significant axon branching in the microchannels which is known to occur after regeneration.

If axon numbers do in fact decrease to significantly lower levels by 50% or more, there are some approaches which could be implemented to help mitigate this reduction. The study presented in Aim 1 of this thesis left the distal stump of the amputated nerve

free, as in un-sutured to any target. Clinically it is common to denervate an unused muscle at the end of an amputated limb and then suture an ‘important’ nerve into said muscle to help maintain chronic stability of the nerve. The same approach could be utilized here to help maintain the stability of the nerve after it has regenerated through the microchannels. Another approach could be to seed cells on the distal end of the microchannels to provide a target for reinnervation after regeneration. However this approach is not as clinically translatable as suturing the end of the microchannels into a denervated muscle. Another interesting approach could be to coapt the distal end of the microchannels with the distal nerve stump to the side of another uninjured nerve. A previous study showed connecting the distal portion of a transected nerve to an uninjured nerve helps sustain the distal nerve segment. [78] While this study looked at sustaining the distal nerve segment, it is likely that doing so with the end of the nerve regenerating through microchannels would also help sustain the nerve chronically.

Another important issue regarding nerve – interface stability is the stability of the action potentials being recorded through the microchannel interface. While action potentials were recorded using the GT-RE at the early time point of 3 weeks, the axons generating these APs are undoubtedly still undergoing the regenerative process. As weeks and months progress these axons will likely increase in diameter as well as have thicker myelin sheaths. These changes will lead to changes in AP waveform and perhaps even new APs will appear at later time points. Furthermore if axons are degenerating as is known to happen over the course of regeneration, APs which are recorded at early time points will disappear. This general instability in APs will make driving a prosthetic limb challenging due to changing control inputs. These changes need to be evaluated on a chronic timescale just as the nerve stability. Furthermore the effect of these changes regarding reliable control signals for advanced prosthetics needs to be determined and solutions generated if the effect is too detrimental.

6.2.2 Microchannel Interface Technology Development

While evaluating the stability of the nerve and APs is important, there also remains significant future work regarding technology development of the GT-RE, microchannel interfaces in general, and peripheral nerve interfacing at large. As noted, delamination was observed between the substrate and insulation layers of the GT-RE regardless of whether these materials were PDMS or Parylene C. This was largely unexpected given the literature supporting both of these materials and the relative *lack* of literature detailing the challenges of insulation and packaging. In general, significant attention is commonly placed on the design and fabrication of electrodes. In hindsight, this author feels insulation and packaging are actually far more challenging and get far less attention than they deserve. Insulation and packaging cannot be left to an afterthought of device fabrication and admittedly, this author was initially at fault for this. Initial material and substrate selection for electrode and device development must be made with an insulation and packaging solution in mind from the beginning. For instance utilizing a silicone adhesive or other silicone derivatives as a substrate material may be highly pragmatic based on the *in vivo* results of this thesis. It is the strong suggestion of this author to investigate device development using silicone adhesives as a substrate. Not only will this help with insulation and packaging challenges, but the fabrication techniques developed in Aim 2 can be directly applied. Another important note is that the importance of insulation and packaging must also be reflected in literature and cannot be left as a single line item as is commonly done where authors merely state ‘wires were encapsulated in silicone’. Cleaning and surface treatment procedures need to be elucidated and reviewers of manuscripts must demand this level of detail as it is already expected generally for electrode fabrication.

Regarding future work, it would also be worthwhile to investigate universally applicable packaging solutions. This is inherently extremely challenging as it requires the ability to circumvent material issues as well as application specific issues such as

mechanical stress in the case of peripheral nerve interfacing. Industry standard approaches are to utilize a metal enclosure for microchips and other non-lead components, which has been the case for decades. Polymers are potentially the way of the future. However, this remains to be fully investigated and validated. In many ways it is not just the polymer that matters but the approach used for packaging as well. Parylene C was initially thought to be a universally applicable material based on its room temperature deposition which was easily applied to many devices and applications. However its inability to stretch limits its capabilities drastically in mechanically or physically demanding environments. For this reason, this author feels that silicone derivatives hold much more promise. A final note on insulation and packaging is that much of the techniques used in this thesis were hand based. It would be advisable to develop more batch oriented techniques to increase efficiency and reduce inherent variability with hand fabrication.

In addition to future work investigating the challenging issues of insulation and packaging, the integration of on board microchips enabling multiplexing, amplification and wireless communication would be highly beneficial for a peripheral nerve interface. Work is currently being performed in the Ghovanloo lab at the Georgia Institute of Technology and undoubtedly elsewhere towards this end. Various electrophysiology companies such as Intan Technologies LLC, Plexon Inc., and Blackrock Microsystems also have commercially available headstages that enable multiplexing and amplification, but none of these are designed for implantation. A small footprint implantable microchip with multiplexing and amplification capabilities would reduce the number of wires and size of headcaps used during awake and freely moving electrophysiology. Furthermore, amplification of APs near the acquisition site could drastically help SNR. Finally, if these microchips were to integrate wireless communication it would completely eradicate the need for signal extraction wires and a headcap. This would in many ways simplify device

fabrication if the microchips were SMDs and the SMT integration technique from Aim 2 was utilized.

Regarding SMT integration, it would be worthwhile to investigate methods of non-permanent integration. The technique developed in Aim 2, while widely applicable, is permanent in that any SMD device attached cannot be removed without destroying the substrate MEA. It would be highly advantageous if SMD components could be replaced with other SMDs as needed or as more advanced capabilities are invented. This would however necessitate abandoning conductive epoxy as the junction between the SMD and substrate MEA. Metals with low melting temperatures such as gallium based alloys could have some utility here if cavities connecting sets of bonding pads are filled with the liquid metal. To remove the electrical components the device could merely be heated to melt the gallium alloy junction enabling the component to be replaced. Upon cooling the gallium alloy would harden again.

Finally, new methods for developing microchannels with embedded electrodes could be developed. In this thesis a long sheet of microchannels with embedded electrodes was rolled to form a 3-D conduit matching the shape and size of a nerve. Another approach could be to lay sheets of microchannels with embedded electrodes on top of each other. The difficulty with this approach is how to navigated having metal traces for each layer of microchannels and embedded electrodes in different planes. One approach to navigate this issue could be to use a PCB with through-hole pins. The leads from the embedded electrodes could connect to ring-shaped bonding pads where the pins from the PCB could penetrate through the center. Conductive epoxy can be applied to this junction facilitating the electrical connection. As long as each layer of microchannels with embedded electrodes has leads of different lengths from the other layers there would be no overlap and each layer could be connected using the pin strategy. This approach has the advantage of circumventing the rolling and open core of the rolled microchannel scaffolds. It is envisioned that placing layers of microchannels on top of each other would

also be easier and less variable than hand rolling a sheet of microchannels. Another approach could be to utilize sheets of microchannels laid upon each other as just stated. However here, instead of integrated electrodes, needle like electrodes or the Transverse Intrafascicular Multichannel Electrode (TIME) could be inserted transversely through the microchannels. The footprint of these electrodes, if sufficiently small, would not hinder regeneration and could make the overall device fabrication drastically simpler.

6.2.3 Motor and Sensory AP Signal Interpretation and Use

Once nerve – interface stability and technology development have been fully investigated, there lies the question of whether the AP signals recorded are enough to drive an advanced prosthetic. The key question is, how many action potential inputs are needed to replicate the motion of a limb using today's prosthetics? Following from this, the next question is how many electrodes are needed to reliably record those APs? DARPA's relatively recent Broad Agency Announcement for Reliable Peripheral Interfaces (DARPA-BAA-11-08) mandated funded projects describe a credible trajectory to 22 independent output channels from a peripheral nerve interface. This suggests a minimum of 22 independent APs in order to derive the 22 output channels from a peripheral nerve interface, but this does not take into account recording APs which cannot be used as viable control signals, sensory APs for example. So the total number of recorded APs would need to be larger and this does not elucidate the number of electrodes needed to achieve this goal either. Furthermore, it is likely not possible to fully answer the questions of minimum APs and minimum electrodes yet as they are inherently dependent on each other. One cannot determine the minimum number of APs needed to control a prosthetic without first having enough electrodes in a peripheral nerve interface to do so. In order to determine how many electrodes are sufficient, one must know the minimum number of APs that need to be recorded. In the end researchers must first make larger count micro-electrodes, such as the 30 microelectrode GT-RE presented here, with

the hope that it has enough electrodes. AP recordings must then be performed to evaluate the number of usable APs that can be recorded and whether these are enough to drive prosthetic motion. If not, the peripheral nerve interface must have an even larger number of electrodes integrated and the cycle repeated.

To enable evaluation of the minimum number of APs needed, one can envision an interfacing experiment with the sciatic nerve where rats are ambulating during AP recordings, muscles electrodes record EMG activity from muscles of the leg, and motion tracking of the leg all occur at once. This experiment would allow correlation of recorded APs to muscle activation to leg movement and could help identify how many electrodes of those that record APs, are actually recording APs useful in determining leg movement. This could then be used to determine whether there are enough APs being recorded to replicate the full motion of the leg. This number of electrodes and APs is likely different from interface to interface and would need to be tested for each, regardless of whether it is a microchannel interface or a Utah Slanted Electrode Array.

An important consideration to the recording of APs for prosthetic control is whether single unit APs are even needed for prosthetic control. It could for instance be argued that multi-unit activity from multiple axons firing in synchrony corresponding to limb movement likely occurs in peripheral nerves. This is would be expected due to the redundancy in the peripheral nerve where multiple axons innervate the same muscle fibers and therefore would also carry the same signal and fire at the same interval. Furthermore, the inherent spatial organization of the nerve, while different on a micro-scale from person to person, would likely place these axons next to each other making it easier to record a larger amplitude multi-unit AP. As such, recording these multi-unit APs could be used to drive prosthetic control. However, while this may be the case in an uninjured nerve, it is important to remember this may not be the case in a regenerated nerve and especially so with regenerative microchannel interfacing. Transected axons do not regenerate in straight lines and therefore do not hold the same spatial location as they

did prior to regeneration and would no longer lie next to each other. This may reduce or eliminate the multi-unit AP if the axons are too far apart from each other for an electrode to record from them at the same time. Furthermore, it is possible that these axons could regenerate into different microchannels thereby eliminating the multi-unit AP that previously existed and necessitating the recording of single unit APs. In the end it would need to be assessed whether enough of these multi-unit APs exist post regeneration to enable prosthetic control in the same way that the number of single unit APs needs to be assessed.

Another pertinent question is whether stimulation can be performed simultaneously during AP recording to enable sensory feedback for closed loop control of advanced prosthetics. Future studies should investigate whether sensory feedback for microchannel interfaces is only viable in 'non-motor' related microchannels. If so, it is necessary to determine whether a full spectrum of sensation is capable of being evoked. Experiments evaluating sensory feedback from peripheral nerve stimulation could utilize voltage sensitive dye and/or MRI techniques to image cortical activity in response to the peripheral stimulation. This also brings up the crucial issue of motor vs. sensory axon population distributions within and across microchannels. In an ideal scenario sensory axons would be contained to separate microchannels from those containing motor axons. This is highly unlikely to occur on its own, but techniques for mapping the axonal population of microchannels could elucidate the population differences between different microchannels. This could enable treating certain microchannels as predominantly motor or sensory to benefit of interfacing.

A clinically relevant technique that may lend itself to this identification challenge is microneurography and is similar to the stimulation ramp performed in Aim 1. The nerve after regenerating through the microchannels could be stimulated significantly proximal to the microchannel interface. This would allow APs of different conduction velocity to be separated over time and allow a mapping of the microchannel interface

based on time of AP occurrence. Conduction velocity is directly related to axon diameter which can be *loosely* correlated to predominantly motor or predominantly sensory populations. While this is not a perfect method to determine motor vs. sensory, it may be good enough given the large number of electrodes that can be integrated into a microchannel interface. Another potential method that is clinically relevant is to ask the patient or amputee to think about moving their limb and map the AP responses and do so for a variety of intended movements. Each microchannel could then be stimulated and sensation assessed to map the sensory component. A final method could be to use non-invasive stimulation of the spinal cord to initiate a walking pattern while the body is raised. This would allow predominately motor activity, aside from proprioception, to be present in the peripheral nerve and may allow mapping of the microchannel interface.

Given the need to investigate motor vs sensory axon populations, it would be warranted to also investigate methods of inducing segregated motor and sensory regeneration. Developmental biology may have some interesting approaches given that axon pathfinding during development follows extremely specific trajectories for both motor and sensory axon types. However more biological studies may need to be performed to understand these pathfinding mechanisms before they can be implemented in nerve regeneration.

6.2.4 Clinical Translation

While it is important to evaluate the next steps for microchannel interfacing in terms of technology development and the ability to interface with the nervous system, it is equally important to evaluate what is needed for clinical translation. Advanced prosthetics currently on the market largely have 8 EMG electrodes or fewer as control inputs. One might therefore assume than a peripheral nerve interface with greater than 8 electrodes would be superior. While this is possible, it is important to note that the 8 EMG electrodes are *always* motor control inputs whereas AP recordings from a

microchannel interface may or may not be motor related activity. For this reason the number of electrodes recording APs would need to be higher in the microchannel interface. However, if studies show that with 'X' number microchannel electrodes greater than 8 can be reliably used to record motor APs for prosthetic control then clinical translation ought to be considered. This is because, with regard to clinical translation, the goal should *not* be to develop a device that acquires all the motor signals from a nerve to enable the full functionality of an advanced prosthetic limb. Instead, the goal should be to develop technology that is better than what is currently available. Once that occurs it should be made available to amputees and patients so as to improve the standard of care and their quality of life as soon as possible. Attempting to build the perfect microchannel interface, or any peripheral nerve interface for that matter, which would enable perfect advance prosthetic function is likely a never ending goal. Clinical translation should not be tied to it.

6.2.5 Failure Analyses and the Standardization of Neural Interfacing Research

The findings of this thesis show that microchannel can be used to record single unit APs from peripheral nerves. While it is unknown whether the APs recorded were motor or sensory units, the overarching question driving future microchannel technology development should no longer be '*can* microchannels be used for peripheral nerve interfacing'? Instead, with clinical translation in mind, the question to answer in the future is 'what causes microchannel devices to *fail* during peripheral nerve interfacing'? In reality this is also what the entire field of peripheral nerve interfacing should be asking. By and large much of the work still being performed is focused on showing the possibilities for peripheral nerve interfacing; either the ability to record AP's or stimulate and generate responses of some kind. This is not to say the work being done is not valuable, but merely that future work needs a slightly different trajectory. Issues of failure and/or replicability are the major upcoming hurdles for peripheral nerve

interfacing in general and for microchannel interfacing. Future work needs to incorporate, if not focus on, *failure analyses*. Mechanisms of failure are as important as success at this point because, in order to realize clinical translation, showing something is possible is not the same as showing something does not fail. Once these questions are asked researchers can target specific aspects of the failure and develop innovations that solve these issues.

This thesis is a perfect example of showing that microchannel interfacing is possible, however in the end failure was encountered due largely to issues with delamination. The delamination is an important finding as it directs future work. Silicone adhesives appear to be a path forward towards this end and could bring microchannel interfacing significantly closer to clinical translation. Additional, future chronic experiments with microchannel interfaces are also needed to elucidate failure mechanisms of the device, nerve or interaction between the two on a chronic timeframe. Along the same lines, experiments which do not evaluate failure mechanisms of devices are not as valuable at this stage of technology development. Examples include a number of acute studies where PDMS passivation was employed using the sacrificial post fabrication approach. As far as this author is aware, this is the first time a device using this approach has been implemented *in vivo* through implantation and failure was observed. This is likely because previous studies never evaluated these devices in a non-acute scenario or evaluated potential failure mechanisms of the devices.

In some ways this seems to be a difference between science and engineering. The field of neural interfacing needs to progress to more of an engineering mindset where universally applied metrics and standards are used to evaluate research being conducted and results being published. An easy example is the vast number of papers using different equations to calculate SNR. Even worse are the numerous papers that don't even report how they calculated SNR! In addition to a standardized method of reporting SNR, key characteristics of electrophysiology rigs should mandated by journals and reported to ensure researchers are using largely equivalent setups that would enable reproduction of

data as well as others to build off of published work. These characteristics should include baseline noise amplitude of the rig during recording sessions and a report of the frequency distribution of the noise. Furthermore, sampling, amplification, and filtering metrics should be standardized at least for all experiments recording single unit action potentials. It is well known that different filters will change the raw signal to different degrees making it difficult to easily compare results across experiments and researchers.

Standard design and implementation criteria for peripheral nerve interfaces should also be mandated and if not used or withheld, reasons should be enumerated. An example is the use of an implantable electrical shield as implemented with the Utah Slanted Electrode Array (USEA) [131] and also here through a stainless steel foil wrap. If the implantable electrical shield is not implemented there should be a good reason for not doing so which is published for others to view. Along these same lines outsourcing device fabrication and parts to industry should always be considered in the effort of standardization and reliability. This will help remove variability in handmade devices and aid in reproducibility across multiple research groups. An example is the outsourcing of the signal extraction wiring for the GT-RE to the Omnetics Connector Corp., which was enabled by the SMT integration technique developed in Aim 2. The electronics industry, and the Omnetics Connector Corp specifically, has spent years refining approaches for connecting and insulating small wires making them an ideal outsourcing option. Furthermore, industry has the metrics and standards previously mentioned already in place making their products reliable and more trustworthy.

6.2.6 Strategy for Market Translation

Finally, it is worth mentioning that peripheral nerve interfacing as a solution to the loss of function with amputees and even clinical segments where nerve stimulation is an option, is likely *not* a viable business opportunity. Meaning, it is unlikely peripheral nerve interfacing will be profitable given the extreme costs associated with developing,

producing, and translating this technology and the incredibly small market size as enumerated in the Chapter 2. If peripheral nerve interfacing is to ever truly be market translatable, one would likely need to identify uses beyond recovery of function for disabled individuals.

In many ways the true greatness of a peripheral nerve interface, and neural interfacing in general, lies in the potential to interface with any electronic device. While helping amputees and disabled individuals is key, it will not make enough profit to sustain an industry sector. If however, the business goal is to enable interfacing with a host of electronics on the market today, the market segment for neural interfacing gets effectively multiplied by the number of new devices one could interface with. Any electronic consumer device that requires the input of a hand could be theoretically replaced with a peripheral nerve interface in the arm of an amputee or disabled individual. Instead of interfacing to a robotic arm and using a 'mouse' with a computer, the amputee could purchase an 'app' that enables them to bypass the robotic arm, and merely move the mouse by thinking. In fact this is done when training amputees to use advanced prosthetics today. However this could be a product that is sold. In the same way instead of a computer mouse, it could be a computer keyboard, a car, videogame controller or any number of other devices. In this way a business could potentially expand their effective market size, recoup the cost of the peripheral nerve interface and hopefully generate profit. This is of course making the optimistic assumption that the technology development of these 'apps' would not be a significant burden compared to the development of the neural interface itself.

In the end, a successful business strategy for neural interfacing would likely be far more intricate and may not even approach market translation with this same mindset. Nevertheless, this serves to initiate thoughts regarding market translation. While this aspect of technology development is not often focused on in an academic environment, it is a necessary component of making peripheral nerve interfacing a valuable technology to

mankind. Without it, the people originally intended to benefit from this technology will largely only ever see it as a media showcase or in the movies.

APPENDIX

A.1. Supplemental Figures

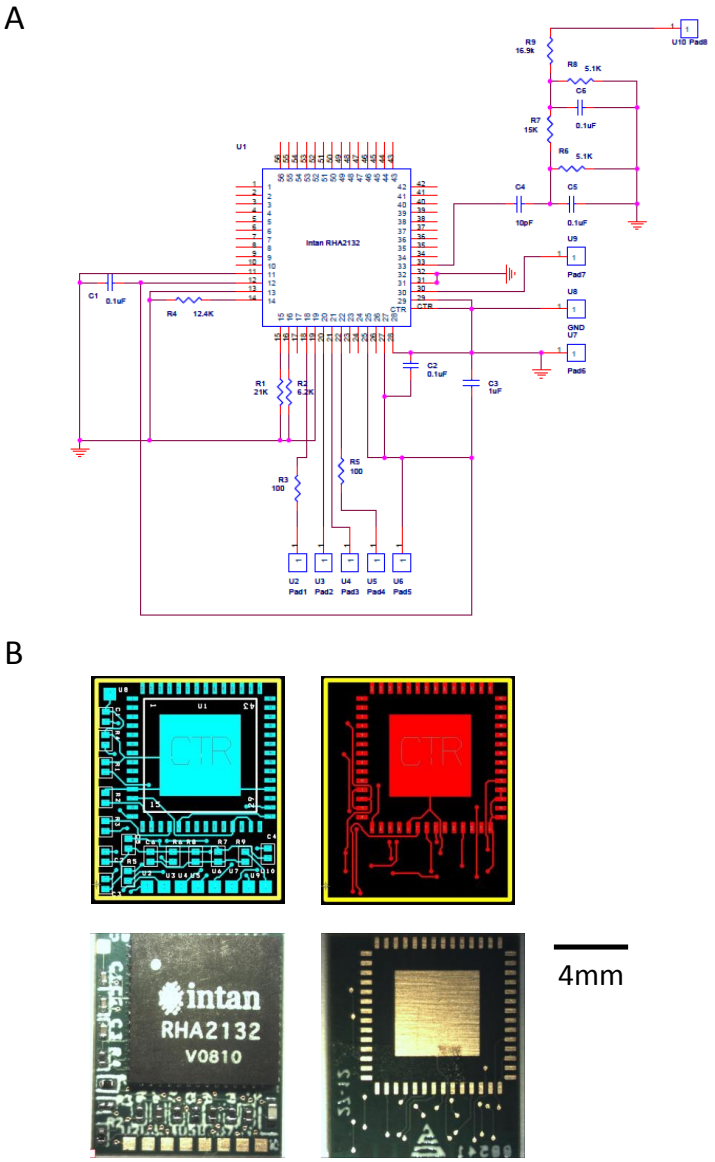

Figure A 1. Intan Technologies microchip PCB layout and components.
(A) Custom PCB wiring layout with off-chip components detailed. (B) Custom PCB design where the top of the PCB is shown on the left and the bottom of the PCB is shown on the right. Actual images of the PCB are shown in the bottom row.

A.2. Supplemental Results

The following is additional work performed in Chapter 3 (Aim 1) specifically with regard to the study involving the regenerative microchannel interface that utilized permanently integrated microwire electrodes with the PDMS/SU-8 microchannel scaffolds.

A.2.1. Nerve regeneration through the regenerative microchannel interfaces

Robust growth of axons and Schwann cells were observed through all microchannel interfaces after 5 months of implantation evidenced by immunohistochemical staining for NF160 and S100 markers, respectively (Figures A2(A) and (B)). Microwires running along the periphery of the microchannel scaffold can be seen in Figures A2(A) because the microwire insulation auto-fluoresces at the 594 nm wavelength used to visualize the axons. Within the microchannels, axons and Schwann cells were co-localized as expected and formed well consolidated mini-cords of regenerated tissue (microchannel fascicles). Additionally, these microchannel fascicles were surrounded by extracellular tissue similar to the fascicular organization of a normal nerve (Figures A2(C) and (D)). A number of channels could not be analyzed due to mechanical damage resulting in loss of microchannel integrity during the sectioning process. However, in all cases analyzed, microchannels containing electrodes also contained regenerated axons and Schwann cells. Furthermore, 88% of all microchannels in the device contained regenerated axons and Schwann cells. In general, the few microchannels that did not contain regenerated axons were positioned along the outer rings of the microchannel interface.

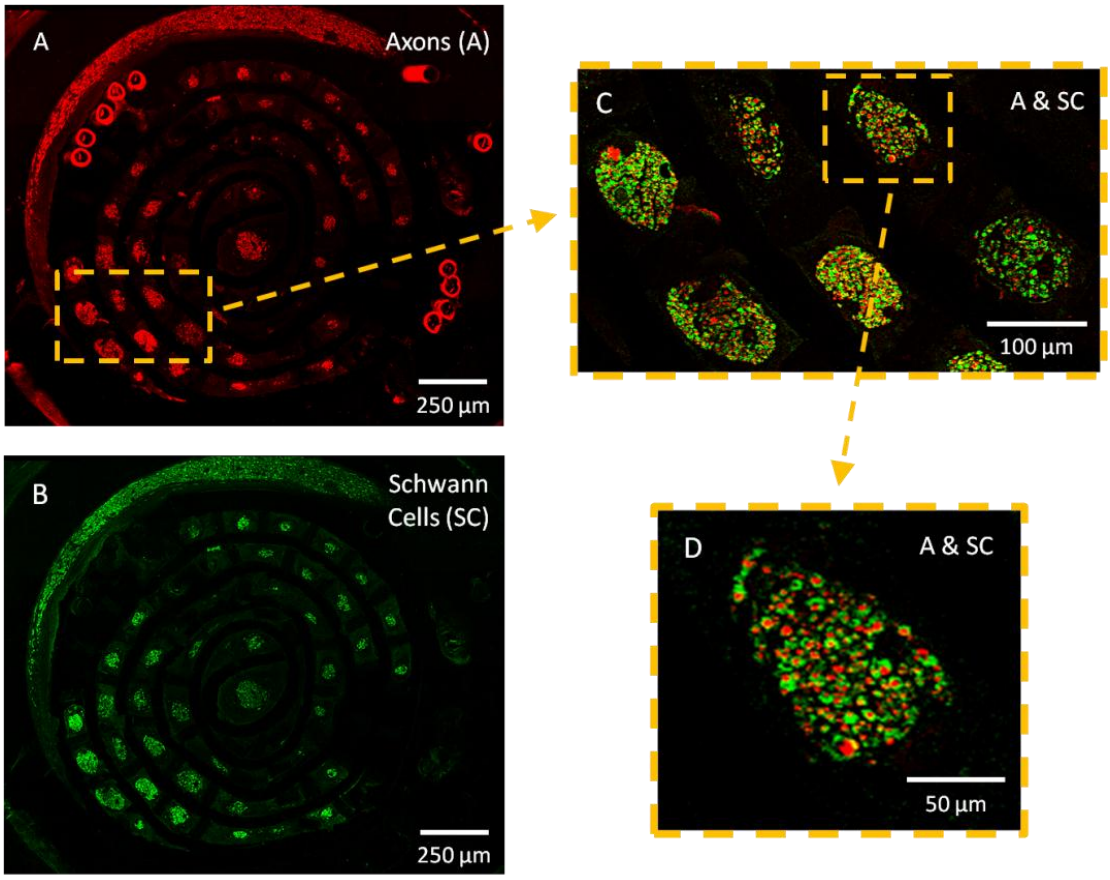

Figure A2. Regenerative Microchannel Interface Cross-Section.
Stained for Axons (red) and Schwann Cells (green). (a) Axons; (b) Schwann cells; (c) Magnified overlay of axons and Schwann cells; (d) Further magnified overlay of axons and Schwann cells.

A.2.2. SNR comparison between tripolar, bipolar and distant low impedance referencing paradigms

A.2.2.1. Average SNR of single unit APs

A tripolar, bipolar, and distant low impedance reference were used in conjunction with spontaneous and sensory evoked single unit recordings taken using the regenerative microchannel interfaces. This allowed differences between the three referencing paradigms to be evaluated in an *in-vivo* setting using SNR as a measure of signal quality. Each SNR calculated for a unit represents a mean value of individual waveform amplitudes compared to the noise band taken during the recording time window. If one

referencing paradigm consistently yields higher SNRs than the other references, an average of the SNRs would also be higher. Accordingly, average SNRs obtained from selected units across tripolar, bipolar, and distant low impedance references were statistically compared. This is depicted graphically with standard error means in Figures A3. The tripolar, bipolar, and distant low impedance average SNRs were calculated to be 1.56 ± 0.17, 1.55 ± 0.23, and 1.58 ± 0.19, respectively. There was no statistically significant difference between any of the three referencing paradigms using a Repeated Measures One-way ANOVA with the post hoc Tukey's Multiple Comparison Test.

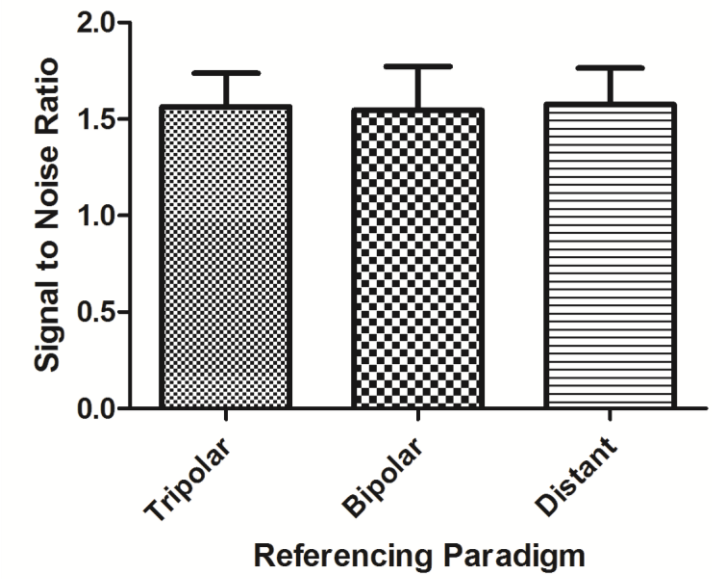

Figure A3. Average SNR for tripolar, bipolar and distant low impedance referencing paradigms.
Stained for Axons (red) and Schwann Cells (green). (a) Axons; (b) Schwann cells; (c) Magnified overlay of axons and Schwann cells; (d) Further magnified overlay of axons and Schwann cells.

A.2.2.2. Average SNR variance of single unit APs

Another aspect of SNR that can be evaluated, in addition to the actual size, is the variability present within the SNR from each individual unit. This can have implications on spike sorting capabilities as greater variability means a less consistent action potential waveform. One way to evaluate this is to compare variances of the individual waveform

amplitudes used to calculate the SNRs across each referencing paradigm. If a specific reference is more reliable, the variance of individual waveform amplitudes within each unit will be smaller than that recorded using the other two references. This would also hold true for an average of waveform amplitude variances from all units within each referencing paradigm. Accordingly, average variances of waveform amplitudes from units recorded across the three referencing paradigms are depicted graphically in Figures A4. The tripolar, bipolar, and distant low impedance average waveform amplitude variances were 0.13, 0.18, and 0.32, respectively. There appears to be a trend where the average variance for the tripolar and bipolar reference are relatively similar, but lower than the distant low impedance variance. However, further statistics need to be performed to determine whether there are any significant differences.

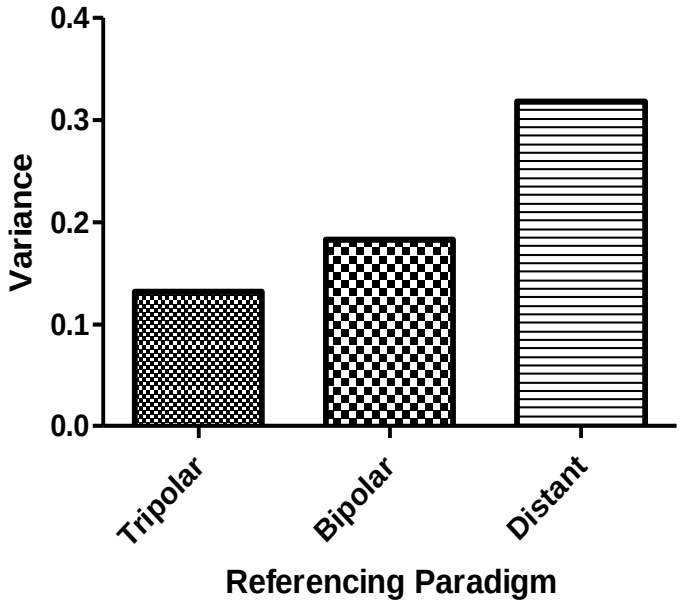

Figure A4. Average Variance of SNRs for tripolar, bipolar and distant low impedance referencing paradigms.
Stained for Axons (red) and Schwann Cells (green). (a) Axons; (b) Schwann cells; (c) Magnified overlay of axons and Schwann cells; (d) Further magnified overlay of axons and Schwann cells.

REFERENCES

[1] Dhillon GS, Lawrence SM, Hutchinson DT, Horch KW. Residual function in peripheral nerve stumps of amputees: implications for neural control of artificial limbs. J Hand Surg Am 2004;29:605–15; discussion 616–8. doi:10.1016/j.jhsa.2004.02.006.

[2] Tyler DJ, Durand DM. Functionally selective peripheral nerve stimulation with a flat interface nerve electrode. IEEE Trans Neural Syst Rehabil Eng 2002;10:294–303. doi:10.1109/TNSRE.2002.806840.

[3] Grill WM, Mortimer JT. Neural and connective tissue response to long-term implantation of multiple contact nerve cuff electrodes. J Biomed Mater Res 2000;50:215–26.

[4] Branner A, Stein RB, Fernandez E, Aoyagi Y, Normann RA. Long-term stimulation and recording with a penetrating microelectrode array in cat sciatic nerve. IEEE Trans Biomed Eng 2004;51:146–57. doi:10.1109/TBME.2003.820321.

[5] Ramachandran A, Schuettler M, Lago N, Doerge T, Koch KP, Navarro X, et al. Design, in vitro and in vivo assessment of a multi-channel sieve electrode with integrated multiplexer. J Neural Eng 2006;3:114–24. doi:10.1088/1741-2560/3/2/005.

[6] Fitzgerald JJ, Lacour SP, McMahon SB, Fawcett JW. Microchannels as axonal amplifiers. IEEE Trans Biomed Eng 2008;55:1136–46. doi:10.1109/TBME.2007.909533.

[7] HESS A, YOUNG JZ. The nodes of Ranvier. Proc R Soc Lond B Biol Sci 1952;140:301–20.

[8] Ziegler-Graham K, MacKenzie EJ, Ephraim PL, Travison TG, Brookmeyer R. Estimating the prevalence of limb loss in the United States: 2005 to 2050. Arch Phys Med Rehabil 2008;89:422–9. doi:10.1016/j.apmr.2007.11.005.

[9] Li Y, Burrows NR, Gregg EW, Albright A, Geiss LS. Declining rates of hospitalization for nontraumatic lower-extremity amputation in the diabetic population aged 40 years or older: U.S., 1988-2008. Diabetes Care 2012;35:273–7. doi:10.2337/dc11-1360.

[10] U.S. Centers for Disease Control and Prevention. National diabetes fact sheet: national estimates and general information on diabetes and prediabetes in the United States, 2011. US Dep Heal Hum Serv Centers Dis Control Prev 2011;3:1–12.

[11] Schmidt CE, Leach JB. Neural tissue engineering: strategies for repair and regeneration. Annu Rev Biomed Eng 2003;5:293–347. doi:10.1146/annurev.bioeng.5.011303.120731.

[12] Mueller M, Leonhard C, Wacker K, Ringelstein EB, Okabe M, Hickey WF, et al. Macrophage Response to Peripheral Nerve Injury: The Quantitative Contribution of Resident and Hematogenous Macrophages. Lab Investig 2003;83:175–85. doi:10.1097/01.LAB.0000056993.28149.BF.

[13] Griffin JW, George R, Ho T. Macrophage systems in peripheral nerves. A review. J Neuropathol Exp Neurol 1993;52:553–60.

[14] Williams LR, Longo FM, Powell HC, Lundborg G, Varon S. Spatial-Temporal progress of peripheral nerve regeneration within a silicone chamber: Parameters for a bioassay. J Comp Neurol 1983;218:460–70. doi:10.1002/cne.902180409.

[15] Williams LR, Danielsen N, Müller H, Varon S. Exogenous matrix precursors promote functional nerve regeneration across a 15-mm gap within a silicone chamber in the rat. J Comp Neurol 1987;264:284–90. doi:10.1002/cne.902640211.

[16] Liu HM. The role of extracellular matrix in peripheral nerve regeneration: a wound chamber study. Acta Neuropathol 1992;83:469–74.

[17] Frostick SP, Yin Q, Kemp GJ. Schwann cells, neurotrophic factors, and peripheral nerve regeneration. Microsurgery 1998;18:397–405.

[18] Taniuchi M, Clark HB, Johnson EM. Induction of nerve growth factor receptor in Schwann cells after axotomy. Proc Natl Acad Sci U S A 1986;83:4094–8.

[19] GUTMANN E, GUTTMANN L, MEDAWAR PB, YOUNG JZ. The Rate of Regeneration of Nerve. J Exp Biol 1942;19:14–44.

[20] Mukhatyar V, Karumbaiah L, Yeh J, Bellamkonda R. Tissue Engineering Strategies Designed to Realize the Endogenous Regenerative Potential of Peripheral Nerves. Adv Mater 2009;21:4670–9. doi:10.1002/adma.200900746.

[21] Campbell WW. Evaluation and management of peripheral nerve injury. Clin Neurophysiol 2008;119:1951–65. doi:10.1016/j.clinph.2008.03.018.

[22] Aebischer P, Gue´nard V, Winn SR, Valentini RF, Galletti PM. Blind-ended semipermeable guidance channels support peripheral nerve regeneration in the

absence of a distal nerve stump. Brain Res 1988;454:179–87. doi:10.1016/0006-8993(88)90817-7.

[23] Aebischer P, Guénard V, Brace S. Peripheral nerve regeneration through blind-ended semipermeable guidance channels: effect of the molecular weight cutoff. J Neurosci 1989;9:3590–5.

[24] Jenq C-B, Coggeshall RE. Regeneration of transected rat sciatic nerves after using isolated nerve fragments as distal inserts in silicone tubes. Exp Neurol 1986;91:154–62. doi:10.1016/0014-4886(86)90033-6.

[25] Zhang W, Ochi M, Takata H, Ikuta Y. Influence of distal nerve segment volume on nerve regeneration in silicone tubes. Exp Neurol 1997;146:600–3. doi:10.1006/exnr.1997.6539.

[26] Williams LR, Powell HC, Lundborg G, Varon S. Competence of nerve tissue as distal insert promoting nerve regeneration in a silicone chamber. Brain Res 1984;293:201–11. doi:10.1016/0006-8993(84)91227-7.

[27] Snider WD, Thanedar S. Target dependence of hypoglossal motor neurons during development and in maturity. J Comp Neurol 1989;279:489–98. doi:10.1002/cne.902790312.

[28] Xu Q-G, Forden J, Walsh SK, Gordon T, Midha R. Motoneuron survival after chronic and sequential peripheral nerve injuries in the rat. J Neurosurg 2010;112:890–9. doi:10.3171/2009.8.JNS09812.

[29] Vanden Noven S, Wallace N, Muccio D, Turtz A, Pinter MJ. Adult spinal motoneurons remain viable despite prolonged absence of functional synaptic contact with muscle. Exp Neurol 1993;123:147–56.

[30] Gordon T, Gillespie J, Orozco R, Davis L. Axotomy-induced changes in rabbit hindlimb nerves and the effects of chronic electrical stimulation. J Neurosci 1991;11:2157–69.

[31] Fu SY, Gordon T. Contributing factors to poor functional recovery after delayed nerve repair: prolonged axotomy. J Neurosci 1995;15:3876–85.

[32] Fu SY, Gordon T. The cellular and molecular basis of peripheral nerve regeneration. Mol Neurobiol 1997;14:67–116. doi:10.1007/BF02740621.

[33] Titmus MJ, Faber DS. Axotomy-induced alterations in the electrophysiological characteristics of neurons. Prog Neurobiol 1990;35:1–51. doi:10.1016/0301-0082(90)90039-J.

[34] Kuiken TA, Miller LA, Lipschutz RD, Lock BA, Stubblefield K, Marasco PD, et al. Targeted reinnervation for enhanced prosthetic arm function in a woman with a proximal amputation: a case study. Lancet 2007;369:371–80. doi:10.1016/S0140-6736(07)60193-7.

[35] Kuiken T. Targeted reinnervation for improved prosthetic function. Phys Med Rehabil Clin N Am 2006;17:1–13. doi:10.1016/j.pmr.2005.10.001.

[36] Fisher LE, Tyler DJ, Anderson JS, Triolo RJ. Chronic stability and selectivity of four-contact spiral nerve-cuff electrodes in stimulating the human femoral nerve. J Neural Eng 2009;6:046010. doi:10.1088/1741-2560/6/4/046010.

[37] Fisher LE, Miller ME, Bailey SN, Davis JA, Anderson JS, Rhode L, et al. Standing after spinal cord injury with four-contact nerve-cuff electrodes for quadriceps stimulation. IEEE Trans Neural Syst Rehabil Eng 2008;16:473–8. doi:10.1109/TNSRE.2008.2003390.

[38] Ortiz-Catalan M, Hakansson B, Branemark R. An osseointegrated human-machine gateway for long-term sensory feedback and motor control of artificial limbs. Sci Transl Med 2014;6:257re6–257re6. doi:10.1126/scitranslmed.3008933.

[39] Navarro X, Krueger TB, Lago N, Micera S, Stieglitz T, Dario P. A critical review of interfaces with the peripheral nervous system for the control of neuroprostheses and hybrid bionic systems. J Peripher Nerv Syst 2005;10:229–58. doi:10.1111/j.1085-9489.2005.10303.x.

[40] Yoo PB, Durand DM. Selective recording of the canine hypoglossal nerve using a multicontact flat interface nerve electrode. IEEE Trans Biomed Eng 2005;52:1461–9. doi:10.1109/TBME.2005.851482.

[41] Branner A, Normann RA. A multielectrode array for intrafascicular recording and stimulation in sciatic nerve of cats. Brain Res Bull 2000;51:293–306. doi:10.1016/S0361-9230(99)00231-2.

[42] Branner A, Stein RB, Normann RA. Selective stimulation of cat sciatic nerve using an array of varying-length microelectrodes. J Neurophysiol 2001;85:1585–94.

[43] Micera S, Navarro X, Carpaneto J, Citi L, Tonet O, Rossini PM, et al. On the use of longitudinal intrafascicular peripheral interfaces for the control of cybernetic hand prostheses in amputees. IEEE Trans Neural Syst Rehabil Eng 2008;16:453–72. doi:10.1109/TNSRE.2008.2006207.

[44] Badia J, Boretius T, Andreu D, Azevedo-Coste C, Stieglitz T, Navarro X. Comparative analysis of transverse intrafascicular multichannel, longitudinal

intrafascicular and multipolar cuff electrodes for the selective stimulation of nerve fascicles. J Neural Eng 2011;8:036023. doi:10.1088/1741-2560/8/3/036023.

[45] Dhillon GS, Horch KW. Direct neural sensory feedback and control of a prosthetic arm. IEEE Trans Neural Syst Rehabil Eng 2005;13:468–72. doi:10.1109/TNSRE.2005.856072.

[46] Lago N, Udina E, Ramachandran A, Navarro X. Neurobiological assessment of regenerative electrodes for bidirectional interfacing injured peripheral nerves. IEEE Trans Biomed Eng 2007;54:1129–37. doi:10.1109/TBME.2007.891168.

[47] Clements IP, Mukhatyar VJ, Srinivasan A, Bentley JT, Andreasen DS, Bellamkonda R V. Regenerative scaffold electrodes for peripheral nerve interfacing. IEEE Trans Neural Syst Rehabil Eng 2013;21:554–66. doi:10.1109/TNSRE.2012.2217352.

[48] Garde K, Keefer E, Botterman B, Galvan P, Romero MI. Early interfaced neural activity from chronic amputated nerves. Front Neuroeng 2009;2:5. doi:10.3389/neuro.16.005.2009.

[49] FitzGerald JJ, Lago N, Benmerah S, Serra J, Watling CP, Cameron RE, et al. A regenerative microchannel neural interface for recording from and stimulating peripheral axons in vivo. J Neural Eng 2012;9:016010. doi:10.1088/1741-2560/9/1/016010.

[50] Minev IR, Chew DJ, Delivopoulos E, Fawcett JW, Lacour SP. High sensitivity recording of afferent nerve activity using ultra-compliant microchannel electrodes: an acute in vivo validation. J Neural Eng 2012;9:026005. doi:10.1088/1741-2560/9/2/026005.

[51] Negredo P, Castro J, Lago N, Navarro X, Avendaño C. Differential growth of axons from sensory and motor neurons through a regenerative electrode: a stereological, retrograde tracer, and functional study in the rat. Neuroscience 2004;128:605–15. doi:10.1016/j.neuroscience.2004.07.017.

[52] Lago N, Ceballos D, Rodríguez FJ, Stieglitz T, Navarro X. Long term assessment of axonal regeneration through polyimide regenerative electrodes to interface the peripheral nerve. Biomaterials 2005;26:2021–31. doi:10.1016/j.biomaterials.2004.06.025.

[53] Rutten WLC. Selective electrical interfaces with the nervous system. Annu Rev Biomed Eng 2002;4:407–52. doi:10.1146/annurev.bioeng.4.020702.153427.

[54] Lago N, Udina E, Ramachandran A, Navarro X. Neurobiological assessment of regenerative electrodes for bidirectional interfacing injured peripheral nerves. IEEE Trans Biomed Eng 2007;54:1129–37. doi:10.1109/TBME.2007.891168.

[55] Salzer JL. Clustering sodium channels at the node of Ranvier: close encounters of the axon-glia kind. Neuron 1997;18:843–6.

[56] FitzGerald JJ, Lacour SP, McMahon SB, Fawcett JW. Microchannel electrodes for recording and stimulation: in vitro evaluation. IEEE Trans Biomed Eng 2009;56:1524–34. doi:10.1109/TBME.2009.2013960.

[57] Lacour SP, Fitzgerald JJ, Lago N, Tarte E, McMahon S, Fawcett J. Long micro-channel electrode arrays: a novel type of regenerative peripheral nerve interface. IEEE Trans Neural Syst Rehabil Eng 2009;17:454–60. doi:10.1109/TNSRE.2009.2031241.

[58] Chew DJ, Zhu L, Delivopoulos E, Minev IR, Musick KM, Mosse C a, et al. A microchannel neuroprosthesis for bladder control after spinal cord injury in rat. Sci Transl Med 2013;5:210ra155. doi:10.1126/scitranslmed.3007186.

[59] Delivopoulos E, Chew DJ, Minev IR, Fawcett JW, Lacour SP. Concurrent recordings of bladder afferents from multiple nerves using a microfabricated PDMS microchannel electrode array. Lab Chip 2012;12:2540–51. doi:10.1039/c2lc21277c.

[60] Bunge RP, Bunge MB, Eldridge CF. Linkage between axonal ensheathment and basal lamina production by Schwann cells. Annu Rev Neurosci 1986;9:305–28. doi:10.1146/annurev.ne.09.030186.001513.

[61] Klinge PM, Vafa MA, Brinker T, Brandis A, Walter GF, Stieglitz T, et al. Immunohistochemical characterization of axonal sprouting and reactive tissue changes after long-term implantation of a polyimide sieve electrode to the transected adult rat sciatic nerve. Biomaterials 2001;22:2333–43. doi:10.1016/S0142-9612(00)00420-8.

[62] Lindenlaub T, Sommer C. Partial sciatic nerve transection as a model of neuropathic pain: a qualitative and quantitative neuropathological study. Pain 2000;89:97–106. doi:10.1016/S0304-3959(00)00354-7.

[63] Carlton SM, Dougherty PM, Pover CM, Coggeshall RE. Neuroma formation and numbers of axons in a rat model of experimental peripheral neuropathy. Neurosci Lett 1991;131:88–92. doi:10.1016/0304-3940(91)90343-R.

[64] Munger BL, Bennett GJ, Kajander KC. An experimental painful peripheral neuropathy due to nerve constriction. I. Axonal pathology in the sciatic nerve. Exp Neurol 1992;118:204–14. doi:10.1016/0014-4886(92)90037-Q.

[65] Coderre TJ, Grimes RW, Melzack R. Deafferentation and chronic pain in animals: an evaluation of evidence suggesting autotomy is related to pain. Pain 1986;26:61–84.

[66] Wall PD, Gutnick M. Ongoing activity in peripheral nerves: the physiology and pharmacology of impulses originating from a neuroma. Exp Neurol 1974;43:580–93.

[67] Fried K, Govrin-Lippmann R, Rosenthal F, Ellisman MH, Devor M. Ultrastructure of afferent axon endings in a neuroma. J Neurocytol 1991;20:682–701. doi:10.1007/BF01187069.

[68] Devor M, Govrin-Lippmann R, Angelides K. Na+ channel immunolocalization in peripheral mammalian axons and changes following nerve injury and neuroma formation. J Neurosci 1993;13:1976–92.

[69] Breward J, Gentle MJ. Neuroma formation and abnormal afferent nerve discharges after partial beak amputation (beak trimming) in poultry. Experientia 1985;41:1132–4. doi:10.1007/BF01951693.

[70] Tyner TR, Parks N, Faria S, Simons M, Stapp B, Curtis B, et al. Effects of collagen nerve guide on neuroma formation and neuropathic pain in a rat model. Am J Surg 2007;193:e1–6. doi:10.1016/j.amjsurg.2006.08.026.

[71] Srinivasan A, Guo L, Bellamkonda R V. Regenerative microchannel electrode array for peripheral nerve interfacing. 2011 5th Int. IEEE/EMBS Conf. Neural Eng., IEEE; 2011, p. 253–6. doi:10.1109/NER.2011.5910535.

[72] Clements IP, Kim Y, English AW, Lu X, Chung A, Bellamkonda R V. Thin-film enhanced nerve guidance channels for peripheral nerve repair. Biomaterials 2009;30:3834–46. doi:10.1016/j.biomaterials.2009.04.022.

[73] Mukhatyar V, Pai B, Clements I, Srinivasan A, Huber R, Mehta A, et al. Molecular sequelae of topographically guided peripheral nerve repair. Ann Biomed Eng 2014;42:1436–55. doi:10.1007/s10439-013-0960-x.

[74] Ceballos D, Valero-Cabré A, Valderrama E, Schüttler M, Stieglitz T, Navarro X. Morphologic and functional evaluation of peripheral nerve fibers regenerated through polyimide sieve electrodes over long-term implantation. J Biomed Mater Res 2002;60:517–28.

[75] Fawcett JW, Keynes RJ. Peripheral nerve regeneration. Annu Rev Neurosci 1990;13:43–60. doi:10.1146/annurev.ne.13.030190.000355.

[76] Carpenter MB, Jerome S. Human neuroanatomy. 8th ed. Baltimore: Williams & Wilkins; 1983.

[77] Furey MJ, Midha R, Xu Q-G, Belkas J, Gordon T. Prolonged target deprivation reduces the capacity of injured motoneurons to regenerate. Neurosurgery 2007;60:723–32. doi:10.1227/01.NEU.0000255412.63184.CC.

[78] Ladak A, Schembri P, Olson J, Udina E, Tyreman N, Gordon T. Side-to-side nerve grafts sustain chronically denervated peripheral nerve pathways during axon

regeneration and result in improved functional reinnervation. Neurosurgery 2011;68:1654–65; discussion 1665–6. doi:10.1227/NEU.0b013e31821246a8.

[79] Bunge RP. The role of the Schwann cell in trophic support and regeneration. J Neurol 1994;242:S19–21. doi:10.1007/BF00939235.

[80] Rossini PM, Micera S, Benvenuto A, Carpaneto J, Cavallo G, Citi L, et al. Double nerve intraneural interface implant on a human amputee for robotic hand control. Clin Neurophysiol 2010;121:777–83. doi:10.1016/j.clinph.2010.01.001.

[81] Guo L, DeWeerth SP. An effective lift-off method for patterning high-density gold interconnects on an elastomeric substrate. Small 2010;6:2847–52. doi:10.1002/smll.201001456.

[82] Liang Guo, Guvanasen GS, Xi Liu, Tuthill C, Nichols TR, DeWeerth SP. A PDMS-based integrated stretchable microelectrode array (isMEA) for neural and muscular surface interfacing. IEEE Trans Biomed Circuits Syst 2013;7:1–10. doi:10.1109/TBCAS.2012.2192932.

[83] Seung Bae Lee, Hyung-Min Lee, Kiani M, Uei-Ming Jow, Ghovanloo M. An Inductively Powered Scalable 32-Channel Wireless Neural Recording System-on-a-Chip for Neuroscience Applications. IEEE Trans Biomed Circuits Syst 2010;4:360–71. doi:10.1109/TBCAS.2010.2078814.

[84] Lacour SP, Wagner S, Narayan RJ, Li T, Suo Z. Stiff subcircuit islands of diamondlike carbon for stretchable electronics. J Appl Phys 2006;100:014913. doi:10.1063/1.2210170.

[85] Graz IM, Cotton DPJ, Robinson A, Lacour SP. Silicone substrate with in situ strain relief for stretchable thin-film transistors. Appl Phys Lett 2011;98:124101. doi:10.1063/1.3570661.

[86] Romeo A, Liu Q, Suo Z, Lacour SP. Elastomeric substrates with embedded stiff platforms for stretchable electronics. Appl Phys Lett 2013;102:131904. doi:10.1063/1.4799653.

[87] Meyer J-U, Stieglitz T, Scholz O, Haberer W, Beutel H. High density interconnects and flexible hybrid assemblies for active biomedical implants. IEEE Trans Adv Packag 2001;24:366–74. doi:10.1109/6040.938305.

[88] Stieglitz T, Schuettler M, Koch KP. Implantable biomedical microsystems for neural prostheses. IEEE Eng Med Biol Mag 2005;24:58–65.

[89] Rousche PJ, Pellinen DS, Pivin DP, Williams JC, Vetter RJ, Kipke DR. Flexible polyimide-based intracortical electrode arrays with bioactive capability. IEEE Trans Biomed Eng 2001;48:361–71. doi:10.1109/10.914800.

[90] Guo L, DeWeerth SP. High-density stretchable electronics: toward an integrated multilayer composite. Adv Mater 2010;22:4030–3. doi:10.1002/adma.201000515.

[91] Li W, Rodger DC, Meng E, Weiland JD, Humayun MS, Tai Y-C. Flexible Parylene Packaged Intraocular Coil for Retinal Prostheses. 2006 Int. Conf. Microtechnologies Med. Biol., IEEE; 2006, p. 105–8. doi:10.1109/MMB.2006.251502.

[92] Li W, Rodger DC, Tai YC. Implantable RF-coiled chip packaging. 2008 IEEE 21st Int. Conf. Micro Electro Mech. Syst., IEEE; 2008, p. 108–11. doi:10.1109/MEMSYS.2008.4443604.

[93] Li W, Rodger DC, Meng E, Weiland JD, Humayun MS, Tai Y-C. Wafer-Level Parylene Packaging With Integrated RF Electronics for Wireless Retinal Prostheses. J Microelectromechanical Syst 2010;19:735–42. doi:10.1109/JMEMS.2010.2049985.

[94] Hassler C, von Metzen RP, Ruther P, Stieglitz T. Characterization of parylene C as an encapsulation material for implanted neural prostheses. J Biomed Mater Res B Appl Biomater 2010;93:266–74. doi:10.1002/jbm.b.31584.

[95] Lawrence SM, Dhillon GS, Horch KW. Fabrication and characteristics of an implantable, polymer-based, intrafascicular electrode. J Neurosci Methods 2003;131:9–26. doi:10.1016/S0165-0270(03)00231-0.

[96] Vetter RJ, Williams JC, Hetke JF, Nunamaker EA, Kipke DR. Chronic neural recording using silicon-substrate microelectrode arrays implanted in cerebral cortex. IEEE Trans Biomed Eng 2004;51:896–904. doi:10.1109/TBME.2004.826680.

[97] Patterson WR, Song Y-K, Bull CW, Ozden I, Deangellis AP, Lay C, et al. A microelectrode/microelectronic hybrid device for brain implantable neuroprosthesis applications. IEEE Trans Biomed Eng 2004;51:1845–53. doi:10.1109/TBME.2004.831521.

[98] Hassler C, Boretius T, Stieglitz T. Polymers for neural implants. J Polym Sci Part B Polym Phys 2011;49:18–33. doi:10.1002/polb.22169.

[99] Bandodkar AAJ, Jia W, Yardımcı C, Wang X, Ramirez J, Wang J. Tattoo-based noninvasive glucose monitoring: a proof-of-concept study. Anal Chem 2015;87:394–8. doi:10.1021/ac504300n.

[100] Nambiar S, Yeow JTW. Conductive polymer-based sensors for biomedical applications. Biosens Bioelectron 2011;26:1825–32. doi:10.1016/j.bios.2010.09.046.

[101] Bandodkar AJ, Wang J. Non-invasive wearable electrochemical sensors: a review. Trends Biotechnol 2014;32:363–71. doi:10.1016/j.tibtech.2014.04.005.

[102] Bandodkar AJ, Molinnus D, Mirza O, Guinovart T, Windmiller JR, Valdés-Ramírez G, et al. Epidermal tattoo potentiometric sodium sensors with wireless signal transduction for continuous non-invasive sweat monitoring. Biosens Bioelectron 2014;54:603–9. doi:10.1016/j.bios.2013.11.039.

[103] Vashist SK. Non-invasive glucose monitoring technology in diabetes management: a review. Anal Chim Acta 2012;750:16–27. doi:10.1016/j.aca.2012.03.043.

[104] Rosset S, Shea HR. Flexible and stretchable electrodes for dielectric elastomer actuators. Appl Phys A 2012;110:281–307. doi:10.1007/s00339-012-7402-8.

[105] Kim D-H, Ghaffari R, Lu N, Rogers J a. Flexible and stretchable electronics for biointegrated devices. Annu Rev Biomed Eng 2012;14:113–28. doi:10.1146/annurev-bioeng-071811-150018.

[106] Kudo H, Sawada T, Kazawa E, Yoshida H, Iwasaki Y, Mitsubayashi K. A flexible and wearable glucose sensor based on functional polymers with soft-MEMS techniques. Biosens Bioelectron 2006;22:558–62. doi:10.1016/j.bios.2006.05.006.

[107] Benight SJ, Wang C, Tok JBH, Bao Z. Stretchable and self-healing polymers and devices for electronic skin. Prog Polym Sci 2013;38:1961–77. doi:10.1016/j.progpolymsci.2013.08.001.

[108] Park S, Vosguerichian M, Bao Z. A review of fabrication and applications of carbon nanotube film-based flexible electronics. Nanoscale 2013;5:1727–52. doi:10.1039/c3nr33560g.

[109] Srinivasan A, Tahilramani M, Bentley JT, Gore RK, Millard DC, Mukhatyar VJ, et al. Microchannel-based regenerative scaffold for chronic peripheral nerve interfacing in amputees. Biomaterials 2015;41:151–65. doi:10.1016/j.biomaterials.2014.11.035.

[110] Harder TA, Yao T-JYT-J, He QHQ, Shih C-YSC-Y, Tai Y-CTY-C. Residual stress in thin-film parylene-c. Tech Dig MEMS 2002 IEEE Int Conf Fifteenth IEEE Int Conf Micro Electro Mech Syst (Cat No02CH37266) 2002.

[111] Guo L, Meacham KW, Hochman S, DeWeerth SP. A PDMS-based conical-well microelectrode array for surface stimulation and recording of neural tissues. IEEE Trans Biomed Eng 2010;57:2485–94. doi:10.1109/TBME.2010.2052617.

[112] Campo a Del, Greiner C. SU-8: a photoresist for high-aspect-ratio and 3D submicron lithography. J Micromechanics Microengineering 2007;17:R81–R95. doi:10.1088/0960-1317/17/6/R01.

[113] Kubenz M, Ostrzinski U, Reuther F, Gruetzner G. Effective baking of thick and ultra-thick photoresist layers by infrared radiation. Microelectron Eng 2003;67-68:495–501. doi:10.1016/S0167-9317(03)00106-0.

[114] Taherabadi LH, Madou MJ. A novel method for the fabrication of high-aspect ratio C-MEMS structures. J Microelectromechanical Syst 2005;14:348–58. doi:10.1109/JMEMS.2004.839312.

[115] Kuo JTW, Kim BJ, Hara S a, Lee CD, Gutierrez C a, Hoang TQ, et al. Novel flexible Parylene neural probe with 3D sheath structure for enhancing tissue integration. Lab Chip 2013;13:554–61. doi:10.1039/c2lc40935f.

[116] Kim BJ, Chen B, Gupta M, Meng E. Formation of three-dimensional Parylene C structures via thermoforming. J Micromechanics Microengineering 2014;24:065003. doi:10.1088/0960-1317/24/6/065003.

[117] Kim BJ, Kuo JTW, Hara S a, Lee CD, Yu L, Gutierrez C a, et al. 3D Parylene sheath neural probe for chronic recordings. J Neural Eng 2013;10:045002. doi:10.1088/1741-2560/10/4/045002.

[118] Meacham KW, Giuly RJ, Guo L, Hochman S, DeWeerth SP. A lithographically-patterned, elastic multi-electrode array for surface stimulation of the spinal cord. Biomed Microdevices 2008;10:259–69. doi:10.1007/s10544-007-9132-9.

[119] Garra J, Long T, Currie J, Schneider T, White R, Paranjape M. Dry etching of polydimethylsiloxane for microfluidic systems. J Vac Sci Technol A Vacuum, Surfaces, Film 2002;20:975. doi:10.1116/1.1460896.

[120] Branner A, Stein RB, Normann RA. Selective stimulation of cat sciatic nerve using an array of varying-length microelectrodes. J Neurophysiol 2001;85:1585–94.

[121] Clements IP, Mukhatyar VJ, Srinivasan A, Bentley JT, Andreasen DS, Bellamkonda R V. Regenerative scaffold electrodes for peripheral nerve interfacing. IEEE Trans Neural Syst Rehabil Eng 2013;21:554–66. doi:10.1109/TNSRE.2012.2217352.

[122] Lago N, Ceballos D, Rodríguez FJ, Stieglitz T, Navarro X. Long term assessment of axonal regeneration through polyimide regenerative electrodes to interface the peripheral nerve. Biomaterials 2005;26:2021–31. doi:10.1016/j.biomaterials.2004.06.025.

[123] Sabatier MJ, To BN, Nicolini J, English AW. Effect of Axon Misdirection on Recovery of Electromyographic Activity and Kinematics after Peripheral Nerve Injury. Cells Tissues Organs 2011;193:298–309. doi:10.1159/000323677.

[124] Hamilton SK, Hinkle ML, Nicolini J, Rambo LN, Rexwinkle AM, Rose SJ, et al. Misdirection of regenerating axons and functional recovery following sciatic nerve injury in rats. J Comp Neurol 2011;519:21–33. doi:10.1002/cne.22446.

[125] Quiroga RQ, Nadasdy Z, Ben-Shaul Y. Unsupervised Spike Detection and Sorting with Wavelets and Superparamagnetic Clustering. Neural Comput 2004;16:1661–87. doi:10.1162/089976604774201631.

[126] Gore RK, Choi Y, Bellamkonda R, English A. Functional recordings from awake, behaving rodents through a microchannel based regenerative neural interface. J Neural Eng 2015;12:016017. doi:10.1088/1741-2560/12/1/016017.

[127] Pang C, Cham J, Nenadic Z, Musallam S, Tai Y-C, Burdick J, et al. A new multi-site probe array with monolithically integrated parylene flexible cable for neural prostheses. Conf Proc . Annu Int Conf IEEE Eng Med Biol Soc IEEE Eng Med Biol Soc Annu Conf 2005;7:7114–7. doi:10.1109/IEMBS.2005.1616146.

[128] RODGER D, FONG A, LI W, AMERI H, AHUJA A, GUTIERREZ C, et al. Flexible parylene-based multielectrode array technology for high-density neural

stimulation and recording. Sensors Actuators B Chem 2008;132:449–60. doi:10.1016/j.snb.2007.10.069.

[129] Rodger DC, Weiland JD, Humayun MS, Tai Y-C. Scalable high lead-count parylene package for retinal prostheses. Sensors Actuators B Chem 2006;117:107–14. doi:10.1016/j.snb.2005.11.010.

[130] Hsu J-M, Rieth L, Normann R a, Tathireddy P, Solzbacher F. Encapsulation of an integrated neural interface device with Parylene C. IEEE Trans Biomed Eng 2009;56:23–9. doi:10.1109/TBME.2008.2002155.

[131] Clark G a, Ledbetter NM, Warren DJ, Harrison RR. Recording sensory and motor information from peripheral nerves with Utah Slanted Electrode Arrays. Conf Proc . Annu Int Conf IEEE Eng Med Biol Soc IEEE Eng Med Biol Soc Annu Conf 2011;2011:4641–4. doi:10.1109/IEMBS.2011.6091149.